Molecular Design of Ordering Transitions
in Block Copolymers

by

Anne-Valérie G. Ruzette

Engineering Degree in Materials Science and Engineering
Catholic University of Louvain-la-Neuve, Belgium, 1995

Submitted to the Department of Materials Science and Engineering
in Partial Fulfillment of the Requirements for the Degree of

Doctor of Philosophy
in
Polymer Science

at the
MASSACHUSETTS INSTITUTE OF TECHNOLOGY
June, 2000

Signature of Author:_____
Department of Materials Science and Engineering
February 17, 2000

Certified by: _____
Anne M. Mayes
Associate Professor of Polymer Physics
Thesis Supervisor

Accepted by: _____
Linn W. Hobbs
Professor of Materials Science
Chairman, Departmental Committee on Graduate Students

Molecular Design of Ordering Transitions
in Block Copolymers

by
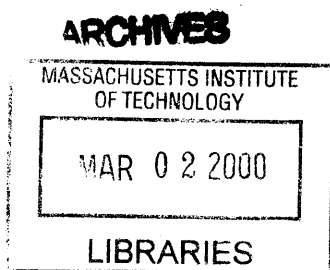
Anne-Valérie G. Ruzette

Submitted to the Department of Materials Science and Engineering
on February 17, 2000 in Partial Fulfillment of the Requirements
for the Degree of Doctor of Philosophy in Polymer Science

ABSTRACT

The tendency of block copolymers (BCP's) to microphase separate at the molecular level, producing a wide array of ordered nanostructures, is of particular interest from an engineering standpoint due to the unique mechanical, optical or electrical properties that ensue. Upon considering the potential applications of these materials, however, one limitation arises from the lack of control over bulk thermodynamics and the appearance of order/disorder (solid-like/liquid-like) transitions in these materials. To address this problem, this thesis aims to, firstly, develop a more quantifiable understanding of the molecular factors governing BCP phase behavior, and, secondly, use that knowledge to molecularly engineer new BCP's with enhanced processibility.

While most BCP's microphase separate upon cooling through an upper disorder-to-order transition (UDOT), polystyrene-*block*-poly *n*-butyl methacrylate, PS-*b*-PBMA, undergoes ordering upon heating through a lower disorder-to-order transition (LDOT). Preliminary studies on this material revealed a unique pressure sensitivity of this ordering transition. By applying pressure, this material could be forced into the segmentally mixed liquid state, implying "baroplasticity", a highly attractive property from a processing standpoint. To better understand the molecular origin of this behavior, the bulk thermodynamics of a family of BCPs formed from styrene and a homologous series of *n*-alkyl methacrylates (PS-*b*-P*n*AMA, *n* ranging from 1 to 12) was investigated, both as a function of pressure and temperature. The results of this study reveal an unexpected, though systematic, dependence of the phase behavior of these BCP's on monomer architecture. In short, over a certain range of alkyl side chain length, PS-*b*-P*n*AMA block copolymers are marginally compatible and exhibit unexpectedly large pressure coefficients for the ordering transition, ranging from 60 to 150°C/kbar.

In an attempt to identify molecular parameters responsible for these thermodynamic trends, as well as those displayed by other systems reported in the literature, combined group contribution/lattice fluid model calculations of the cohesive properties of the corresponding homopolymers are performed. Based on this analysis, the homopolymer mass density is proposed as a macroscopic parameter that appears to govern phase behavior in weakly interacting block copolymers or polymer blends. Using this new criterion, a simple tool for the molecular design of phase behavior into weakly interacting BCP's is identified, which is successfully used to engineer "baroplastic" behavior into several new systems of commercial relevance, including elastomers and adhesives based on styrene and low T_g acrylates.

In light of the improved understanding of BCP phase behavior emerging from these studies, a simple phenomenological free energy expression is proposed for compressible polymer mixtures, that can be extended to block copolymers. Its ability to predict qualitative phase diagrams for the systems investigated in this thesis as well as many other polymer pairs is demonstrated. Using this expression, basic principles regarding polymer thermodynamics are outlined.

Thesis Supervisor: Anne M. Mayes
Title: Associate Professor of Polymer Physics

Table of Contents

3

CHAPTER IV: A PREDICTIVE TOOL FOR THE DESIGN OF BLOCK COPOLYMER PHASE BEHAVIOR. **90**

CHAPTER V: NEW "BAROPLASTIC" ELASTOMERS AND ADHESIVES BASED ON STYRENE AND ALKYL ACRYLATES **120**

CHAPTER VI: A COMPRESSIBLE FREE ENERGY EXPRESSION **141**

CHAPTER VII: CONCLUSIONS AND FUTURE WORK **168**

LIST OF FIGURES

7

8

LIST OF TABLES

ACKNOWLEDGEMENTS

The completion of this thesis would have been impossible without the prodigious support, help and guidance I received from a great number of people throughout the years.

Above all, and with all my heart, I thank my thesis advisor, Anne M. Mayes, for her invaluable teaching and spiritual support. Through her example of unfailing perseverance, strength and extraordinary vision, she has lead me to summits I feared insurmountable. She has instilled in me a passion for polymer science which I perceive as the finest gift of all.

To my grandfather and first mentor, Charles Coppieters, who shared with me his love for spiritual and intellectual beauty and introduced me to a life of learning, I am forever grateful.

For this gift of life, for her unconditional support through every path I have chosen, and, above all, for her infallible love, I thank my mother, Marie-Rose Ruzette. Though his time with me was short, I thank my father, Alexis Ruzette, for the inexhaustible spring of enthusiasm and vitality he placed in me. I further thank my childhood companion and big brother, Laurent Ruzette.

To Cyrille Foillard, my husband and dearest friend, I offer my thanks for his generous and loving support, and for sharing his wife with her Block Copolymers.

I wholeheartedly thank all the members of the Mayes team, an unforgettable group of colleagues and dear friends who have helped me greatly, starting by teaching me American colloquialism...: Dave Walton, Michael Fasolka, Philip Soo, Jonathan Hester, Darrell Irvine, Pallab Banerjee, Stella Park, Rafal Mickiewicz, Solar Olugabefola and Aryia Akthakul. In particular, I thank Pallab Banerjee for making an important part of this work possible by synthesizing most of the anionic diblock copolymers.

Several other people have contributed enormously to this study. First and foremost, I extend my gratitude to T. P. Russell, my co-advisor, collaborator and mentor, whose guidance and support have helped me tremendously. For his partnership in this study, I thank his graduate student, Michael Pollard. For their precious help with the SANS experiments, I am most grateful to the people at NIST, the Argonne National Laboratory and the Los Alamos National Laboratory. In particular, I thank Steve Kline, Boualem Hammouda, and Tania Slawecki (NIST), Denis Wozniak, Kenneth Litrell and P. Thiyagarajan (ANL), and Rex Hjelm (LANSCE). For their help with the synthesis, I thank Professor Jérôme and his research group.

I also wish to thank Professors Marcel Crochet, Francis Delannay and Jean-Marie Streydio for their pivotal role in preparing me for my graduate education. Thanks also to the people in the Department of Materials Science and Engineering at MIT, and in particular, to Professor Rubner.

Finally, I wish to thank the members of my thesis committee: Professors Gerbrand Ceder, T. P. Russell and Chris Scott.

CHAPTER I: BACKGROUND AND MOTIVATION

I.1. INTRODUCTION TO BLOCK COPOLYMERS (BCP'S)

Block copolymers are macromolecules comprised of two or more chemically

distinct polymers covalently bonded together. Depending on the degree of

thermodynamic compatibility between the different blocks, such copolymers can either

be segmentally mixed or microphase separated into microdomains consisting of the

different block segments, with the covalent junctions residing at the interface. Indeed,

while incompatible homopolymer mixtures phase separate macroscopically, the covalent

junction between the polymer components in block copolymers forces the phase

separation to occur on a size scale on the order of the radius of gyration R_g of the

molecule, i.e. ~ 10-100 nm.[1-4] This tendency of block copolymers to microphase separate

or self-assemble at the molecular level, producing a wide array of highly ordered

nanostructures, is of particular interest from an engineering standpoint due to the unique

mechanical, optical or electrical properties that ensue.[5] The most commonly encountered

morphologies in A-B diblock and A-B-A triblock copolymers are illustrated in Figure I.1.

The particular morphology formed upon self-assembly is dictated under equilibrium

conditions by three parameters: the copolymer molecular weight, the composition and the

degree of thermodynamic compatibility between the two segment types, the latter being

quantitatively represented by the interaction parameter χ_{AB}.[3]

11
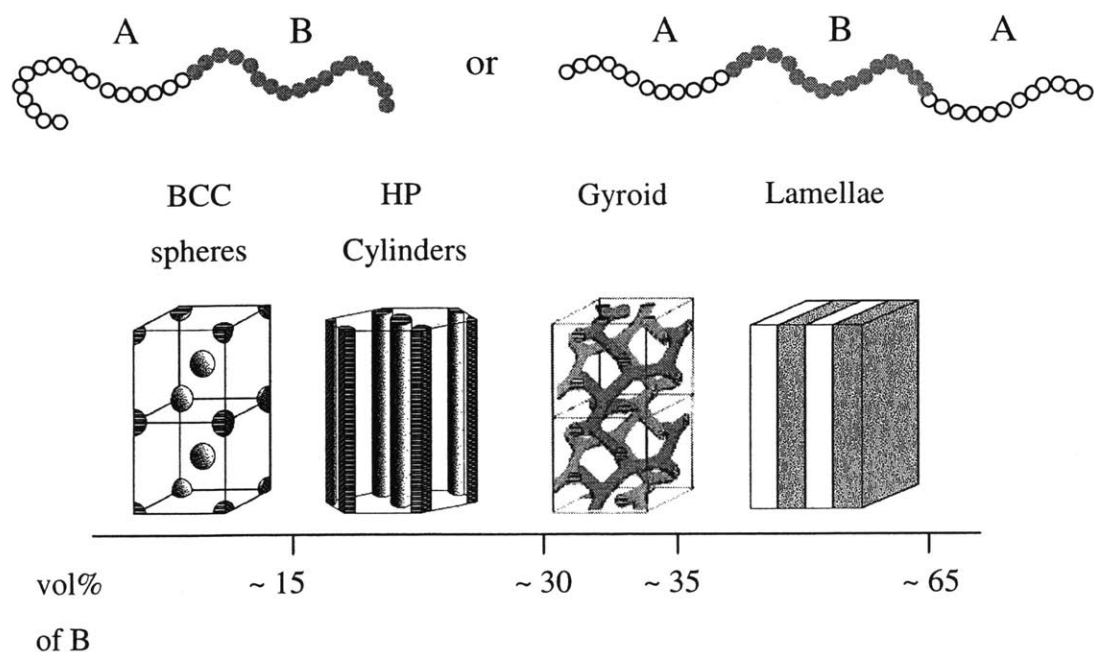
Figure I.1: A-B diblock and A-B-A triblock copolymer morphologies

Thermodynamically, self-assembly into one of the ordered morphologies shown in Figure I.1 results from the fact that, in block copolymers, the incompatibility between segments A and B driving phase separation is counterbalanced by entropic forces arising from the covalent link between the two blocks. Indeed, to keep the two blocks of a diblock copolymer away from each other and, therefore, minimize the unfavorable contacts between the two incompatible segment types, copolymer chains must adopt an extended configuration compared to their equilibrium (unperturbed) random coil dimensions. This stretching of the copolymer chains upon microphase separation is limited by the entropic frustration that ensues. Therefore, the particular morphology formed upon self-assembly and its equilibrium period D are dictated by a competition

between two free-energy contributions: the enthalpic interaction energy and the entropic (elastic) restoring force.[6]

Microphase separation in block copolymers has dramatic effects on their viscoelastic properties. Indeed, the localization of polymer chains in ordered microdomains of each segment type with the chemical junctions residing at the interface strongly *restricts flow* compared to segmentally mixed systems or pure homopolymers.[4,7] This distinct feature of block copolymers has lead to their widespread use as thermoplastic elastomers[8] and pressure sensitive adhesives[9], and holds promise for the development of new solid polymer electrolytes.[10] Moreover, self-assembly of block copolymers into spatially ordered microdomains provides new avenues for the development of nanotechnologies,[11-16] optically active materials[17-19] and biomaterials.[20] Finally, the recent development of more versatile and industrially amenable synthetic routes for the preparation of block copolymers has now unveiled new opportunities for optimizing the resulting properties of these molecules via a judicious choice of both chemistry and molecular architecture.[21]

Upon considering the potential applications of block copolymers, one limitation arises, however, from the lack of control over *bulk thermodynamics* and, more particularly, the temperature of order/disorder transitions in these materials. From an applications standpoint, the strong thermodynamic incompatibility typically found for block copolymers is highly advantageous, as it results in remarkably stable solid-like microphase separated morphologies. However, for melt processing where flow is essential, the ability to access the segmentally mixed liquid state is clearly desirable.[4,8] Therefore, being able to fine tune the degree of thermodynamic compatibility between

13

the various blocks of a block copolymer would not only lead to better control over the particular morphologies that are formed upon self-assembly, but also improve the processibility of these materials. In an attempt to address this need, and perhaps design new block copolymers with tunable levels of interactions, this thesis focused on understanding the structure/property relationship between monomer architecture and phase behavior of weakly interacting block copolymer melts.

Since they are central themes to the present thesis, the phase behavior and thermodynamic compatibility of diblock copolymers as a function of temperature and pressure are reviewed in the next three sections. The two types of ordering transitions most commonly encountered in diblock copolymers, namely the upper disorder-to-order and lower disorder-to-order transitions, denoted **UDOT** and **LDOT**[22-24], are presented in section I.2 and I.3 respectively, along with some of the existing theories aimed at reproducing and/or predicting these phase behaviors. The effect of pressure on these two types of transitions is discussed separately in section I.4. Finally, section I.5 presents the main premise of this thesis, namely, that block copolymer phase behavior and resulting rheological properties can be controlled via architectural modifications of the block segments. The approach that was chosen to demonstrate this postulate is briefly presented.

I.2. UPPER DISORDER-TO-ORDER TRANSITION (UDOT)

I.2.1. UDOT-type phase diagram

It is well known that most pairs of dissimilar high molecular weight polymers are immiscible. This results from the very limited role played by combinatorial entropy in macromolecular systems, which, combined with the mostly weak dispersive nature of intermolecular interactions in organic materials, typically leads to strong thermodynamic incompatibility. Hence, in most instances, the segmentally mixed (disordered) state of a block copolymer (phase mixed state of a polymer blend) is only observed for very low molecular weights at high enough temperatures such that the entropy gain upon mixing outweighs the unfavorable enthalpic interactions between the two components. In practice, however, segmental mixing is preferably achieved by the addition of a common solvent such that the unfavorable enthalpic interactions are sufficiently weakened.

The temperature above which two incompatible homopolymers are phase mixed is referred to as the upper critical solution transition (UCST).[25] The analogous thermodynamic transition in block copolymers consisting of two incompatible blocks is called the upper disorder-to-order transition, denoted UDOT. Figure I.2 gives a schematic representation of the UDOT-type phase diagram. Model UDOT-type systems which have been extensively studied experimentally include: polystyrene-*block*-polyisoprene (PS-*b*-PI)[4,26-28], polyethylene-*block*-polyethylethylene (PE-*b*-PEE) and other polyolefin based block copolymers[29-31] and polystyrene-*block*-poly methyl methacrylate (PS-*b*-PMMA)[32-35]. Typical UDOT temperatures for 50/50 (symmetric) block copolymers

of these systems are summarized in Table I.1. As can be seen, this transition lies within an experimentally accessible temperature range only for very low molecular weights. For larger molecular weights of commercial relevance (50 to 100,000 g/mol), the UDOT lies above the degradation temperature of the copolymer, and segmental mixing can only be achieved by the addition of a common solvent.

TABLE I. 1: TRANSITION TEMPERATURES OF UDOT BCP'S

A-B Copolymer	M_n (10^3 g/mol)	wt% A	T_{UDOT}
PS-b-PI	18	50	120^{27}
	14	40	70^{26}
PE-b-PEE	27.5	50	136^{31}
PS-b-PMMA	29.7	50	157^{34}
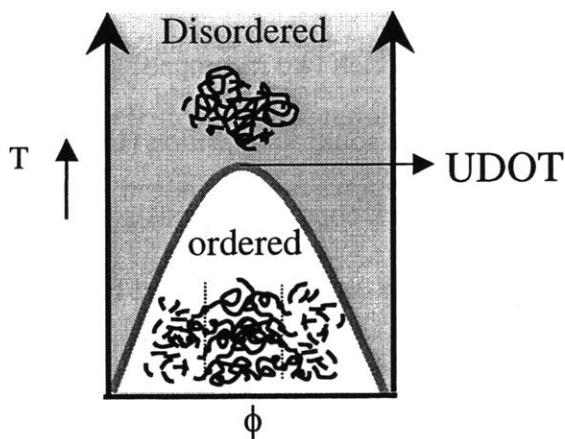
Figure I.2: UDOT-type Phase Diagram

I.2.2. Thermodynamic treatments of the UDOT

I.2.2.a. The Flory-Huggins incompressible regular solution model.

The thermodynamics of the upper critical transition in polymer blends (UCST) was first analyzed independently by Flory[36,37] and Huggins[38] who developed, within a rigid lattice framework, the following regular solution model for the molar free energy of mixing two chemically distinct homopolymers A and B (per mole of lattice sites):

$$\Delta G / RT = \frac{\phi_A}{N_A} \ln \phi_A + \frac{\phi_B}{N_B} \ln \phi_B + \phi_A \phi_B \chi^{FH} \qquad (I.1)$$

where ϕ_i is the volume fraction and N_i the number of lattice sites of fixed size occupied by molecules i and χ^{FH} is the so-called Flory-Huggins interaction parameter. The first two terms represent the entropy of mixing species A and B on the same lattice, while the last term represents the usually unfavorable enthalpic contribution. χ^{FH} is related to the excess exchange interaction energy $\Delta \varepsilon$ according to equation I.2:

$$\chi^{FH} = z \left[\varepsilon_{AB} - \frac{\varepsilon_{AA} + \varepsilon_{BB}}{2} \right] / RT = z \Delta \varepsilon / RT \qquad (I.2)$$

where z is the lattice coordination number and ε_{ij} is the molar attractive (-) nearest neighbor van der Waals interaction energy between segments i and j (J/mol). The Flory-Huggins theory is a mean field formalism that assumes the system to be *incompressible* and hence ignores non-zero changes in volume upon mixing. It further assumes that the same lattice can be used to describe the configurations of both the pure components and

the mixture, which requires that the geometry of the two molecular species be virtually identical. Finally, it defines χ as being inversely proportional to temperature and independent of composition, molecular weight, chain architecture and pressure.

From the free energy expression given in equation I.1, the spinodal condition for phase separation can be derived. For a binary mixture of homopolymers A and B, the Flory-Huggins theory predicts that the system will phase separate at a critical value of the product of χ and the degree of polymerization, N, of $\chi N = 2$ when $N_A = N_B = N$. Leibler[39] was the first to predict that a simple 50:50 diblock copolymer containing $N_{tot}=2N$ monomer units, N of each type, has a larger critical χ value: $\chi(2N)\cong 10.495$ or $\chi N=5.25$. Alternatively, one can approximate quite simply this critical value for the order/disorder transition in a symmetric block copolymer by equating the free energy of the disordered state to that of the ordered state:[6]

$$G_{\text{disordered}} = G_{\text{ordered}} \text{ at the UDOT}$$

In the disordered state where the A and B segments are intimately mixed, the free energy per chain can be approximated by the A-B contact energy alone:

$$G_{disordered} / kT \approx \chi f_A f_B N_{tot} = \frac{\chi N_{tot}}{4} \tag{I.3}$$

where N_{tot} is the total number of segments or monomer units in the block copolymer chain ($2N$) and f_i is the fraction of each monomer type, which is 0.5 for a symmetric diblock copolymer.

The free energy per chain in the ordered, lamellar phase for a symmetric block copolymer is, on the other hand, given by the sum of an elastic (stretching) energy term and an interaction term:

$$G_{ordered} / kT = G_{el} / kT + G_{int} / kT = \frac{3}{2}\left(\frac{(D/2)^2}{\langle R^2 \rangle_o}\right) + (\frac{\gamma_{AB}}{kT})\Sigma \qquad (I.4)$$

where D is the equilibrium lamellar period, $<R_2>_o$ is the unperturbed radius of gyration of

a gaussian coil, which is equal to $N_{tot}a^2$ where a is the statistical length of a segment,

γ_{AB}/kT is the interfacial tension between the two blocks (in units of kT) and Σ is the

interfacial area per chain between A and B microdomains. The first term on the right

hand side of equation I.4 represents the entropic cost for stretching the copolymer blocks

away from their junction points upon the formation of the lamellar phase. This entropic

penalty leads to an elastic (Hookian) force which is proportional to the ratio of the

extended chain dimensions (equal to $D/2$) to the unperturbed coil dimensions $<R^2>_o$. The

second term of equation I.4 represents the interaction free energy which, in the ordered

state, is confined to the narrow interfacial region between the A and B microdomains.

According to the classical theory of polymer interfaces[169], the interfacial tension γ_{AB}

between two polymers can be related to the interaction parameter χ by the following

expression:

$$\gamma_{AB} / kT = \frac{1}{a^2}\sqrt{\frac{\chi}{6}} \qquad (I.5)$$

while the volume filling constraint of the lamellar microdomains leads to the following

expression for Σ:

$$\Sigma = \frac{N_{tot}a^3}{D/2} \qquad (I.6)$$

Upon inserting equation I.5 and I.6 into equation I.4 and minimizing with respect to the

lamellar period D, one obtains the following expressions for the equilibrium lamellar

period and the free energy in the ordered (lamellar) state:

19

$$D \approx 1.03a\chi^{1/6}N_{tot}^{2/3} \qquad (I.7)$$

and

$$G_{ordered} \approx 1.19(\chi N_{tot})^{1/3} \qquad (I.8)$$

By equating this expression for the lamellar free energy to the free energy in the disordered state (equation I.3), an estimate of the location of the order/disorder transition can be obtained, yielding $\chi N_{tot} = 10.4$, which is remarkably close to the value of 10.495 predicted by Leibler.

Since χ is inversely proportional to temperature, this higher critical χ value for block copolymers implies that microphase separation in these systems is more difficult than macrophase separation in the analogous homopolymer mixtures. Hence, chemically joining two homopolymers of the same size to form a diblock copolymer reduces the transition temperature by a factor of ~ 2.6. Following a similar type of reasoning, a yet more favorable critical χ value is obtained for A-B-A triblock copolymers.

Based on the considerations presented above, it appears that the phase behavior of UDOT/UCST-type block copolymers or polymer blends is dictated by a single parameter: χ, or equivalently, ε_{AB}. Attempts have been made to predict χ from homopolymer properties, without requiring the fitting of any experimental data on the phase behavior of a given polymer pair. This, however, necessitates an assumption regarding the type of mixing rules that prevail in the segmentally mixed system. The well-known Berthelot's mixing rule has been typically used.[40] It is a regular solution model that assumes ε_{AB}, the cross interaction energy, to be the geometric average of the pure component interaction energies ε_{AA} and ε_{BB}:

$$\varepsilon_{AB} = \sqrt{\varepsilon_{AA}\varepsilon_{BB}} \qquad\qquad (I.9)$$

Therefore, the sole knowledge of ε_{AA} and ε_{BB} is sufficient to predict the mixture

properties. These two parameters are in turn related to the experimental Hildebrand

solubility parameter δ, which is the square root of the cohesive energy density and has

units of ($J^{1/2}cm^{-3/2}$). According to the regular solution theory[40], χ is related to the

individual component solubility parameters through:

$$\chi = \frac{v}{RT}(\delta_A - \delta_B)^2 \qquad\qquad (I.10)$$

where v is the average segmental molar volume $(v_A v_B)^{1/2}$. The assumptions underlying

equations I.1 and I.10 are (1) no volume changes on mixing, (2) ideal entropy of mixing,

(3) weak forces of the induced dipole type (dispersive interactions), and (4) Berthelot's

rule for the cross interaction energy (equation I.9). Such a formalism implies χ is always

positive, and miscibility only occurs when the solubility parameters of the individual

components are of similar magnitude. The weakness of this treatment is twofold.

Firstly, because direct measurements of cohesive energies and solubility

parameters are intractable for macromolecules, δ must be determined indirectly. This

explains the large disparity in experimental values of δ obtained by different authors.[41]

The use of group contribution methods,[42] which evaluate homopolymer properties based

on the contribution of each chemical group present in the repeat unit, circumvents the

problem of experimental evaluation of δ. The basic assumption of such calculations is

that the contribution of a given chemical group, such as a methyl (CH_3) group, is

independent of its chemical and structural environment. Several databases of group

contributions have been built, using PVT data for homopolymers or small molecule

analogues. Different formalisms for the evaluation of δ have been proposed by several authors[42], some of whom include contributions not only from dispersive van der Waals interactions, but also dipole/dipole and hydrogen bonding interactions. For example, Van Krevelen proposed a three component cohesive energy density:

$$\delta^2 = \delta_d{}^2 + \delta_p^2 + \delta_H^2 \qquad\qquad (I.11)$$

Although such calculations permit the evaluation of δ for any given chemistry, the second weakness of Berthelot's mixing rule still remains, namely that deviations from a geometric average for the cross interaction energy have been reported for several polymer mixtures and solutions.[43,44] Such deviations result in what is referred to as irregular mixing. Equation I.9 has therefore been only moderately successful in reproducing experimental data and accurately predicting phase behavior of new block copolymers or homopolymer blends. Nevertheless, the solubility parameter approach has been widely used as a rule of thumb when considering potentially miscible polymer pairs. A small difference in the solubility parameters of two homopolymers has indeed been shown to correlate with thermodynamic compatibility.[45-47] Intuitively, if two polymers A and B have solubility parameters of the same magnitude, it indicates that the degree of cohesion and hence the strength of A-A and B-B segmental interactions are comparable. In the absence of a strong specific interaction such as H-bonding between the two unlike segments, this makes mixing of segments A and B more favorable than in the case where ε_{AA} and ε_{BB} strongly differ.

I.2.2.b. The IRPA and effective χ parameters.

Owing to the very limited success of equations I.9 and I.10 in accurately predicting χ values, different techniques that allow direct measurement of the phase behavior of block copolymers and polymer blends have been investigated. Typically, χ has been extracted from small angle neutron scattering (SANS) experiments using the incompressible random phase approximation (IRPA) initially developed by de Gennes[48] for polymer blends, and modified for block copolymers by Leibler.[39] Within the RPA formalism, a relation can be established between the intensity scattered by a given mixture or block copolymer, and the strength of thermodynamic fluctuations, which imply the phase behavior of the system. The scattering function for diblock copolymers, which will be described in chapter II along with the details of SANS, consists of the scattering function for ideal noninteracting Gaussian diblock chains and an interaction term which accounts for the interactions among different segment types. When the Flory-Huggins model is used to express the interaction term, the IRPA is obtained. The effective χ values extracted as a function of temperature from SANS data using the IRPA are typically fit to a linear form:

$$\chi = A + B/T \tag{I.12}$$

where B is the purely enthalpic term related to $\Delta\varepsilon$, and the constant term A is given an entropic origin.[32,49,50]

The effective χ parameters extracted in this fashion from SANS data have been shown to violate several assumptions of the incompressible mean-field Flory-Huggins theory. Firstly, χ values are often composition dependent and χ for diblock copolymers

23

can differ from the value obtained for mixtures.[51,52] Secondly, pressure has been shown to

affect thermodynamic compatibility of UDOT-type block copolymers and mixtures,

despite their limited compressibility. These effects will be presented in section I.4.

Thirdly, and perhaps most importantly, expression I.1 fails to predict phase separation

upon heating, which has been systematically observed for miscible or marginally

miscible polymer mixtures and diblock copolymers, and will be presented in the next

section. The wide body of experimental data on extracted χ values thus points to some

serious shortcomings of the Flory-Huggins incompressible mean-field free energy

expression. In fact, a systematic study of the effect of local structure on thermodynamic

compatibility in blends and block copolymers consisting entirely of polyolefins has

shown that, even for these very simple systems, the effective χ parameter displays a

complex, and not necessarily predictable, dependence on the local structure of the

individual components.[46,53-61] These experimental findings on polyolefins have lead to the

development of several on-lattice and off-lattice theories and numerical simulations

aimed at understanding the molecular factors controlling the phase behavior of polymer

blends and block copolymers. Lattice-based analytical treatments include the lattice

cluster theory (LCT), developed by Freed and coworkers,[62-65] which is a modification of

the Flory-Huggins free energy expression that accounts for compressibility and local

monomer structure. In the standard lattice model of block copolymers and mixtures, the

different monomer types are assumed to fit into the same lattice site, and hence, have

essentially the same volume. In the more generalized lattice model of the LCT, however,

monomers are allowed to have specified molecular structures that can cover several

neighboring lattice sites. Moreover, free volume and compressibility are accounted for

by the introduction of empty lattice sites. Earlier, Sanchez and Lacombe developed a free energy expression for compressible multicomponent systems based on their Lattice-Fluid equation of state.[44,66] This treatment will be described in the next section, since special emphasis was given by the authors to its ability to predict (micro)phase separation upon heating. Another analytical treatment was proposed by Fredrickson, Liu and Bates[67] who argued that local structure asymmetries result in an entropic frustration in the segmentally mixed state. Using a field theory, these authors computed purely entropic corrections to the Flory-Huggins theory for athermal (non-interacting) systems characterized by structural asymmetry. On-lattice and off-lattice numerical calculations, on the other hand, include the Monte-Carlo simulations carried out by Yethiraj et al[68] and Müller[69], the numerical studies of Curro[70] and Schweizer et $al.$[71-73], based on the polymer reference interaction site model (PRISM) theory, and the molecular dynamics simulations of Maranas et $al.$[74,75] A common evidence emerging from all these treatments is that structural asymmetry, which can arise from differences in monomer shape, size, degree of side group branching or backbone persistence length (i.e. chain stiffness), strongly influences local packing, thereby resulting in both *enthalpic* and entropic excess contributions to the free energy of mixing. Deviations from regular mixing (equation I.3-I.4) favorable or unfavorable to miscibility will ensue, depending on whether the effect of conformational and interaction asymmetries tend to reinforce or compensate each other. However, it is important to note that such systematic studies of the dependence of χ on local monomer structure have been carried out only for polyolefin model systems. The energetics of these systems are expected to be much simpler than for chemically distinct

homopolymers, where asymmetries in both bare interaction energies (ε_{ij}'s) *and* local

structure (monomer size, chain stiffness etc.) are expected.

I.3. LOWER DISORDER-TO-ORDER TRANSITION (LDOT)

I.3.1. LDOT-type phase diagrams

Perhaps one of the most important shortcomings of the incompressible Flory-

Huggins theory is its inability to predict (micro)phase separation upon heating. Indeed,

in a departure from the classical UDOT behavior presented above, diblock copolymers of

styrene and n-butyl methacrylate, denoted here PS-*b*-PBMA, have been shown to be

miscible in some temperature range for intermediate molecular weights and undergo a

transition from the disordered to the ordered state upon heating.[22,76] This thermodynamic

transition, referred to as the lower disorder-to-order transition (LDOT), is analogous to

the lower critical solution transition (LCST) observed in most compatible polymer

mixtures[77] and solutions.[44,78] Figure I.3 illustrates the LDOT-type phase diagram, as well

as the lens-shaped phase diagram resulting from the simultaneous appearance of a UDOT

and a LDOT. Very few systems, PS-*b*-PBMA being one, have been found to exhibit the

latter kind of phase behavior in an experimentally accessible temperature range. A

schematic representation of the phase diagram obtained experimentally for PS-*b*-PBMA

is given in Figure I.4, along with the observed transition temperatures for 50/50

(symmetric) compositions.[22,76] Unfortunately, the UDOT region of this phase diagram is

difficult to investigate due to its proximity to the glass transition temperature T_g of the

copolymer.

(a)   (b)
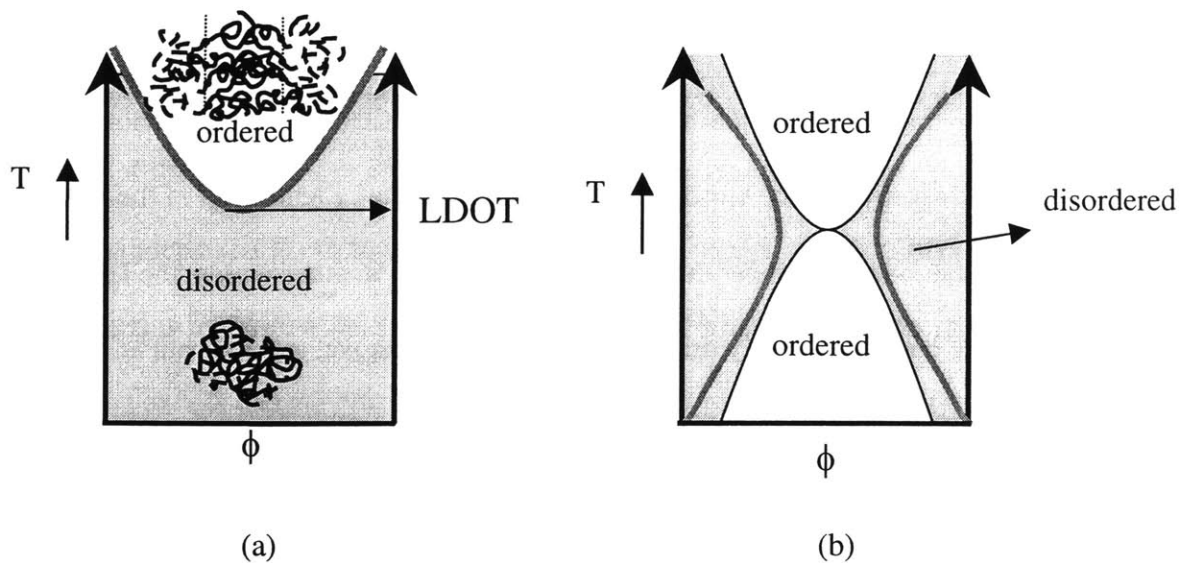
Figure I.3: LDOT (a) and lens-shaped (b) phase diagrams
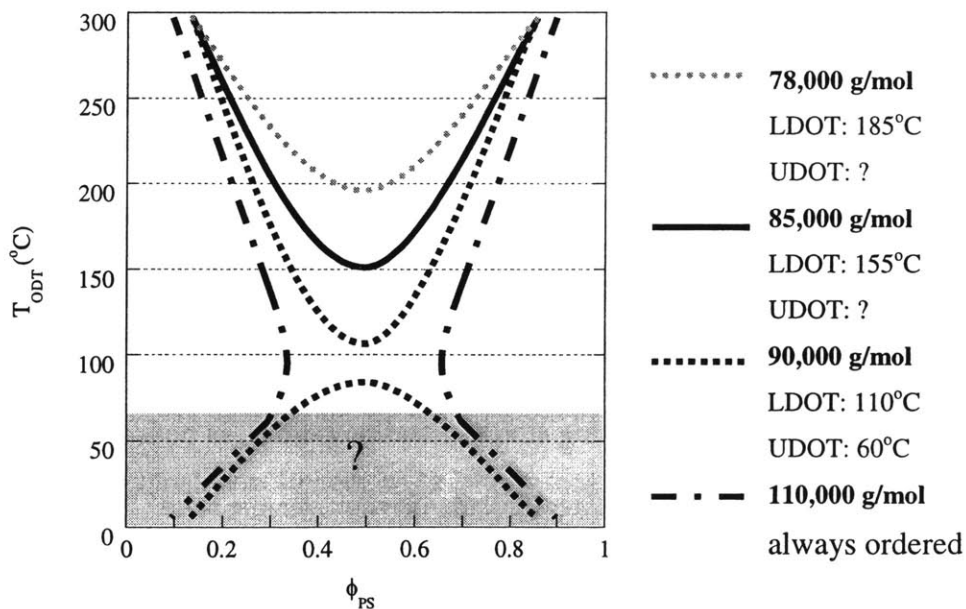
Figure I.4: Schematic phase diagram for PS-*b*-PBMA

27

I.3.2. Thermodynamic treatments of the LDOT

A straightforward thermodynamic analysis of LDOT phase behavior shows that both the enthalpy and the entropy changes upon ordering (demixing) of the block segments at elevated temperatures must be positive.[79] In other words, the LDOT, in contrast to the enthalpically driven UDOT discussed above, results from an increase in entropy, or an increase in the number of configurations available to the system, at high temperatures in the ordered state compared to the disordered state.[79] Empirically, microphase separation upon heating is always accompanied by a positive change in volume, which explains the systematic pressure dependence reported for this transition.[80-82] High pressures favor the denser segmentally mixed state, thereby raising the ordering temperature. The effect of pressure on the LDOT, which will be presented in more detail in section I.4, has important implications from an engineering standpoint. Small angle neutron scattering studies on PS-*b*-PBMA under hydrostatic pressure reveal that the LDOT can increase by as much as 147°C per kbar.[82] Pressure has an equally profound effect on the rheological properties of this material, enhancing flow by forcing segmental miscibility. From a processing viewpoint, such "baroplastic" behavior could offer increased flexibility in controlling structure and properties, as both temperature and pressure might equally be used to affect the thermodynamic state.

The compressible nature of systems that exhibit phase separation upon heating has led to the development of several theoretical treatments aimed at predicting such transitions and understanding their molecular origin. Typically, equation of state (EOS)

effects are incorporated into the classic free energy balance of two component systems to account for compressibility and non-zero volume changes upon mixing. One popular approach consists in treating a binary mixture of components A and B as a three component system, the third component being holes, or free volume. The main consequence of the introduction of holes into the system is that the free energy expression now depends independently on the three interaction energies ε_{ij}'s, which is in contrast to the Flory-Huggins incompressible regular solution model, where the free energy only depends on the excess thermodynamic quantity $\Delta\varepsilon$ (excess exchange interaction energy).[65] Such dependence on pure component interaction energies in compressible formalisms results from the difference in energetic costs for breaking A-A, B-B and A-B contacts upon the introduction of a vacancy. The knowledge of equation of state properties of the individual components and the mixture is thus necessary and, in fact, might be sufficient, to understand thermodynamic compatibility in compressible systems.

I.3.2.a. Equation of state (EOS) theories

Several equations of state have been developed which express the equilibrium density for homopolymers and mixtures at a given pressure and temperature.[83] These thermodynamic treatments have all shown that phase separation and ordering upon heating in blends and block copolymers, respectively, can be related to dissimilarities in the equation of state properties of the pure components. The first equation of state presented for chain molecules was the general corresponding states theory of Prigogine and collaborators.[84] It is a cell model theory, assuming a hard sphere repulsive potential.

Flory et al.[85,86] later presented a modified version of this theory, replacing the generalized

Lennard-Jones potential by a van der Waals type potential. Patterson[87] derived a simpler

EOS theory which is formally identical to the Flory-Huggins theory, except that the

interaction parameter χ also contains equation of state contributions. Sanchez and

Lacombe[44,66,79] developed the lattice-fluid (LF) equation of state which is also formally

similar to the Flory-Huggins theory, except that a free-volume term is accounted for via

the introduction of vacant sites on the lattice. This equation of state is described in more

detail since it was used in this work to calculate PVT behavior for the corresponding

homopolymers of the diblock copolymers investigated.

As is the case for most equation of state theories, the LF theory requires the

knowledge of three equation of state parameters for each pure component. It is founded

on a lattice model description of the fluid and a mean-field (random mixing)

approximation is used to determine the number of configurations available to a system of

N_o vacant sites or holes and N molecules, each of which occupy r lattice sites. The

chemical potential of the mixture, μ, is given by:

$$\mu = rN\varepsilon^*\left[-\tilde{\rho} + \tilde{P}\tilde{v} + \tilde{T}\tilde{v}\{(1-\tilde{\rho})\ln(1-\tilde{\rho}) + \frac{\tilde{\rho}}{r}\ln(\tilde{\rho})\}\right] \qquad (I.13)$$

where $\tilde{P}$, $\tilde{T}$, $\tilde{v}$ and $\tilde{\rho}$ are the reduced pressure, temperature, specific volume and

density defined as:

$$\tilde{P} \equiv P/P^* \qquad (I.14)$$

$$\tilde{T} \equiv T/T^*, \ T^* = \varepsilon^*/k = P^*v^*/k \qquad (I.15)$$

$$\tilde{v} \equiv 1/\tilde{\rho}, \ \tilde{\rho} \equiv \rho/\rho^* \qquad (I.16)$$

where k is the Boltzman's constant, and P, T and ρ are the system pressure, absolute temperature and density, respectively. The parameters with an asterisk represent the close-packed *equation of state parameters* of the pure component or mixture: ε^* is the interaction per mer, v^* is the close-packed mer volume, ρ^* is the close-packed density and P^* the internal pressure related to the mer interaction energy by equation I.15. The knowledge of the three parameters P^*, ρ^* and T^* is sufficient to fully describe a given homopolymer. The equation of state is derived from the condition of minimal chemical potential at equilibrium:

$$\tilde{\rho}^2 + \tilde{P} + \tilde{T}[\ln(1 - \tilde{\rho}) + (1 - \frac{1}{r})\tilde{\rho}] = 0 \tag{I.17.a}$$

In the long chain limit (large r), this expression can be simplified to:

$$\tilde{\rho}^2 + \tilde{P} + \tilde{T}[\ln(1 - \tilde{\rho}) + \tilde{\rho}] = 0 \tag{I.17.b}$$

Solving for equation I.17.a or b for a given pressure and temperature yields the equilibrium density and fractional free volume of pure components or mixtures. Such predictions of homopolymer densities have been shown to accurately reproduce experimental PVT data.[83]

Typically, the equation of state parameters P^*, ρ^* and T^* are extracted from PVT data using a least-squares fitting procedure over extended ranges of pressure and temperature. Alternatively, Boudouris *et al.*[88] recently reported a very attractive procedure for evaluating these parameters using group contribution methods. Their analysis uses a pre-established database of constant contributions to P^*, ρ^* and T^* for the most commonly encountered chemical groups in commercial polymers. This combination of group contribution methods with an equation of state model offers the

highly valuable opportunity to predict PVT behavior for polymeric systems without requiring any experimental data.

When equation I.17 is used to model thermodynamic properties of multicomponent systems, "combining" or "mixing rules" need to be adopted. Such rules, though often quite arbitrary, are required in all statistical mechanical theories of mixtures and relate the mixture parameters to those of the pure components. For example, Sanchez and Lacombe propose the following mixing rules for $P*$ and $\rho*$ of polymer mixtures:

- $P* = \phi_A P_A^* + \phi_B P_B^* - \phi_A \phi_B \Delta P *$ (I.18.a)

  with $\Delta P* = P_A^* + P_B^* - 2P_{AB}^*$ (I.18.b)

  and $\phi_A = \dfrac{m_A / \rho_A^*}{m_A / \rho_A^* + m_B / \rho_B^*}$ (I.18.c)

- $1/\rho^* = m_A / \rho_A^* + m_B / \rho_B^*$ (I.18.d)

where ϕ_i is the close-packed volume fraction and m_i the mass fraction of component i and $P_{AB}^* = \varepsilon_{AB}^* / v^* = kT_{AB}^* / v^*$. The only unknown parameter of the LF model is the cross interaction parameter P_{AB}^*, or, equivalently, ε_{AB}^*.

I.3.2.b. Compressible random phase approximation (CRPA)

Different equations of state have been used in combination with the random phase approximation (RPA) to extract intersegmental interaction energies ε_{AB} from SANS data and predict phase diagrams for polymer blends[89-91] and diblock copolymers[23,24,92] known to exhibit the LCST/LDOT.

Immediately following the discovery of the LDOT in PS-*b*-PBMA, Yeung *et al.*[23] presented a theoretical justification for this observation based on a combination of the LF equation of state and the random phase approximation. They modeled the compressible system by treating the free volume as small solvent molecules in an incompressible polymer/solvent system and hence used a formalism identical to the theory of block copolymer solutions. Upon doing so, they showed that the two main corrections to χ arising from the introduction of compressibility into the system are: **(1)** a dilution of the effective interactions due to the presence of unoccupied sites and **(2)** an equation of state term which is always positive and destabilizes the segmentally mixed state as temperature increases. Although the authors did not present any quantitative comparison between their predictions and experimental data on PS-*b*-PBMA, they qualitatively showed that both UDOT and LDOT behaviors can be predicted by a compressible RPA formalism. The relative positioning of the two transitions depends on the magnitude of the bare interaction parameter χ, the total molecular weight and the disparity in equation of state parameters of the pure components.

Freed and coworkers[89] had previously developed a similar compressible RPA formalism for blends and block copolymers and applied it to the styrene/vinyl methyl ether system, another system known to phase separate upon heating.[90,92] Shortly after the publications of Freed and coworkers, Sanchez *et al*[91] developed another compressible RPA formalism for polymer blends based on their LF equation of state and the compressible RPA developed by Ackasu *et al.* for scattering from multicomponent polymer blends.

Recently, Hino and Prausnitz[24] reported a compressible RPA similar to that of

Yeung *et al.*, except that they used a more recent continuous space (non-lattice based)

equation of state and further presented a rigorous comparison between theory and

experiments. The authors quantitatively applied their theory to PS-*b*-PBMA and

extracted a cross interaction energy ε_{AB} for this system by fitting their compressible RPA

to the reported experimental coexistence curves for both blends[93] and block

copolymers.[22,76] They found a deviation from the regular (Berthelot's) mixing rule of κ_{AB}

=0.00782, namely:

$$\varepsilon_{AB} = (1 - \kappa_{AB})\sqrt{\varepsilon_{AA}\varepsilon_{BB}} = 0.99218\sqrt{\varepsilon_{AA}\varepsilon_{BB}} \tag{I.19}$$

For this particular value, they were able to quantitatively reproduce the phase behavior of

PS/PBMA blends and block copolymers and further predicted a strong pressure

coefficient of about $200^{\circ}C/kbar$ for the LDOT of this system. However, the authors also

showed that, as is the case for all equation of state theories, the predicted phase diagram

is highly sensitive to the exact value of κ_{AB} used.

The weakness of the compressible theoretical treatments briefly presented here is

threefold. Firstly, they remain very involved, especially when applied to diblock

copolymers. Secondly, they rely heavily on the knowledge of an extremely sensitive

parameter, namely, ε_{AB}, which must be determined experimentally. So far, their use as a

simple predictive tool has therefore been at best very limited. Finally, although they have

helped in some way understanding the thermodynamics of entropically-driven phase

separation, a clear physical and quantitative understanding of the molecular-level factors

that govern the LDOT is still lacking .

I.3.2.c. A tentative molecular explanation of the LDOT

Typically, systems exhibiting the LDOT/LCST have been categorized either as those with strong specific interactions (e.g., hydrogen bonding, strong dipole/dipole or electron donor/electron acceptor interactions), or more weakly interacting systems with molecular packing differences (EOS effects). In both cases, it has been argued that the denser nature of the disordered (phase mixed) state equates to a loss of molecular configurations compared to the ordered (phase separated) state, which drives the LDOT(LCST).[79] For strongly interacting systems such as PMMA/PVDF[94,95] and, to a lesser extent, PS/PVME[96-102] and PS/poly(2,6-dimethyl phenylene oxide) (PS/PPO)[103,104], the loss of configurations is thought to arise from the preferred orientation of the interacting chemical groups. For weakly interacting systems, on the other hand, molecular packing differences (EOS effects) lead to differences in free volume of the pure components that are reflected in their densities and thermal expansion coefficients. These disparities result in an enthalpically favorable and entropically unfavorable densification, or reduction in free volume, of the segmentally mixed state.[105] PS/PBMA is thought to fall into the latter category, since both upper and lower critical temperatures have been found for diblock copolymers and low molecular weight blends of this polymer pair. Indeed, the presence of the UDOT precludes the possibility of strong specific interactions between styrene and butyl methacrylate segments. Clearly, there remain important questions concerning the molecular origin of the LDOT in such weakly interacting systems. Of special importance is the lack of experimental facts that would greatly help to further elucidate the mechanism of this transition.

I.4. PRESSURE DEPENDENCE OF ORDERING TRANSITIONS

As discussed above, equation of state (EOS) theories predict non-zero volume changes on mixing and, therefore, the effect of pressure on miscibility for polymer mixtures and diblock copolymers. While the phase behavior of block copolymers as a function of temperature has been extensively studied and was reviewed by Bates and Fredrickson,[3,4] the effect of pressure has remained relatively unexplored. For diblock copolymers exhibiting UDOT behavior, the incompressible random phase approximation is usually employed to extract the Flory-Huggins χ parameter, although the few reported pressure studies clearly show an effect of pressure on polymer compatibility, even for this enthalpically driven phase transition.[106-110] Experimental variation of pressure hence offers the opportunity to further understand the molecular origin of phase behavior and access thermodynamic quantities, such as the packing efficiency of two polymer chains consisting of dissimilar segment types, which are not available through variation of temperature only. Given the phenomenological relation between local structure, packing, and thermodynamic compatibility described in the previous sections, such information should indeed shed additional light onto the mechanisms responsible for the specific phase behavior of a given polymer pair.

The phase behavior of a polymer blend under pressure is governed by the sign of the excess volume change on mixing and the type of transition. This is evident upon considering the general thermodynamic relation between pressure and transition temperature along a spinodal:[79]

$$\left.\frac{\delta T_s}{\delta P}\right|_x = \frac{v_{xx}}{s_{xx}} = \frac{T_s v_{xx}}{h_{xx}}$$ (I.20)

where T_s is the spinodal temperature, P is pressure, x is a composition variable, and v_{xx}, s_{xx} and h_{xx} are the second derivatives with respect to composition of the intensive system volume, entropy and enthalpy, respectively. Alternatively, the well known Clausius-Clapeyron equation can equally be used:[79,111]

$$\left.\frac{dT_s}{dP}\right|_x \cong \Delta V_{mix} / \Delta S_{mix} = T_s \Delta V_{mix} / \Delta H_{mix}$$ (I.21.a)

Likewise, for a block copolymer undergoing an order/disorder transition, the following expression relates the pressure coefficient of the transition to the change in system enthalpy, entropy and volume upon disordering (segmental mixing):

$$\left.\frac{dT_{dis}}{dP}\right|_x \cong \Delta V_{dis} / \Delta S_{dis} = T_{dis} \Delta V_{dis} / \Delta H_{dis}$$ (I.21.b)

I.4.1. Effect of pressure on the UDOT

For the enthalpically driven UDOT, the system enthalpy and entropy increase upon disordering ($\Delta S_{dis} > 0$, $\Delta H_{dis} > 0$) and the sign of dT_{UDOT}/dP is thus governed by the sign of ΔV_{dis}. From equation I.14, it follows that an increase in the transition temperature will be observed under applied pressure if $\Delta V_{dis} > 0$ since pressure tends to favor the more dense microphase separated (ordered) state. For a system with $\Delta V_{dis} < 0$, i.e. wherein segmental mixing is accompanied by volume contraction, high pressures favor the more dense segmentally mixed state and lower the transition temperature. These considerations are summarized on the phase diagrams of Figure I.5.a and b.

37

$\Delta V_{dis} < 0$ $\Delta V_{dis} > 0$

(a)   (b)
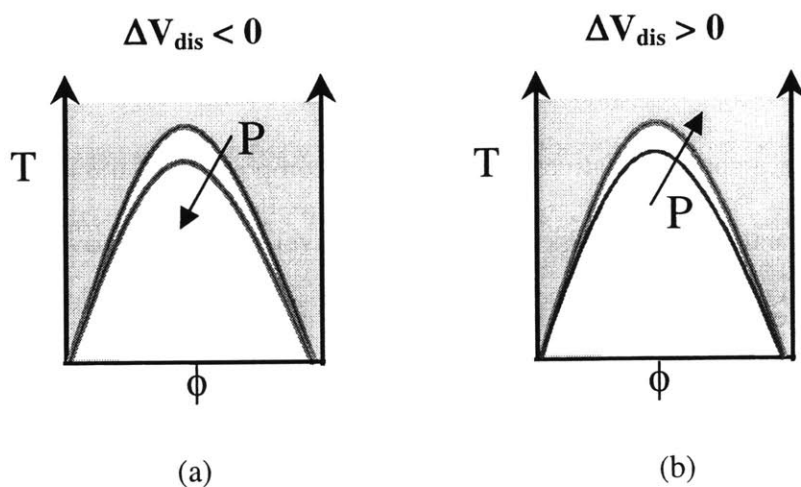
Figure I.5: Effect of Pressure on the UDOT

A few experimental studies of the pressure dependence of the UDOT have been recently reported. Hajduk et al.[106,107] studied diblock copolymers of polystyrene and polyisoprene and found that the UDOT increased with increasing pressure by about 20°C/kbar. They further measured an excess fractional change in volume upon disordering $\Delta V_{dis}/V$ of about $5*10^{-4}$ (0.05 %) for this material. Stühn and coworkers[112,113] studied the same system and reported a similar pressure coefficient of 19°C/kbar at high pressure. Schwann and coworkers[109] studied the effect of pressure on block copolymers of poly(ethylenepropylene) and polydimethylsiloxane and observed a change in sign for the pressure coefficient as a function of pressure. For pressures lower than ~0.5 kbar, they report a negative pressure coefficient of about 10 to 20°C/kbar, while at higher pressures (> 1 kbar), a positive coefficient of similar magnitude is found. Finally, Frielinghaus et al.[110] reported a negative pressure coefficient of ~ -20°C/kbar over the entire experimental pressure range for diblock copolymers of poly(ethylene propylene) and poly(ethyl ethylene).

Such complex dependence of the UDOT on pressure can be ascribed to two competing effects. Predominantly, application of pressure decreases the free volume, thereby concentrating net repulsive segmental contacts and reducing block miscibility for these incompatible systems. However, if the system exhibits a small negative change in volume upon disordering, then the application of pressure might first enhance miscibility by favoring the more dense segmentally mixed state.

I.4.2. Effect of pressure on the LDOT

In contrast to the UDOT, the system volume always decreases upon disordering for the entropically driven LDOT (ΔV_{dis} always < 0). Hence, dT_{LDOT}/dP is always positive.[79] The effect of pressure on the LDOT is illustrated in Figure I.6.
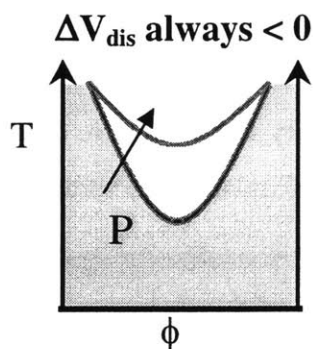
Figure I.6: Effect of Pressure

on the LDOT

A few theoretical and experimental studies of the pressure dependence of the LDOT/LCST have been recently reported. Janssen and coworkers[80] reported a pressure coefficient of ~12°C/kbar for blends of PS and PVME close to the critical composition, while Hammouda and Bauer[81] observed shifts of ~20-25°C/kbar for asymmetric mixtures of the same homopolymers. These results are in good qualitative agreement with the

predictions of Dudowicz and Freed.[52] Hammouda and Bauer also investigated pressure

effects on the scattering from mixtures of polystyrene and poly n-butyl methacrylate, but

did not report the magnitude of the pressure coefficient for the LCST of this system.

Early on during this thesis, measurements were performed in collaboration with Professor

T. Russell and M. Pollard on diblock copolymers of the same components. A strong

pressure coefficient of ~ 147°C/kbar was extracted, which is about 10 times greater than

the pressure coefficients reported so far for any system.[82] The strong effect of pressure on

the LDOT of this system, which is in agreement with the predictions of Hino and

Prausnitz,[24] has important implications from an engineering standpoint. Indeed, pressure

has an equally profound effect on the rheological properties of this material, enhancing

flow by forcing segmental miscibility. From a processing viewpoint, such *"baroplastic"*

behavior could offer increased flexibility in controlling structure and properties, as

temperature and pressure might equally be used to affect the thermodynamic state. This

motivated part of the present thesis which aims at developing a deeper understanding of

the molecular origin of this strong pressure sensitivity and seeking to control its

appearance in functional diblock copolymers.

I.5. TOWARDS A BETTER CONTROL OF BCP PHASE BEHAVIOR

A direct relation between *monomer structure* and *thermodynamic compatibility*

emerges from the discussion of phase behavior in block copolymers and polymer blends

presented above. However, a systematic study of this relationship has so far only been

carried out on saturated polyolefin systems. Clearly, there remains important questions to

be answered concerning the molecular origin of phase behavior in more complex weakly interacting systems such as PS-*b*-PBMA, which exhibits both a UDOT and a LDOT. Of special importance is the lack of experimental facts that would help further elucidate the origin of such phase behavior. Moreover, the potential application of block copolymers appears to suffer from a lack of simple, engineering-oriented models that could be used as predictive tools for the design of block copolymer phase behavior. In an attempt to address these needs, and perhaps design new block copolymers with tunable levels of interactions, this thesis dissertation focused on, firstly, identifying molecular parameters that control miscibility and the type of order/disorder transition (LDOT versus UDOT) in weakly interacting block copolymers such as PS-*b*-PBMA. Secondly, a simple predictive tool was developed, which could be used to molecularly engineer the phase behavior of new systems of commercial interest. Given the phenomenological relation between block copolymer thermodynamics and their rheological properties, special emphasis was given to the molecular design of order/disorder transitions that would enhance the processibility of these materials.

To better understand the molecular origin of the strong pressure sensitivity of PS-*b*-PBMA, and perhaps identify new block copolymers with similar properties, the phase behavior of a family of diblock copolymers formed from styrene and a homologous series of n-alkyl methacrylates was investigated, both as a function of temperature and pressure. This family of materials, illustrated in Figure I.7, indeed offers the unique opportunity to understand how the systematic variation of a structural parameter (the length of the alkyl side chain of the methacrylate block) affects thermodynamic compatibility between the two blocks and, hence, the type of phase diagram (UDOT versus LDOT) and resulting

properties. For PS-*b*-PMMA, the first member of this family of materials, the classical

UDOT behavior usually found for incompatible polymer pairs is well documented.[32-35,113]

Considering the remarkably different phase behavior of PS-*b*-PBMA compared to this

system,[22] one might expect that lengthening the alkyl side chain of the methacrylate

should enhance the tendency towards LDOT behavior in this family of materials, due to

the increasing disparity in free volume between styrene and the methacrylate block. This

is based on the predictions of the theoretical treatments presented above which indicate

that the presence of the LCST/LDOT in polymer mixtures and diblock copolymers is

directly related to a mismatch in equation of state parameters of the two components.

The phase behavior of this family of block copolymers as a function of temperature and

pressure, determined through a combined use of dynamic rheological testing and small

angle neutron scattering (SANS), is presented in chapter III. In Chapter IV, an

engineering-oriented predictive tool for designing order/disorder transitions into weakly

interacting block copolymers is developed, based on existing group contribution/equation

of state calculations and the experimental results obtained for this family of PS/PnAMA

block copolymers. The success of this semi-quantitative tool at predicting the phase

behavior of new PS/PnAMA block copolymers is demonstrated. In chapter V, this

simple semi-quantitative tool is further applied to new block copolymers of commercial

relevance, namely, polystyrene-*block*-poly alkyl acrylates. These materials are highly

attractive candidate thermoplastic elastomers or adhesives which can now, for the first

time, be prepared using new controlled "living" free radical polymerization techniques

such as Atom Transfer Radical Polymerization (ATRP). The ability to control the

appearance of pressure and temperature-tunable order/disorder (solid like/liquid like)

transitions by molecular design of these systems is demonstrated for the first time.

Finally, in Chapter VI, a simplified expression for the free energy of mixing of a

compressible mixture is derived, which captures the thermodynamic trends observed in

this thesis as well as those reported in the literature for other systems. Its potential use as

a quantitative model for phase diagram prediction is discussed.

Material	n	Phase behavior
PS-b-PMMA	1	UDOT
PS-b-PBMA	4	UDOT + LDOT
others	$1 < n < 4$	?
	$n > 4$	
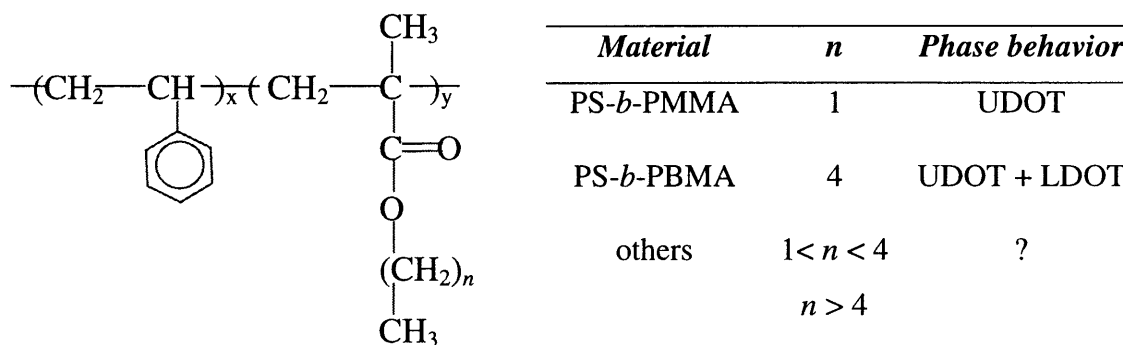
Figure I.7: Schematic representation of PS-b-PnAMA

CHAPTER II: EXPERIMENTAL METHODS

II.1. MATERIALS PREPARATION

Although the results obtained in this thesis are in principle applicable to more complex architectures, only diblock copolymers were considered for simplicity. Two synthesis techniques were employed for the preparation of diblock copolymers, namely, classical anionic polymerization and the new atom transfer radical polymerization (ATRP) recently described by Matyjaszewski et al.[21]

II.1.1. Anionic polymerization of PS-*b*-PnAMA

In order to study the effect of monomer architecture on block copolymer phase behavior in the styrene/alkyl methacrylate system, a series of nearly monodisperse, compositionally symmetric diblock copolymers of styrene and various n-alkyl methacrylates (nAMA), namely, ethyl (EMA), propyl (PMA), hexyl (HMA), octyl (OMA) and lauryl methacrylate (LMA), were synthesized anionically, using sec-butyl lithium as the initiator. Copolymers with octyl and lauryl methacrylate were prepared in the laboratories of Professor R. Jérôme at the University of Liège in Belgium, while the remaining anionic block copolymers were prepared by P. Banerjee in the research group of Professor A. M. Mayes at MIT. The following synthesis protocol was used in both cases.

All monomers were rigorously purified prior to synthesis using two distillations. MMA and EMA (Aldrich), PMA, BMA, HMA, OMA and LMA (Polyscience Inc.) and S (Aldrich) monomers were first dried and distilled over CaH_2 and subsequently stored under a nitogen atmosphere at -10°C until needed. Prior to polymerization, the methacrylate monomers were titrated with a 25 wt% tri-octyl aluminum solution (Aldrich) in hexane until a yellowish-green color developed[114] and were then distilled a second time. For styrene, the second distillation step was carried out over fluorenyllithium. The s-BuLi initiator (Aldrich, 1.3 M solution in cyclohexane) was used as received. The polymerization reaction was carried out under nitrogen in THF that had been refluxed over a freshly prepared sodium-benzophenone complex. The solvent, containing a tenfold excess of dried LiCl with respect to the required number of moles of initiator, was cooled to –78°C and titrated using one or two drops of distilled styrene and a dropwise addition of s-BuLi until a persistent yellow/orange color developed. The required amount of s-BuLi initiator was then injected, followed by the purified styrene monomer. Polymerization of the first block was allowed to proceed for 30 minutes, after which diphenyl ethylene was added in proportion with the amount of initiator used. After 5 minutes, an aliquot of polystyrene was extracted and terminated with methanol for molecular weight determination. The second monomer was then injected and polymerization was allowed to proceed for 2 hours before the reaction was terminated with methanol. Compositions were determined using ^{1}H nuclear magnetic resonance (NMR). Molecular weights were measured by gel permeation chromatography (GPC) in THF using PS standards.

TABLE II.1: CHARACTERISTICS OF THE ANIONIC DIBLOCK COPOLYMERS

copolymer	M_n (kg/mol)	M_w/M_n	PS (wt %)	remarks
30K PS-*b*-PLMA	30	1.03	47.0	-
45K PS-*b*-PLMA	45	1.05	49.5	-
19K PS$_{d8}$-*b*-PLMA	19	1.01	50 (theor.)	-
23K PS-*b*-POMA	23	1.06	55.8	-
43K PS-*b*-POMA	43	1.03	50.7	-
27K PS-*b*-POMA	~ 27	-	54.3	30/70 wt% mixture of
28.6K PS-*b*-PHMA	28.6	1.01	49.0	-
41K PS-*b*-PHMA	41	1.01	49.0	-
34.3 PS-*b*-PHMA	~ 34.3	-	49.0	45/55 wt% mixture of
110K PS-*b*-PPMA	110	1.03	49.2	-
136K PS-*b*-PPMA	136	1.01	49.8	< 5% homopolymer
70K PS-*b*-PEMA	70	1.02	49.1	< 5% homopolymer
110K PS-*b*-PEMA	110	1.01	48.7	< 5% homopolymer
79K PS-*b*-PEMA	~ 77	-	49.0	70/30 wt% mixture of
80K PS-*b*-P(MMA-*r*-LMA)	80	1.01	50	26.5 wt% MMA 23.5 wt% LMA

The characteristics of the different anionic block copolymers used in this thesis are listed in Table II.1. The absolute molecular weights listed are based on the measured weight fraction and molecular weight of the styrene block. For some materials, a small fraction of PS homopolymer was present, as noted in the table. During the study of phase behavior for this family of materials, mixtures of two different molecular weights of the same material were sometimes prepared in order to access thermodynamic transitions

without requiring further synthesis. Such use of mixtures has proven to be very successful, provided the molecular weights of the two copolymers are not too disparate.[76,115,116] The mixtures were prepared by coprecipitating in methanol the desired amounts of each copolymer dissolved in THF. The precipitate was then filtered and allowed to dry in vacuum for several hours.

II.1.2. ATRP of S/AMA and S/AA block copolymers

II.1.2.a. Introduction to ATRP

Because of the control over termination reactions and chain end functionality that it offers, anionic polymerization has been used almost exclusively over the past three decades for the preparation of block copolymers.[8] However, besides requiring extremely rigorous purification procedures of all monomers, solvent and reagents, this technique is also very limited in the types of block copolymers that it can produce. In particular, anionic polymerization of block copolymers comprising an acrylate block has proven very difficult.[117] Such materials are important candidate thermoplastic elastomers and pressure sensitive adhesives, which can now be prepared by the recently reported controlled "living" atom transfer radical polymerization (ATRP) methods. Since it was first described 5 years ago by Matyjaszewski *et al.*[118] and Sawamoto *et al.*[119], ATRP has been widely applied to the preparation of block, graft or random copolymers of various chemistries and architectures.[21]

ATRP is a controlled free radical polymerization technique that relies on the reversible activation of dormant species to yield free radicals capable of propagating the polymerization. Initiation of ATRP involves an equilibrium reaction between a halogen derivative (alkyl halide R-X, where X= Cl, Br) and a transition metal halide catalyst (MX, where M=Cu, Ni, Ru, Fe,… and X=Cl, Br) complexed with an organic ligand. This reaction yields the activated radical (R$^\bullet$) and an oxidized metal complex (MX_2). Subsequently, a similar equilibrium is established between the growing radical and the halogen end-capped chain, and polymerization proceeds by the *activation-propagation-deactivation cycle* depicted in Figure II.1

Activation

$$\text{\textasciitilde\textasciitilde\textasciitilde}X + LnM^{Z+} \longrightarrow \text{\textasciitilde\textasciitilde\textasciitilde}\bullet + LnM^{(Z+1)+}X$$

Propagation

$$\text{\textasciitilde\textasciitilde\textasciitilde}\bullet \quad =\!\backslash \longrightarrow \text{\textasciitilde\textasciitilde\textasciitilde}\bullet$$

Deactivation

$$\text{\textasciitilde\textasciitilde\textasciitilde}\bullet + LnM^{(Z+1)+}X \longrightarrow \text{\textasciitilde\textasciitilde\textasciitilde}X + LnM^{Z+}$$
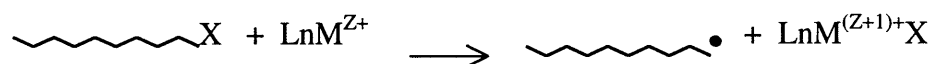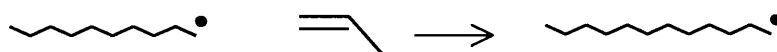
Figure II.1: General mechanism of ATRP

However, because the equilibrium between activated and deactivated species lies heavily on the side of the deactivated (halogen end capped) chain, the overall concentration of activated radicals remains very low throughout the polymerization, and the various termination reactions typically encountered in normal free radical polymerization are

much less probable. This confers to ATRP its almost "living" character and allows for control over molecular weight and polydispersity of the polymer. Moreover, because the chain retains the halogen end functionality at the end of polymerization, chain extension with a second monomer is possible, and block copolymers can thus be prepared. Finally, since ATRP is a free radical polymerization method, it can be applied to a much wider range of chemistries and does not require any rigorous purification of the monomers or reagents, since the only impurity that needs to be removed from the reaction medium prior to polymerization is oxygen. ATRP hence offers a highly versatile and attractive alternative to anionic polymerization for the preparation of block copolymers.

This polymerization technique was used to prepare block copolymers of styrene and various methacrylates and acrylates. The experimental details are given below.

II.1.2.b. ATRP of PS-b-PnAMA

PS-*b*-PnAMA block copolymers were prepared in two steps. First, a methacrylate homopolymer was prepared by ATRP in the bulk. The purified Cl-terminated methacrylate block was then used as a macroinitiator for the polymerization of styrene in N,N-dimethylformamide (DMF).[120] Butyl methacrylate (BMA), methyl methacrylate (MMA) and lauryl methacrylate (LMA) were purchased from Aldrich and used as received. Homopolymers of these monomers were prepared by ATRP in the bulk using methyl-2-bromopropionate (Aldrich, used as received) as the initiator, and Copper[(I)]Cl/1, 1, 4, 4, 10 10- hexamethyltriethylenetetramine (both from Aldrich, used as received) as the transition metal/ligand complex. The choice of a more reactive brominated initiator

49

(R-Br), over a chlorinated one (R-Cl), ensures rapid initiation for the polymerization of the highly reactive methacrylate monomers.[121] In all cases, 25 ml of monomer were combined with 0.06 g CuCl and 0.5 ml of the amine ligand (amine/Cu$^{(I)}$Cl molar ratio = 3:1) in a conical flask containing a stir bar. After capping the flask with a rubber septum, the monomer/catalyst mixture was degassed by refluxing dry, grade 5.0 nitrogen for 15 min. Towards the end of those 15 min., the initiator (68 μl, molar ratio of R-BR:Cu$^{(I)}$Cl = 1:1) was injected under a continuous flow of nitrogen and the reaction vessel was then quickly placed in an oil bath equilibrated at a temperature of 90°C. Polymerization was allowed to proceed for 20 minutes, which, for the concentration of initiator used, corresponds to a conversion of approximately 70%. Indeed, higher conversion was found to be detrimental for the subsequent preparation of block copolymers, since substantial loss of chain end functionality tends to occur towards the end of the polymerization when a brominated initiator is used. The reaction mixture was then dissolved in 20 ml of THF and precipitated in methanol. The resulting methacrylate homopolymer was re-dissolved in THF and precipitated in methanol 3 times to remove unreacted monomer and the catalyst complex. The purified polymer was then dried overnight at 60°C under vacuum. The dried and purified n-alkyl methacrylate homopolymer (PnAMA) was then used as a macroinitiator for the ATRP of styrene (Aldrich, used as received). PnAMA (2g) was dissolved in 20 ml of N,N-dimethylformamide (DMF, Aldrich, used as received) in a Schlenk tube equipped with a stir bar. Cu$^{(I)}$Cl (0.008 g), the amine ligand (65 μl, Cu$^{(I)}$Cl:ligand = 3:1), and styrene monomer (4 ml) were added to the dissolved polymer and the solution was then degassed for 15 min. and subsequently placed in an oil bath equilibrated at a temperature of 130°C. These conditions (DMF, 130°C) have indeed

50

been shown to result in controlled ATRP of styrene.[120] Polymerization was allowed to

proceed for 48 hrs, after which the reaction mixture was precipitated in methanol. The

filtered block copolymer was then purified 3 times by dissolution/precipitation in

THF/methanol and dried overnight under vacuum at 40°C. In some cases, the resulting

block copolymer was found to contain substantial amounts of unreacted methacrylate

homopolymer. Soxhlet extraction with hexane for 2 days was found to result in almost

complete removal of the undesired methacrylate homopolymer.

Compositions of the block copolymers were determined using ^{1}H nuclear magnetic

resonance (NMR). Molecular weights were measured by gel permeation chromatography

(GPC) in THF using PMMA standards. Absolute molecular weights were obtained based

on the measured weight fraction and molecular weight of the methacrylate first block.

The characteristics of the ATRP PS-*b*-PnAMA will be presented in Chapter IV.

II.1.2.c. ATRP of PS-b-PnAA

Block copolymers between styrene and various n-alkyl acrylates (nAA), namely

methyl acrylate (MA), butyl acrylate (BA), hexyl acrylate (HA) and lauryl acrylate (LA)

were prepared by ATRP using a very similar protocol as that developed for PS-*b*-

PnAMA. Again, all monomers, purchased from Aldrich, were used as received. The

acrylate block was prepared first, in bulk, using methyl-2-chloropropionate (Aldrich,

used as received) as the initiator. Indeed, since the propagation is much slower for the

acrylates, initiation can involve the less reactive, but also more stable chlorinated

initiator.[121] This circumvents the problem of chain end functionality loss at high degrees

of conversion of the first block, which leads to the presence of undesired homopolymer in the final block copolymer. The acrylate monomer (25 ml) was combined with 0.06 g $Cu^{(I)}Cl$ and 0.5 ml amine in a conical flask which was then sealed. The initiator (70 μl, $R-Cl:Cu^{(I)}Cl = 1:1$) was added to the degassed mixture and polymerization was carried at 90°C for 12 hrs. The resulting acrylate homopolymer was then purified three times as described above and dried overnight at room temperature under vacuum. The same conditions as those described above for PS-*b*-PnAMA were used for the extension of the acrylate macroinitiator with styrene monomer. In this case, however, no homopolymer was detected in the final block copolymer. Compositions of the block copolymers were determined using ^{1}H nuclear magnetic resonance (NMR). Molecular weights were measured by gel permeation chromatography (GPC) in THF using PMMA standards. Absolute molecular weights were obtained based on the measured weight fraction and molecular weight of the acrylate first block. The characteristics of the ATRP PS-*b*-PnAA will be presented in Chapter V.

II.2. INVESTIGATION OF PHASE BEHAVIOR

The experimental investigation of phase behavior of the various materials prepared in the context of this thesis made use of two major techniques: dynamic rheological testing and small angle neutron scattering (SANS). Because of their extensive use in this work, these two techniques will be described in detail in the sections below.

II.2.1. Dynamic rheological testing

II.2.1.a. Background

When a material is deformed under periodic forces, one refers to its mechanical properties as *dynamic*. These properties are expressed by the dynamic storage modulus G', the loss modulus G'', and mechanical damping or internal friction. The dynamic storage modulus, G', represents the inherent stiffness of the material under dynamic loading conditions. The loss modulus G'' represents the amount of elastic energy which is dissipated as heat under cyclic loading conditions. Both G' and G" are sensitive to molecular motions, relaxation processes, structural heterogeneities, morphologies of multiphase systems and transitions of different types, including *order/disorder transitions*. Dynamic mechanical properties of viscoelastic materials are typically determined by measuring the response to a sinusoidal excitation (stress or strain), as a function of temperature and amplitude and frequency of the excitation. As long as the strain (or stress) applied to the material is below the elastic limit, linear viscoelastic behavior is observed. In this case, the mechanical response to a sinusoidal stimulus is also sinusoidal, but out of phase with the applied stimulus. This phase lag results from the time necessary for molecular rearrangements. For example, upon the application of a sinusoidal strain of amplitude ε_0 and frequency ω:

$$\varepsilon = \varepsilon_o \sin \omega t = \varepsilon_o \exp^{i\omega t} \qquad (II.1)$$

the resulting stress in the material will be given given by:

$$\sigma = \sigma_o \sin(\omega t + \delta) = \sigma_o \exp^{i\omega t + \delta} \qquad (II.2)$$

where σ_0 is the stress amplitude, ω the angular frequency (rad/sec) and δ the phase

angle (rad). By dividing the stress by the strain, one can define a complex modulus, E^*

or G^* (elongation or shear deformation), which consists of a real (storage), and a

complex (loss) part. For shear, these two components depend on the imposed strain, the

measured stress and the phase angle as follows:

$$G^* = \sigma / \varepsilon = \sigma_o / \varepsilon_o \times (\cos \delta + i \sin \delta) = G' + iG'' \qquad \text{(II.3.a)}$$

$$G' = (\sigma_o / \varepsilon_o) \cos \delta \qquad \text{(II.3.b)}$$

$$G'' = (\sigma_o / \varepsilon_o) \sin \delta \qquad \text{(II.3.c)}$$

II.2.1.b. Dynamic rheological testing of diblock copolymers

Intuitively, the drastically different diffusion mechanisms which are expected to

prevail in the ordered state compared to the segmentally mixed state should result in large

changes in the viscoelastic properties of diblock copolymers undergoing an ordering

transition. While the viscoelastic behavior of a copolymer in the segmentally mixed state

should resemble that found for homopolymers, the thermodynamic barrier imposed by

microphase separation should strongly alter diffusion processes in the ordered state.

Several authors investigated these effects.[4] Bates and coworkers[122,123] further illustrated

how they provide an easy means for observing ordering transitions in diblock

copolymers. They found that, upon raising the temperature above the UDOT of diblock

copolymers, the low-frequency dynamic modulus and viscosity decreased dramatically

and the rheological behavior changed from non-Newtonian (shear-dependent viscosity) to

Newtonian (shear-independent viscosity). Upon shifting isothermal frequency scans

along the frequency axis, they found that the low-frequency data exhibited two very distinct power-law behaviors above and below the ordering transition. In the disordered state, a low-frequency power-law behavior similar to that found for homopolymers is observed, namely:

$$G' \sim \omega^2 \text{ and } G'' \sim \omega \quad \text{(disordered state)}$$

In contrast, for a diblock copolymer in the ordered state, a scaling of the modulus with frequency of 0.5 is found for both G' and G'':

$$G', G'' \sim \omega^{0.5} \quad \text{(ordered state)}$$

Finally, for a material undergoing a transition from the ordered to the disordered state in the temperature range studied, a change in scaling of G' from $G' \sim \omega^{0.5}$ to $G' \sim \omega^2$ is found. Dynamic rheological testing thus provides a unique opportunity for studying phase behavior in diblock copolymers. Although rigorously not applicable for materials undergoing morphological changes, time/temperature superposition is commonly used as it provides an elegant way of presenting and interpreting dynamic rheological data.

II.2.1.c. Experimental details

Dynamic rheological measurements were obtained using a Rheometric Scientific ARES rheometer operated in the parallel plate geometry, with 25 mm diameter plates and a 0.5 mm gap size. Bulk polymer samples (17 mm in diameter, 1 mm thick) were melt pressed in a hot press held at a temperature of 100°C or more. To avoid the application of large stresses on the material, the polymer was allowed to warm above the glass

transition of the stiffer block before pressurizing. Once placed in the rheometer, the sample thickness was further reduced to 0.5mm, again well above T_g.

The dynamic storage (G') and loss (G'') moduli of the copolymers were determined isothermally as a function of frequency ($0.1 < \omega < 400$ rad/sec), and temperature was varied from 100 to 200°C in 10 or 20°C increments. A strain of 0.5 to 1% was used, which is in the linear elastic regime for the materials considered in this work. Whenever possible, the isothermal frequency sweeps obtained at various temperatures were superimposed about a reference temperature of 150°C in order to obtain master plots. Data taken at torques lower than 1 g-cm (the lower limit of sensitivity of the transducer) were discarded.

II.2.2. Small angle neuron scattering (SANS)

II.2.2.a. Background

While dynamic rheological measurements offer a clear means of identifying whether a block copolymer is ordered or disordered, they do not provide direct information on the type of phase diagram in hand (UDOT versus LDOT), unless a phase transition is observed in the temperature range studied. Therefore, this technique was used in combination with small angle neutron scattering (SANS), the latter offering the advantage of revealing unambiguously whether composition fluctuations in the disordered state increase or decrease with increasing temperature, as expected for LDOT and UDOT behavior, respectively.

In a scattering experiment, one refers to scattering as the deflection of an incident beam from its original direction by interaction with the nuclei of atoms or molecules in a sample. If the scattering process does not involve any transfer of energy, the scattering is called elastic and the neutrons only undergo a momentum transfer. The momentum transfer q is related to the neutron wavelength λ and the scattering angle θ by:

$$q = (4\pi / \lambda) \sin \theta \qquad (II.4)$$

The spatial arrangement of the atoms or molecules by which the neutrons are scattered in a given sample gives rise to constructive or destructive interference, depending on the phase difference between the scattered neutron beams. Measuring the scattered intensity as a function of the scattering angle hence provides an easy means of studying the local structure and correlations between the atoms or molecules in a particular sample. The number of scattered neutrons per second and per incident neutron for a given nucleus in the sample is called the atomic scattering cross section, and is proportional to b^2, where b is the scattering length. The difference in scattering lengths from one nucleus to another is thus responsible for the contrast needed to extract interesting information on chain configurations and structure from neutron scattering experiments. Table II.2 summarizes the values of b for the atoms most commonly encountered in organic materials.[124]

For a polymer molecule, each repeat unit (monomer) acts as a collection of point scatterers. Therefore, the scattering length of a monomer unit is defined as the sum of all scattering lengths of the constitutive atoms. An important value of b is that of deuterium and how it differs from the value for hydrogen. This difference is at the origin of selective deuterium labeling, a technique extensively used to enhance the level of contrast

in a mixture or diblock copolymer compared to that obtained for fully hydrogenated materials.

TABLE II. 2: SCATTERING LENGTH b FOR ELEMENTS APPEARING IN ORGANIC POLYMERS

Atom	Nuclei	Scattering length b $(10^{-12}$ cm$)$
Hydrogen	^{1}H	-0.374
Deuterium	^{2}H (D)	0.667
Carbon	^{12}C	0.665
Oxygen	^{16}O	0.580

II.2.2.b. SANS on diblock copolymers

As mentioned above, the coherent scattered intensity in SANS carries information on the correlations between atoms or groups of atoms and is therefore a very attractive method for studying microphase separation in block copolymers. For diblock copolymers in the microphase separated state, the periodic structures formed give rise to Bragg reflections (constructive interference between the waves scattered by point scatterers arranged on a lattice). From the detailed structure of the Bragg reflections, one can extract the symmetry and the periodicity of a given morphology. In the disordered state, however, the scattering spectrum is completely different. While polymer blends exhibit a monotonic decrease of scattered intensity with scattering angle (or q vector), the

scattered intensity of diblock copolymers exhibits a broad reflection at non-zero angle, even in the disordered state.[4,39] This reflection, which results from the connectivity of the two blocks, is referred to as the **correlation-hole peak**[48] and occurs at a wave vector $q^* \sim$ 1.86/R_g, where $R_g = N^{1/2}a/6$, is the radius of gyration of a gaussian chain containing N statistical segments of length a. The shape of the correlation hole peak is strongly affected by the degree of thermodynamic compatibility between the two blocks.

Leibler[39] first showed how the evolution of both the peak intensity and shape could be used experimentally to extract the microphase separation temperature and interaction parameter χ from the coherent scattering. The absolute scattered intesity I (cm^{-1}) is related to the scattering function $S(q)$ as follows:

$$I(q) = v^{-1}(b_1 - b_2)^2 S(q) \qquad (II.7)$$

where v is a reference segmental volume and b_i is the scattering length of component i. Within the incompressible random phase approximation (IRPA), the scattering function $S(q)$ is given by:

$$S(q) = W(q) / [\sum_i S_{ii}(q) - 2\chi W(q)] \qquad (II.8)$$

where W is the determinant of the matrix composed of the correlation functions of the ideal independent copolymer chains, $\|S_{ij}\|$, and χ the Flory-Huggins interaction parameter. For ideal gaussian chains of N statistical segments of length a, the correlations functions S_{ij} are given by:

$$S_{11}(q) = Ng_1(f, x) \qquad (II.9.a)$$

$$S_{22}(q) = Ng_1(1-f, x) \qquad (II.9.b)$$

$$S_{12}(q) = S_{21}(q) = N/2[g_1(1, x) - g_1(f, x) - g_1(1-f, x)] \qquad (II.9.c)$$

59

where f is the segment fraction of component 1: $f = N_1/N$, where N_1 is the number of

statistical segment of type 1 in the copolymer, and $g_1(f,x)$, the Debye function, is defined

as:

$$g_1(f,x) = 2[fx + \exp(-fx) - 1]/x^2 \tag{II.10}$$

with

$$x = q^2 N a^2 / 6 = q^2 R_g^2 \tag{II.11}$$

When equations II.9 through 11 are incorporated into equation II.8, the formula for the

scattering function becomes:

$$S(q) = N /[F(x) - 2\chi N] \tag{II.12}$$

where $F(x)$ is a function of the Debye functions only, and is hence independent of

temperature:

$$F(x) = \frac{g_1(1,x)}{g_1(f,x)g_1(1-f,x) - \frac{1}{4}[g_1(1,x) - g_1(f,x) - g_1(1-f,x)]^2} \tag{II.13}$$

The last two equations can then be used in combination with equation II.7 to extract

thermodynamic and configurational information such as χ and R_g.

Equations II.12 and II.13 assume that the two segment types have identical

statistical segment lengths a_i and segment volumes. For copolymers consisting of

structurally dissimilar blocks, this assumption can be relaxed by using a modification to

equation II.13 proposed by Bates[29]:

$$F(x_1, x_2) = \frac{f^2 g(x_1) + 2f(1-f)h(x_1)h(x_2) + (1-f)^2 g(x_2)}{f^2(1-f)^2[g(x_1)g(x_2) - h^2(x_1)h^2(x_2)]} \tag{II.14}$$

where f is now the volume fraction instead of the segment fraction of component 1, and

$g(x_i)$ and $h(x_i)$ are given by:

$$g(x_i) = 2[x_i + \exp(-x_i) - 1] / x_i^2 \qquad\qquad \text{(II.15.a)}$$

$$h(x_i) = x_i^{-1}(1 - \exp(-x_i)) \qquad\qquad \text{(II.15.b)}$$

and

$$x_i = q^2 N_i a_i^2 / 6 = q^2 R_{g_i}^2 \qquad\qquad \text{(II.16)}$$

II.2.2.c. Experimental details

SANS measurements were obtained primarily at the Cold Neutron Research Facility at the National Institute of Standards and Technology (NIST) on beamline NG-3. The instrument configuration was $\lambda = 6.00$ Å, $\Delta\lambda/\lambda = 15\%$, sample-to-detector distance = 6 m, resulting in a q spanning 0.008 to 0.08 Å^{-1}. Some measurements were also taken at the Manuel Lujan Jr. Neutron Scattering Center of the Los Alamos Neutron Science Center at the Los Alamos National Laboratory on the Low-Q Diffractometer (LQD), and at the Intense Pulsed Neutron Source at the Argonne National Laboratory on the Small Angle Neutron Diffractometer (SAND). The wavelength range and q range for these two time-of-flight diffractometers are $0.2 < \lambda < 20$ Å, $0.003 < q < 0.5$ Å^{-1} and $1 < \lambda < 14$ Å, $0.0035 < q < 0.6$ Å^{-1}, respectively. In all cases, melt pressed samples were prepared as described in section II.2.2.c. The scattered intensity was corrected for background and detector inhomogeneity in the standard manner and scaled to absolute units (cm^{-1}) using a silica standard. Temperature was varied by 10 or 20°C increments and sufficient time was provided for thermodynamic equilibration at each temperature. Thermodynamic reversibility of the observed behaviors was verified in each case through temperature

cycling. Effective interaction parameters χ were extracted from the SANS data using the incompressible RPA described above.

In order to obtain additional information on the phase behavior of the materials studied in this thesis, SANS experiments were carried out not only as a function of temperature, but also pressure. SANS measurements under hydrostatic pressure were performed at NIST using a hydraulic pressure cell that permits *in situ* measurements over a pressure range from 1 to 1000 bar and over a T range spanning 25 to 190°C. Silicone oil is used as the pressurizing fluid, with a rubber gasket separating the sample, prepared as described above, from the fluid. As for simple T measurements, reproducibility of pressure measurements was verified by cycling both T and P. Data were reduced in the same manner as regular SANS data. Pressure coefficients were extracted from the variation of the ordering transition temperature with pressure. To this end, pressure was varied isothermally over an interval spanning 0.014 to 1 kbar, at various temperatures ranging from 100 to 190°C.

CHAPTER III: PHASE BEHAVIOR OF PS-*B*-PNAMA

In this chapter, the phase behavior of the series of anionically synthesized symmetric block copolymers between styrene and *n*-alkyl methacrylates listed in Table II.1 is presented. Their phase behavior was determined both as a function of temperature and pressure through a combined use of dynamic rheological testing and SANS. In the following sections, the parameter *n* refers to the number of carbon atoms in the alkyl side chain of the methacrylate block, i.e., $n = 1$ for MMA, 2 for EMA, 3 for PMA, 4 for BMA, etc. The results are divided into two categories, namely, those obtained for block copolymers with long alkyl side chain methacrylates ($n \geq 6$), and those obtained for short alkyl side chains ($2 \leq n \leq 4$).

III.1. PHASE BEHAVIOR AS A FUNCTION OF TEMPERATURE

III.1.1. Copolymers with long side chains ($n \geq 6$)

Figure III.1 shows the storage (*G'*) and the loss (*G''*) moduli of 45K PS-*b*-PLMA as a function of frequency at various temperatures, time/temperature superimposed about a reference temperature of 150°C. The results suggest that this material remains in the ordered state over the entire temperature range studied (100 to 190°C), as is evident from the low frequency power law behavior. Both *G'* and *G''* scale with frequency approximately as $\omega^{0.5}$, which is typical for ordered diblock copolymers.[122,123]
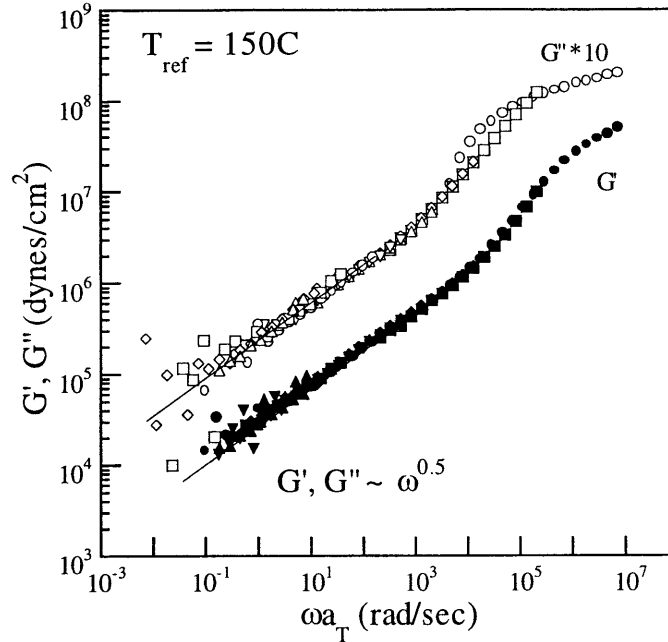
Figure III.1:Master curves for G' and G'' of 45K PS-b-PLMA

Similar results were obtained for the 30K sample. The persistence of the ordered state for temperatures a high as 200°C in these materials is consistent with two distinctly different phase diagrams. One possibility is that the low temperature compatibility between styrene and the methacrylate strongly decreases with increasing alkyl side chain length. This would have the effect of raising the UDOT above the experimentally accessible temperature range, even for these rather low molecular weights. Alternatively, a simultaneous increase of the UDOT and decrease of the LDOT would result in an "lens shaped" phase diagram (see Figure I.3.b in Chapter I) in which the two transitions have essentially merged together such that the copolymer is ordered at all temperatures. To differentiate between these two scenarios, SANS measurements were performed on these materials, as well as a the lower molecular weight PS_{d8}-b-PLMA sample.

Figure III.2 shows the scattering intensity profile as a function of wave vector

$q=4\pi\sin\theta/\lambda$ for 19K PS_{d8}-b-PLMA. At temperatures below 130°C, a Bragg reflection

characteristic of the ordered state is observed at $q \cong 0.041$ Å^{-1}. Increasing the

temperature above 130°C results in a significant decrease in the peak intensity and a

broadening of the scattering maximum. Such "correlation hole" scattering is the

signature of a segmentally mixed state[39], indicating that this material undergoes a classic

UDOT between 130 and 140°C.
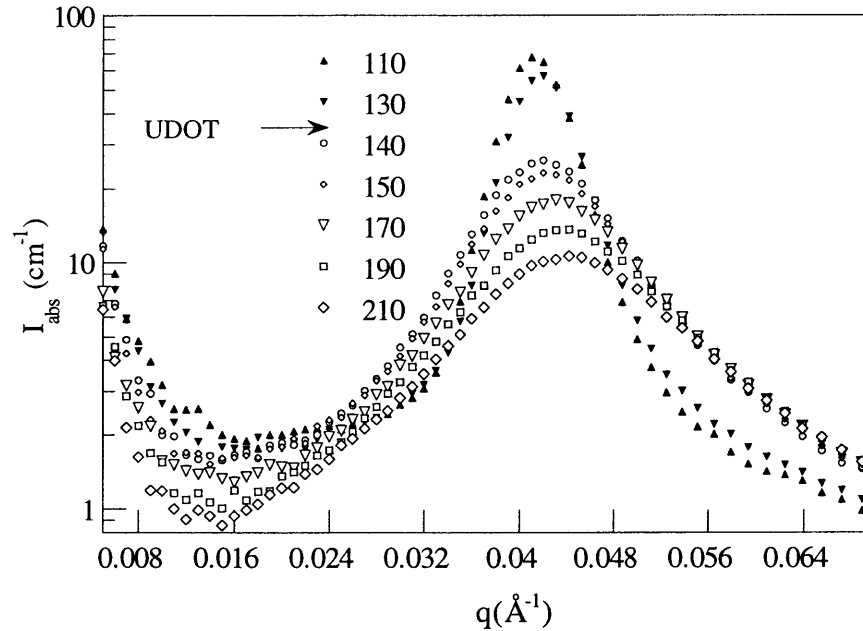
Figure III.2: Scattering intensity profile for 19K PS_{d8}-b-PLMA

A convenient means of locating more precisely an ordering transition in block

copolymers is by plotting the breadth of the scattering maximum and its intensity.[4]

Indeed, at the order/disorder transition, the full width at half maximum intensity of the

peak (FWHM) is expected to increase abruptly, while the peak intensity (I_{max}) should

decrease as sharply. Figure III.3 shows the temperature dependence of these two

parameters, obtained from a gaussian fit to the scattering intensity profile. The abrupt

increase in FWHM (from ~ 0.003 to ~ 0.006) and decrease in I_{max} (from ~ 55 to ~ 25)

between in 130 and 140°C signify the order/disorder transition of the block copolymer,

and a UDOT temperature of ~ 135°C is extracted. Moreover, the magnitude of the

thermodynamic fluctuations in the system, or, equivalently, the intensity of the scattering

maximum I_{max}, monotonically decreases with increasing temperature, thereby precluding

the possibility of LDOT-type phase behavior for this sample in the temperature range

probed (110-210°C). For the 30K and 45K samples, sharp reflections were observed at

all temperatures, confirming the ordered state apparent from the dynamic rheological

measurements. A monotonic decrease in intensity of the first order reflection with

increasing temperature was also found, again ruling out LDOT behavior.

Figure III.3: T-dependence of I_{max} and FWHM for 19K PS_{d8}-b-PLMA
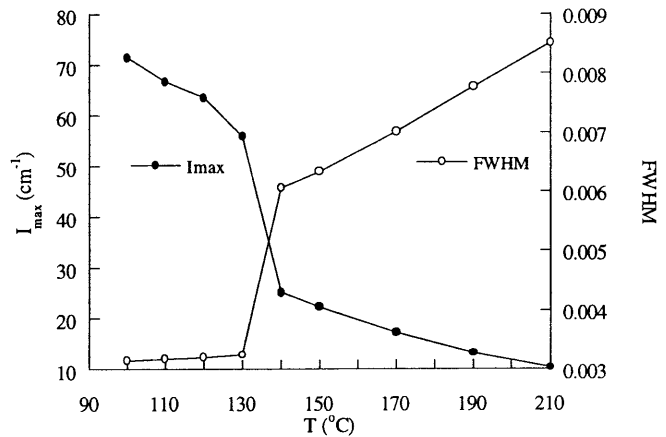
Similar results were obtained for PS-b-POMA and PS-b-PHMA, but with a

distinct increase in block compatibility in going from lauryl to hexyl methacrylate. For

PS-b-POMA, the 23K sample was disordered throughout the experimental temperature

range while the 43K was ordered. As shown in Figure III.4, a UDOT could be observed

between 130 and 140°C for a $\overline{M_n}$ ~ 27K mixture of these two samples containing 70 wt%

of the low molecular weight copolymer and prepared as described in section II.1.1. The

66

inset of Figure III.4 shows the variation of I_{max} and FWHM with temperature. The

UDOT of this block copolymer manifests itself in a strong decrease in I_{max} and increase

in FWHM between 130 and 140°C, while the presence of a LDOT in the temperature-

range investigated is again ruled out by the monotonic decrease in I_{max} and increase in

FWHM.

For PS-*b*-PHMA, the 28.6K sample was disordered over the entire experimental

temperature range, while the 41K sample was always ordered. However, a $\overline{M_n} \sim$ 34.3K

mixture of these two materials containing 45 wt% of the low molecular weight diblock

was found to undergo a UDOT at 162°C, as shown in Figures III.5. Again, no sign of an

LDOT-trend was observed for any of these block copolymers.
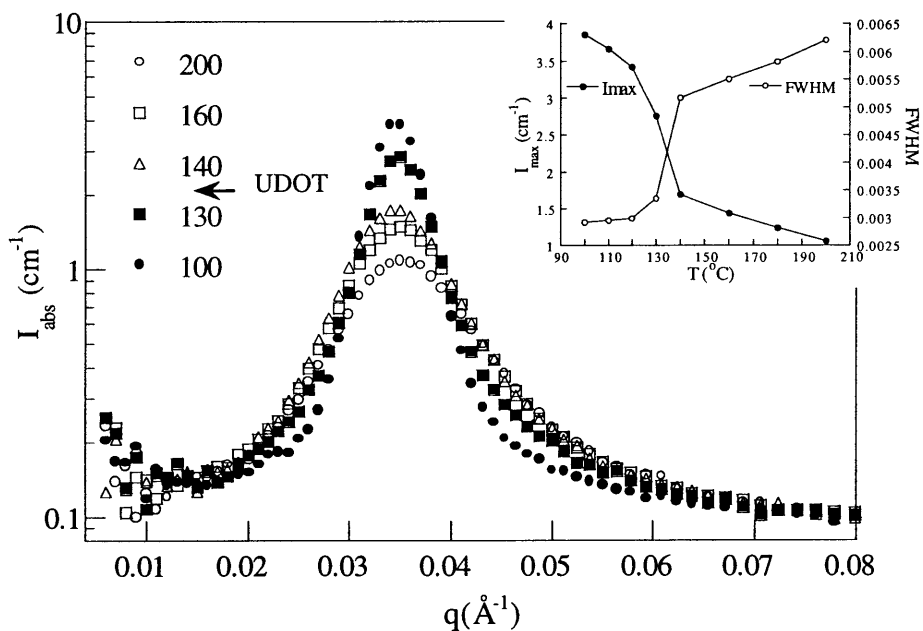
Figure III.4: Scattering intensity profile for 27K PS-*b*-POMA
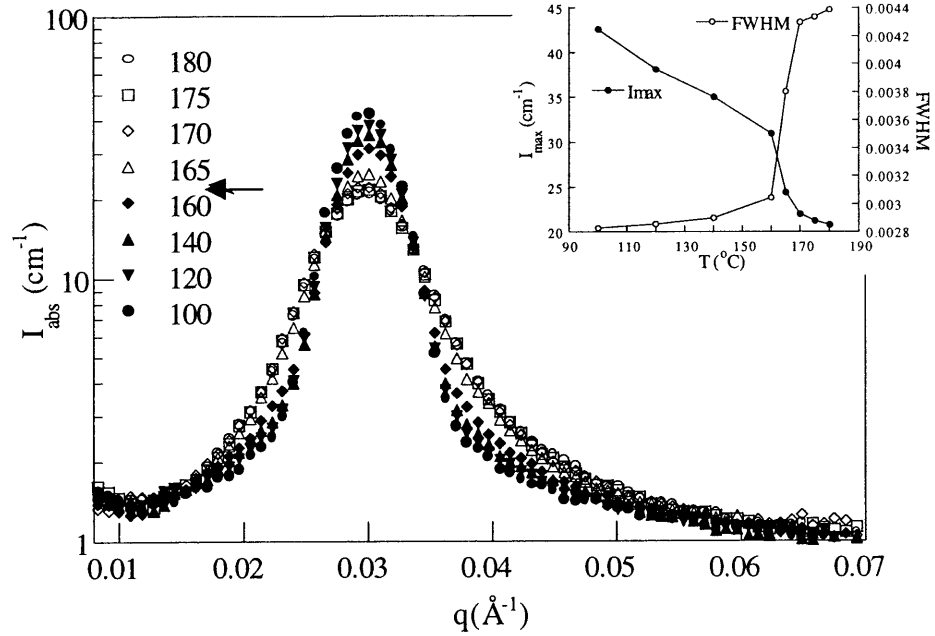
Figure III.5: Scattering Intensity profile for 34.3K PS-*b*-PHMA

To extract χ as function of temperature from the SANS data for these three

UDOT-type systems, the incompressible RPA formalism described in section II.2.2.b was

employed:

$$I(q) = \frac{(b_S - b_{AMA})^2}{v_{ref}} S(q) \qquad \text{(III.1)}$$

where $S(q)$ is given by equation II.12. The number of statistical segments N was equated

to the degree of polymerization of the molecule.[3] For $F(q)$, the expression developed in

the case of disparate statistical segment lengths (equations II.14 through 16) was used.

Neutron scattering data were fit to equation III.1 with χ, the statistical segment length of

the methacrylate block b_{AMA}, and a constant scaling factor as fitting parameters. A

statistical segment length of 6.7 Å was used for PS.[125] Data for the lowest molecular

weight samples were used in all three cases, i.e., 19K PS_{d8}-b-PLMA, 23K PS-b-POMA and 28.6K PS-b-PHMA. For the hydrogenated samples, namely PS-b-POMA and PS-b-PHMA, no suitable fit could be obtained without prior subtraction of an incoherent scattering background due to the high hydrogen content. As a first approximation, a constant background was included as a fitting parameter. An example of the resulting fit is given in Figure III.6 for PS-b-POMA. The average values of the fitting parameters are listed in Table A.1 of the appendix along with the fitting temperature range and N for each material.

The interaction parameters are shown in Figure III.7 where the functional form χ = A + B/T was used, with best fit slope and intercept values as listed. Data obtained by Russell et $al.$[32] for 27.6K PS_{d8}-b-PMMA are included for comparison. The χ values are found to increase from approximately 0.044 to 0.083 when the side chain length is increased from 6 to 12 hydrocarbons, while PS_{d8}-b-PMMA (n = 1) exhibits a slightly greater degree of thermodynamic incompatibility, since the reported χ value for this system is around 0.0373 in the temperature range considered. The increase in χ is found to result from both an increase in B, the temperature dependent enthalpic contribution to χ, and A, the temperature independent entropic contribution. However, an important observation to be made upon considering the data presented in Figure III.7 is the weak temperature dependence and large "entropic" contribution to χ (large A) that characterizes all of these systems. This is in contrast with classical incompatible (UDOT) systems such as styrene/isoprene[4], for which χ is mainly governed by unfavorable enthalpic interactions (B large and positive, A small). This observation strongly suggests that besides $\Delta\varepsilon$, other factors such as differences in packing, chain flexibility and self-

interaction energies of the pure components, play an important role in the phase behavior.

As mentioned in Chapter I of this thesis, such effects have been studied by several

authors, using both lattice-based and off-lattice calculations on polymer mixtures of

dissimilar components. These calculations have shown that disparities in monomer

structure, chain flexibility and Van der Waals self-interaction energies contribute both

entropic and enthalpic terms to the free energy of mixing that result in reduced

compatibility. For PS-b-PMMA, Freed and coworkers[126] argued that the weak

temperature dependence previously reported[32] arises from geometrical packing

constraints on the differently shaped monomers and the distribution of excess free

volume resulting from these constraints.
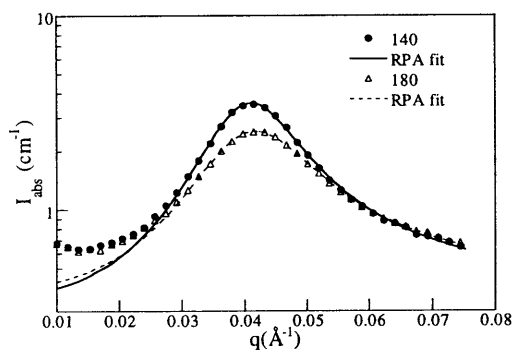
Figure III.6: Scattering intensity profile for 23K PS-b-PnOMA at 140 and 180°C and corresponding IRPA fits.
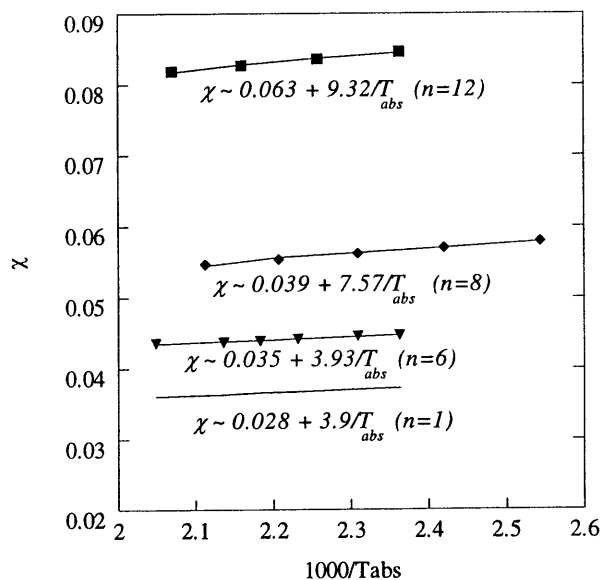
Figure III.7: Interaction parameters χ for UDOT-type PS-b-PnAMA BCP's (n = # hydrocarbons in side chain)

III.1.2. Copolymers with intermediate alkyl side chains (2 ≤ n ≤ 4)

Strikingly different results were obtained for diblock copolymers between styrene

and methacrylates with intermediate alkyl side chains $(2 \leq n \leq 4)$. Master curves for G'

and G'' obtained for 136K PS-b-PPMA ($n=3$) are shown in Figure III.8. The data

indicate that this system is disordered at low temperatures and goes through a LDOT

around 160°C. The transition is evidenced by the change in scaling of G' in the low

frequency regime from $G' \sim \omega^{1.4}$, characteristic of a segmentally mixed system, to $G' \sim$

$\omega^{0.5}$, characteristic of the microphase separated state. In the vicinity of the transition,

good overlap of the data for both G' and G'' cannot be obtained through horizontal

temperature shifts. Such failure of time/temperature superposition is commonly observed

for systems characterized by large concentration fluctuations prior to ordering.[123]
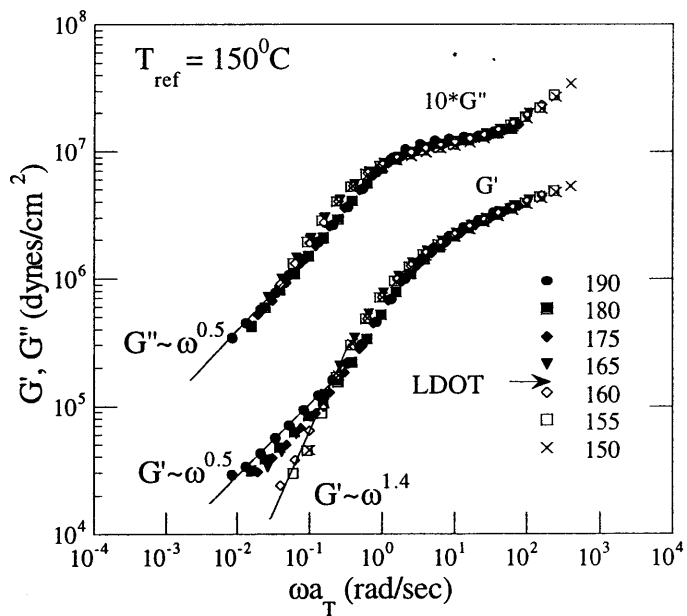
Figure III.8: Master curves
for G' and G'' of
136K PS-b-PPMA

The tendency of this system to microphase separate upon heating through a

LDOT is further evidenced by the neutron scattering data for 110K PS-b-PPMA shown in

Figure III.9. The weak scattering maximum observed at low temperatures (T<175°C)

increases in intensity as the LDOT is approached. Between 195 and 205°C, the distinct

narrowing of the scattering peak and increase in peak intensity together signal the onset

of order (see inset of Figure III.9). The weak scattering observed in the mixed state, far

below the LDOT, witnesses a strong compatibility between styrene and propyl

methacrylate compared with the styrene/n-alkyl methacrylate systems described in the

previous section. Similar data were obtained for 136K PS-b-PPMA, confirming the

LDOT observed by dynamic rheological testing on this material and yielding a better

estimate for the transition temperature of ~ 155°C. Based on these results and the phase

diagram for PS_{d8}-b-PBMA presented in Chapter I (Fig. I.4), PS-b-PPMA appears to be

more miscible than the latter system, since symmetric 110K and 136K PS_{d8}-b-PBMA are

always ordered. (While deuteration is generally known to affect miscibility, SANS

experiments on hydrogenated PS-b-PBMA show that deuteration effects do not

significantly alter the phase diagram for this system[127]).

Figure III.9:
Scattering intensity
profile for
110K PS-b-PPMA
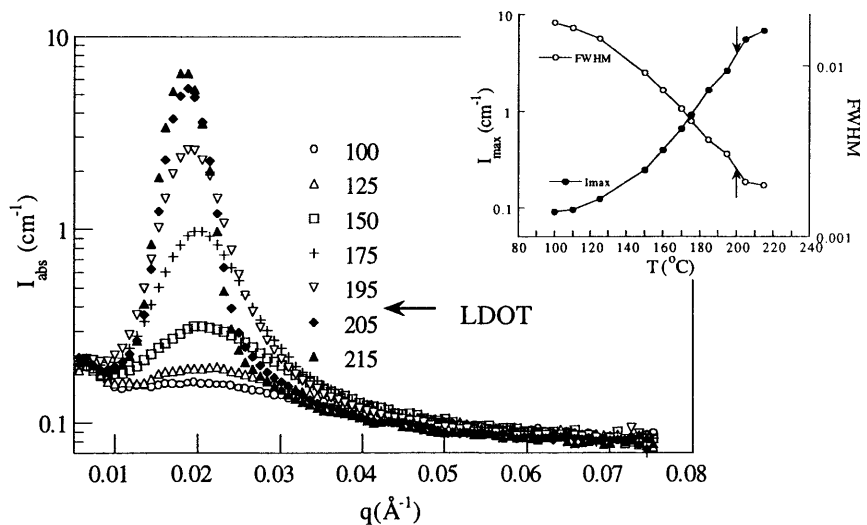
Block copolymers of styrene and ethyl methacrylate ($n=2$), PS-*b*-PEMA, were also found

to exhibit the LDOT-type phase behavior. Figure III.10 shows the scattering profile

obtained for a $\overline{M_n}$ ~79K mixture of 70K and 110K PS-*b*-PEMA containing 70 wt% of the

lower molecular weight diblock. This material undergoes a LDOT at ~ 185°C, as

evidenced by the distinct sharpening and increase in intensity of the scattering peak at

and above this temperature (see inset of Figure III.10). On the other hand, 110K PS-*b*-

PEMA is always ordered in this temperature range. (see Figure III.11)

Figure III.10:
Scattering intensity
profile for
79K PS-*b*-PEMA
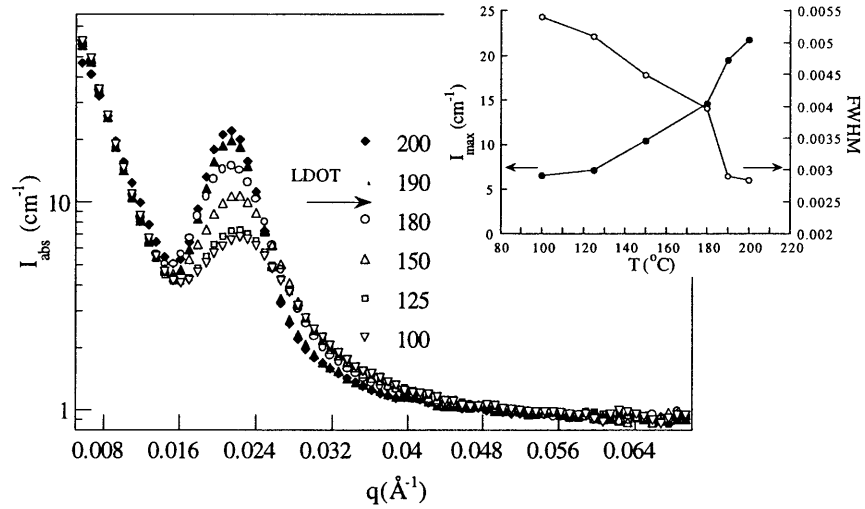
Figure III.11:
Master curves for
G' and G'' of
110K PS-*b*-PEMA
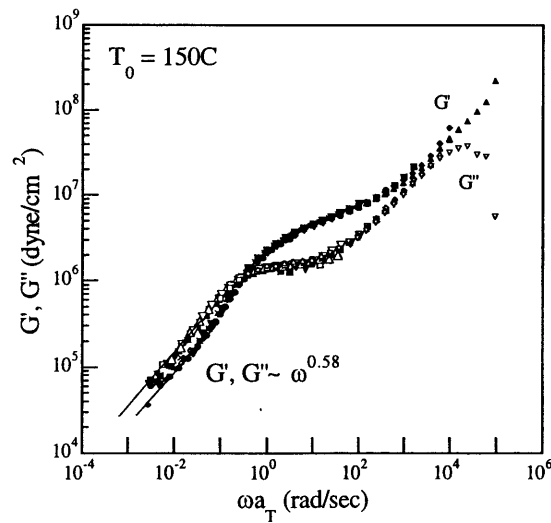
These results indicate that the degree of thermodynamic compatibility between styrene and ethyl methacrylate is quite comparable to that found for PS-*b*-PBMA, since 78K PS-*b*-PBMA undergoes a LDOT at ~ 185°C while 110K PS-*b*-PBMA is always ordered. The results obtained for these three LDOT-type block copolymers, namely, PS-*b*-PEMA, PS-*b*-PPMA and PS-*b*-PBMA, thus point to a *maximum in thermodynamic compatibility* for PS-*b*-PPMA ($n = 3$). Earlier blend studies of PS/PEMA and PS/PPMA by Brannock and coworkers[128] seem to reveal a quite different trend, namely, a higher degree of miscibility for PS/PEMA. However, the use of melt indexes as molecular weight indicators of the polydisperse polymers used in those studies complicates quantitative comparison with the observations presented here.

Strictly speaking, the incompressible RPA formalism used in the previous section to extract χ parameters from SANS data does not apply to compressible LDOT-type systems. However, "effective" χ parameters can still be obtained, which combine the different contributions to the free energy of mixing, namely, the purely enthalpic effects arising from segmental interaction and the equation of state effects described in section I.3.2 of Chapter I. Although the individual contribution to the free energy of mixing for each of these effects can not be resolved without the use of one of the compressible formalisms described in section I.3.2.b, the extracted χ values can still be used as a basis for comparison. The effective interaction parameters for PS-*b*-PPMA, PS-*b*-PEMA and PS$_{d8}$-*b*-PBMA are shown in Figure III.12 where the functional form $\chi = A + B/T$ was used, with best fit slope and intercept values as listed. The parameters used for this fit are listed in Table A.1. As expected, the slope B is negative for these LDOT systems, since

the degree of thermodynamic compatibility decreases with increasing temperature. The

greater value of B for $n = 3$ confirms the larger degree of compatiblity observed for this

system and points to a more negative ΔH_{mix}.
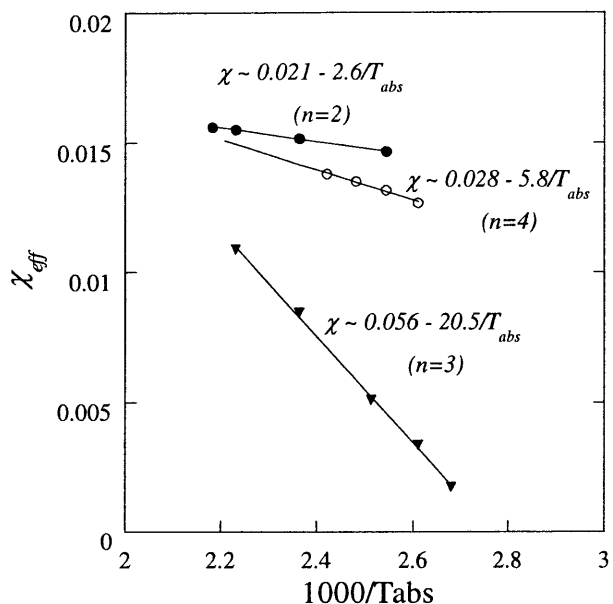
Figure III.12: Interaction parameters χ for LDOT-type PS-b-PnAMA BCP's

III.1.3. Summary

Table III.1 summarizes the results presented so far, namely, the type of behavior

(UDOT versus LDOT) and the transition temperature for each system. Also included are

the results reported for PS-b-PMMA[32] and PS-b-PBMA.[22,76] The results indicate a strong

dependence of the phase behavior of these block copolymers on the degree of branching

of the methacrylate block. For very *short* ($n = 1$, MMA) and *long* ($n \geq 6$, HMA, OMA

and LMA) alkyl side chains, the classical **UDOT**-type phase behavior of block

copolymers consisting of incompatible blocks is observed. For *intermediate side chain*

75

length ($2 \leq n \leq 4$), however, the block copolymer is miscible at low temperatures and

microphase separates upon heating through a **LDOT**. Moreover, a maximum in

thermodynamic compatibility is observed for $n = 3$ (PMA), as evidenced by the variation

of the effective interaction parameter χ as a function of the alkyl side chain length shown

in Figure III.13 for a constant temperature of 150°C.
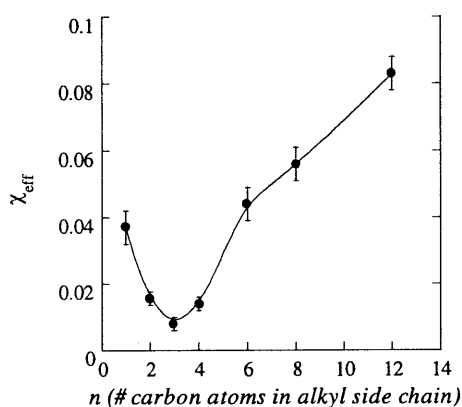
Figure III.13: Interaction parameter χ

for PS-*b*-P*n*AMA BCP's

at 150°C and as a function of n

Given the chemistry involved in the family of materials under investigation, the

presence of strong specific interactions between the non-polar styrene and the polar

methacrylate segment cannot be deemed responsible for the compatibility observed for

intermediate side chain lengths. Indeed, at best, modest dipole/induced dipole

interactions can occur between these two segments. Therefore, other effects, such as a

fine balance between these weak interactions and favorable packing effects in the

segmentally mixed state, have to be invoked to explain the trend observed in these

materials. The investigation of phase behavior as a function of temperature only does not

allow one to assess how energetically favorable or unfavorable packing is to segmental

mixing. However, such information can be easily obtained from SANS measurements

under hydrostatic pressure, since this technique gives access to the pressure coefficient of a thermodynamic transition, and, hence, the sign of ΔV_{mix} through the Clausius-Clapeyron equation. The effect of pressure on the phase behavior of the materials listed in Table III.1 is described in the next sections.

TABLE III.1: SUMMARY OF PHASE BEHAVIOR AND TRANSITION TEMPERATURES FOR SYMMETRIC PS-*b*-PNAMA

Copolymer	Type of behavior	Transition temperature
PS-*b*-PLMA $n=12$	UDOT	30K, 45K: >200°C 19K: 135 ± 5 °C
PS-*b*-POMA $n=8$	UDOT	23K: <100°C 43K: >200°C 27K mixt.: 135 ± 5 °C
PS-*b*-PHMA $n=6$	UDOT	28K: <100°C 46K: >200°C 34.3K mixt.: 162 ± 2.5 °C
PS$_{d8}$-*b*-PBMA* $n=4$	LDOT + UDOT	78K: 185 ± 5°C (LDOT) 85K: 155°C ± 5°C (LDOT) 110K: always ordered
PS-*b*-PPMA $n=3$	LDOT	110K: 200°C ± 5°C 136K: 155 ± 2°C
PS-*b*-PEMA $n=2$	LDOT	77K mixt.: 185°C 110K: always ordered
PS-*b*-PMMA $n=1$	UDOT	28K: <100°C 27K: <100°C

*Only the LDOTs are given.

77

III.2. PHASE BEHAVIOR AS A FUNCTION OF PRESSURE

III.2.1. LDOT-type block copolymers ($2 \leq n \leq 4$)

As explained in Chapter I, LDOT-type block copolymers are expected to display an increase in thermodynamic compatiblity with increasing pressure, which results from the denser nature of the segmentally mixed state in these materials (ΔV_{mix} or $\Delta V_{dis} < 0$). The effect of pressure on the LDOT of 136K PS-b-PPMA is illustrated in Figure III.14 where the scattering profile is shown for a fixed temperature of 190°C as a function of pressure. At this temperature and at atmospheric pressure, the block copolymer is fully microphase separated as evidenced by the sharp reflection at a wave vector $q \sim 0.0158$ Å^{-1}. However, with increasing pressure, the intensity of the reflection decreases dramatically. In fact, at pressures exceeding 0.33 kbar, the intense, narrow reflection of the ordered state changes abruptly to a broad reflection, signifying the onset of segmental mixing upon the application of pressure. Hence, at a fixed temperature of 190°C, an order/disorder transition *pressure* can be identified which lies between 0.33 and 0.5 kbar (see inset of Figure III.14). Likewise, at a fixed pressure of 0.33 kbar, an order/disorder transition *temperature* is observed at $\sim$ 190°C, as shown in Figure III.15. At atmospheric pressure, on the other hand, the transition temperature was approximately 155°C (Table III.2). This indicates that the LDOT has increased by approximately 35°C upon the application of 0.33 kbar of hydrostatic pressure, which yields a rough estimate of the pressure coefficient dT_{LDOT}/dP for the LDOT of this material of about 106°C/kbar.

Unfortunately, the pressure increments used here limit the accuracy of dT_{LDOT}/dP to

within $\pm 10^{\circ}C$.
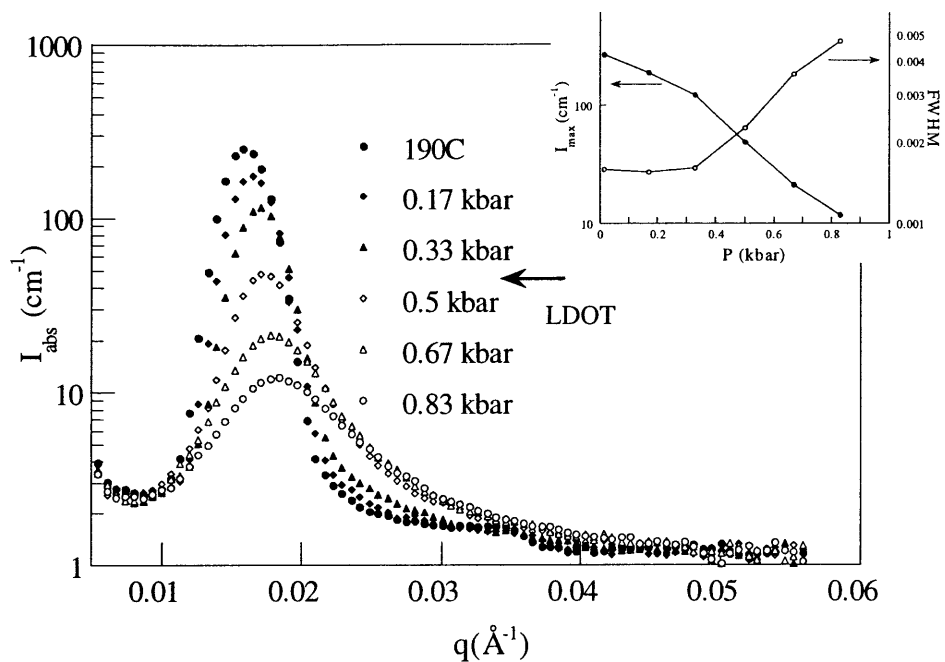
Figure III.14: Scattering intensity profile for 136K PS-*b*-PPMA at 190°C and indicated pressures
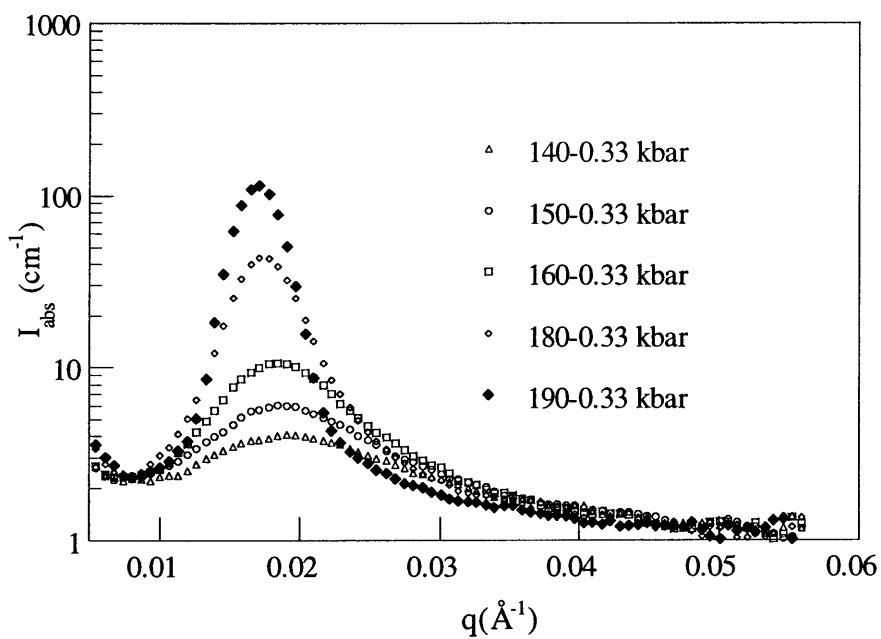
Figure III.15: Scattering intensity profile for 136K PS-*b*-PPMA at 0.33 kbar and indicated temperatures

However, it was found that a more precise estimate of this coefficient could be obtained upon constructing master curves for I_{max} and FWHM as a function of temperature by pressure-temperature superposition, as described below.

Figure III.16 shows the temperature dependence of the FWHM and peak intensity I_{max} at a series of pressures. At each pressure, the FWHM decreases and the peak intensity I_{max} increases with increasing temperature, as expected for this LDOT block copolymer. At atmospheric pressure, a discontinuous decrease in the FWHM and increase in the peak intensity I_{max} are observed between 150 and 160°C, confirming the LDOT at ~ 155°C and atmospheric pressure for this material. At 0.17 kbar, the LDOT has shifted to a higher temperature, between 160 and 180°C. Unfortunately, data taken at 170°C are missing due to a mechanical malfunction which occured at that temperature, and a finer estimate of the LDOT at 0.17 kbar can therefore not be obtained. The examination of the temperature dependence of the FWHM and I_{max} at different pressures indicates that a simple horizontal shift along the temperature axis will generate universal curves for these two parameters. The magnitude of the shift quantifies the equivalence between pressure and temperature for these block copolymers. Shown in Figure III.17 are the master curves at atmospheric pressure for I_{max} and FWHM, generated by horizontal shifting of the data from Figure III.16. The shift factor for each pressure was calculated, assuming the following linear relationship between temperature and pressure:

$$\Delta T = -\frac{dT}{dP}(P - P_o) \qquad\qquad (III.2)$$

where P_o is the reference pressure (one atmosphere) and the negative sign results from the fact that higher pressure data need to be shifted to the left (higher P is equivalent to lower T for LDOT systems). Pressure-temperature superposition using a constant value

80

for *dT/dP* of 90°C results in substantial overlap between data taken at successive

pressures, yielding master curves for I_{max} and FWHM over an extended temperature

range which display discontinuities at ~ 155°C, the LDOT at atmospheric pressure. The

coefficient *dT/dP* used in equation III.2 quantifies the equivalence between pressure and

temperature for this material, yielding a more accurate estimate of dT_{LDOT}/dP of ~

90°C/kbar. This coefficient is about 5 times greater than that obtained for the UDOT-

type systems studied thus far.[106-110]
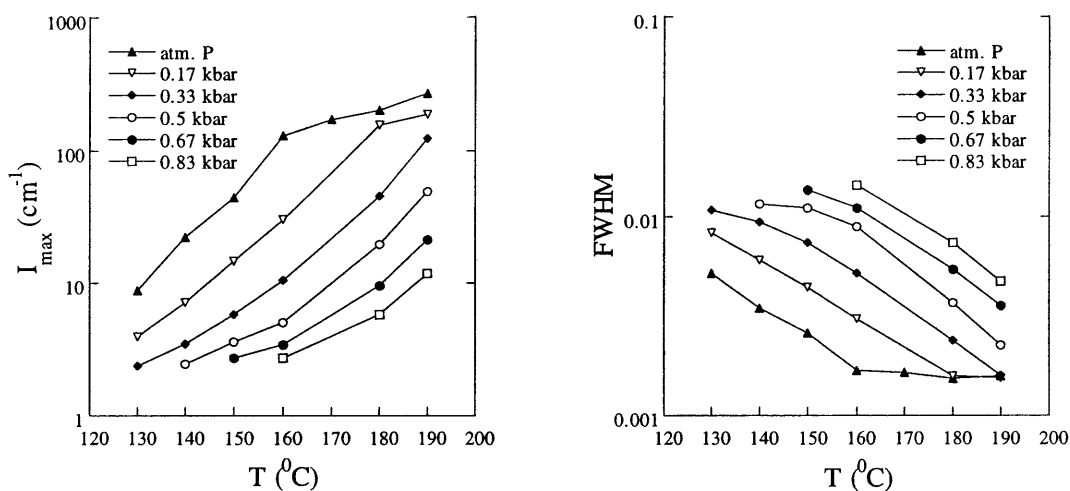
Figure III.16: T- and P-dependence of I_{max} and FWHM for 136K PS-*b*-PPMA
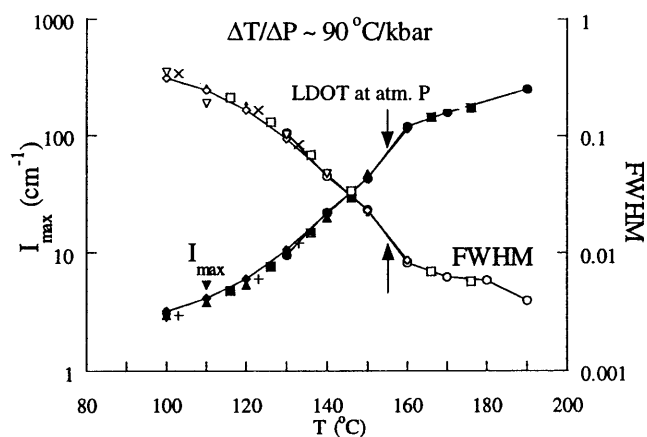
Figure III.17: Master curves for Imax and FWHM for 136K PS-*b*-PPMA

81

Similar results for ~79K PS-b-PEMA yielded a pressure coefficient dT_{LDOT}/dP of

100°C/kbar for this block copolymer, while our preliminary results obtained in

collaboration with M. Pollard and T. P. Russell had yielded an even larger coefficient of

~ 147°C/kbar for PS-b-PBMA.[82] These results indicate that hydrostatic pressure is a very

effective means of driving these LDOT-type block copolymers from the ordered to the

disordered state. In terms of the rheological properties, this means that pressure at a

constant temperature can be used to force the material to flow. Such "*baroplastic*"

behavior could be highly advantageous for processing thermoplastic elastomers.

III.2.2. UDOT-type block copolymers ($6 \leq n \leq 12$ and $n = 1$)

Although the block copolymers with long side chain methacrylates, namely, PS-b-

PHMA, PS-b-POMA and PS-b-PLMA, were found to exhibit very similar behaviors as a

function of temperature, pressure studies revealed important differences among these

materials. For UCST/UDOT-type materials, the sign of the pressure coefficient

dT_{UDOT}/dP is dictated by that of ΔV_{mix}, and, hence, by how efficiently the dissimilar

segment types can pack in the mixed state.

Figure III.18 shows the effect of pressure at a temperature of 140°C on ~ 34.3K

PS-b-PHMA. At atmospheric pressure, this block copolymer undergoes a UDOT at

162°C, and is hence fully ordered at 140°C. However, upon the application of hydrostatic

pressure at 140°C, the material undergoes an order-disorder transition, as evidenced by

the strong decrease in peak intensity and increase in peak width between 0.17 and 0.33

kbar (see inset of Figure III.18). Such a pressure-induced transition implies a negative

change in volume upon disordering (segmental mixing) for this block copolymer ($\Delta V_{mix} <$

0). Hence, although segmental mixing at atmospheric pressure is enthalpically

unfavorable, efficient packing in the segmentally mixed state leads to a strong increase in

thermodynamic compatibility upon applying pressure to this material. From the data

taken at various pressures and temperatures, master curves were constructed for I_{max} and

FWHM, as described above. A constant dT_{UDOT}/dP of -60°C was found to result in

substantial overlap of the curves obtained at a series of pressures, as shown in Figure

III.19. Despite its UDOT-type nature, this block copolymer is thus characterized by a

strong pressure sensitivity, in fact, closer to that of LDOT-type systems. This result is

very encouraging from a processing standpoint, since it points to an additional lever

which could be used in conjunction with temperature to induce flow in these UDOT-type

block copolymers. It is further in contrast with the rather weak pressure dependence

reported for all the other UDOT-type systems studied so far.
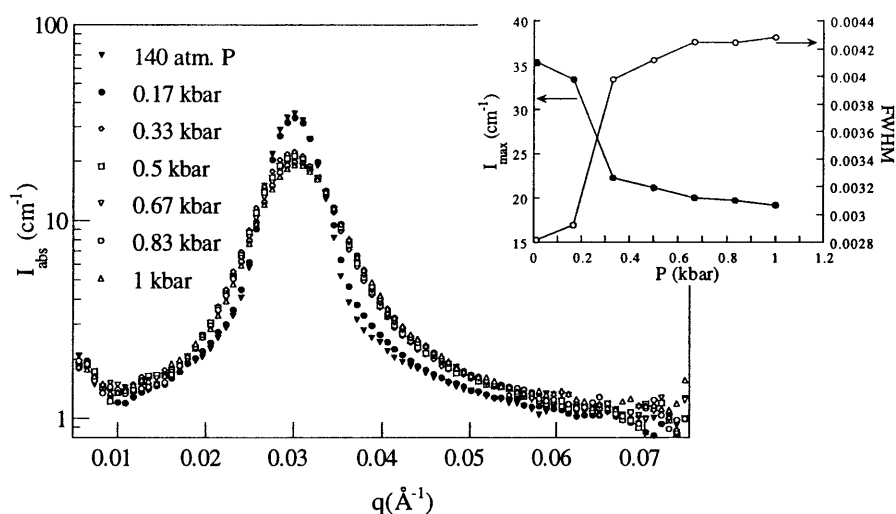
Figure III.18: Scattering intensity profile for 34.3K PS-*b*-PHMA at 140°C and
at indicated pressures.
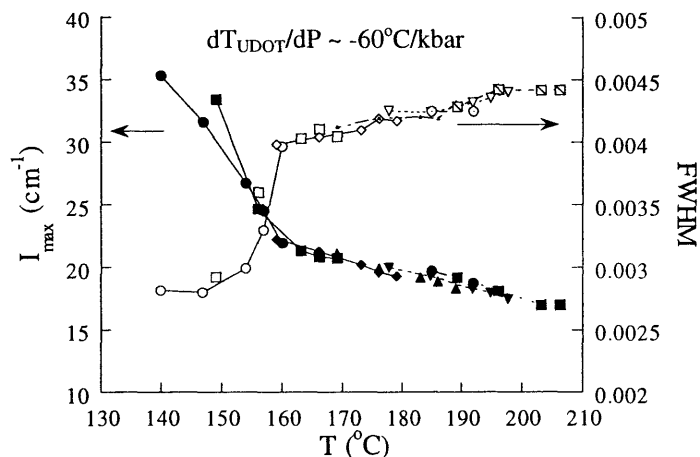
Figure III.19: Master curves for I_{max} and FWHM for 34.3K PS-*b*-PHMA

Although pressure was also found to induce miscibility in PS-*b*-POMA, pointing

to a $\Delta V_{mix} < 0$ for this system, a very small coefficient of ~ -5°C/kbar was obtained. This

decrease in dT_{UDOT}/dP upon lengthening the alkyl side chain from 6 to 8 carbon atoms is

consistent with a simultaneous increase in the unfavorable enthalpic interactions between

the two segment types (larger $\Delta \varepsilon$), and a decrease in packing efficiency in the

segmentally mixed state (ΔV_{mix} negative but smaller in magnitude). In fact, the free

energy to be gained upon squeezing the "excess volume" associated with the ordered state

of this block copolymer is so small that, at the highest pressures, the block miscibility is

actually reduced. This is evident upon considering the master curves for I_{max} and FWHM

shown in Figure III.20, constructed this time by shifting various isotherms along the

pressure axis around a reference temperature of 137°C. At the highest pressures, the peak

intensity starts to increase, while the FWHM starts decreasing. These departures from

the low pressure trend indicate that, at high pressure, the phase behavior is governed by

the increase in unfavorable interaction energy which results from the decrease in free

volume. Similar changes in the effect of pressure on thermodynamic compatibility as pressure increases have been reported by Schwann and coworkers[109] for block copolymers of PEP and PDMS.
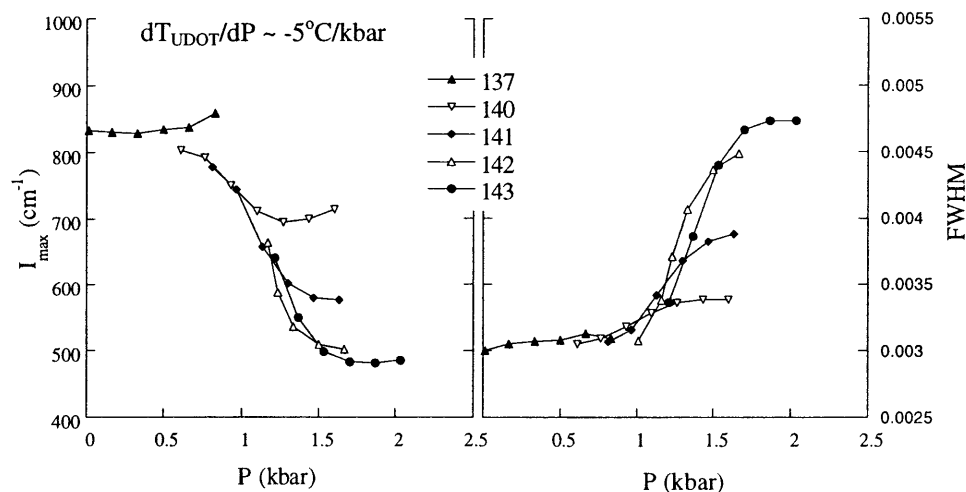
Figure III.20: Master curves for I_{max} and FWHM as a function of pressure at a reference temperature of 137°C for 27K PS-b-POMA

Based on these observations, it is in fact not surprising that upon further increasing the alkyl side chain length to 12 carbon atoms, the pressure coefficient for the UDOT dT_{UDOT}/dP actually *changes sign*. Figure III.21 shows the effect of pressure on 19K PS_{d8}-b-PLMA. This material undergoes a UDOT at atmospheric pressure at ~ 135°C, and is therefore segmentally mixed at 140°C. However, upon the application of pressure, the system becomes incompatible and undergoes an ordering transition between 0.17 and 0.33 kbar at this temperature (see inset of Figure III.21). Upon constructing the master plots for I_{max} and the FWHM shown in Figure III.22, a positive pressure coefficient for the UDOT of dT_{UDOT}/dP ~ + 13°C/kbar is obtained for this material. Thus, for this highly branched methacrylate, the incompatibility between the two blocks

85

results from increasingly unfavorable enthalpic interactions combined with inefficient

packing in the segmentally mixed state ($\Delta V_{mix} > 0$) for these two asymmetric monomers.
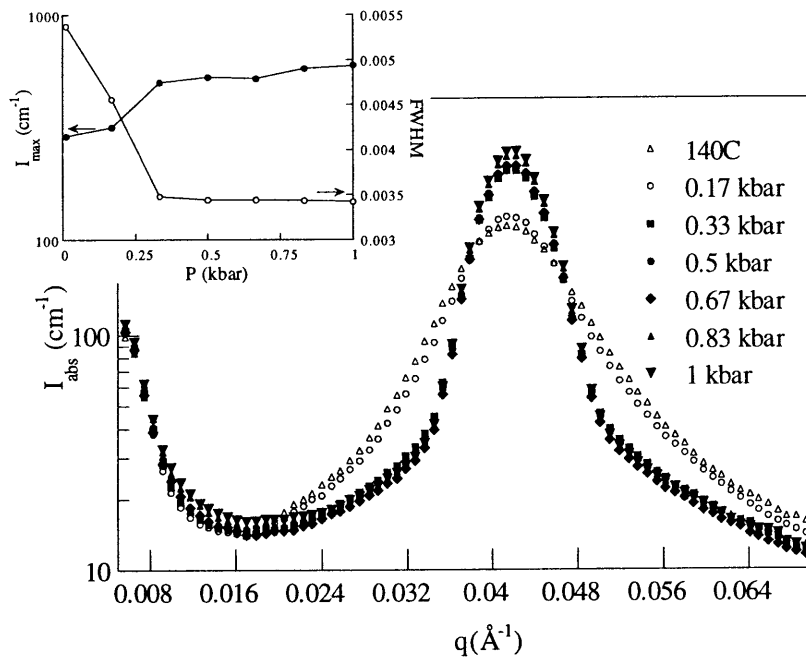
Figure III.21: Scattering intensity profile for 19K PS-b-PLMA at 140°C
and indicated pressures
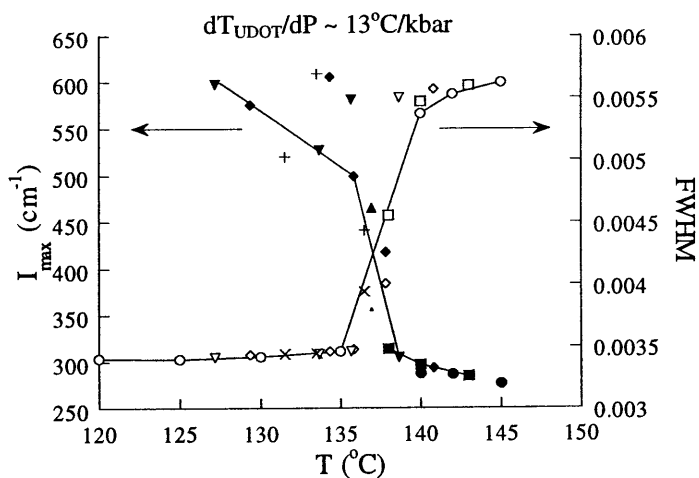
Figure III.22: Master curves for I_{max} and FWHM of 19K PS-b-PLMA at
atmospheric pressure

Similar results were obtained for PS-*b*-PMMA, the first member of the series of block copolymers investigated here. Figure III.23 shows the effect of pressure on 27.6K PS_{d8}-*b*-PMMA at 160°C. Although this block copolymer is always disordered, the distinct increase in I_{max} and decrease in FWHM points to a decrease in thermodynamic compatibility with increasing pressure for this system. Unfortunately, the ordering transition is not accessible for this material since it lies below the glass transition temperature. However, an estimate of the pressure coefficient dT/dP in the segmentally mixed state can still be obtained by superimposing the data obtained at various pressures as a function of temperature. In this manner, a pressure coefficient of ~ 23°C/kbar was extracted for PS_{d8}-*b*-PMMA.
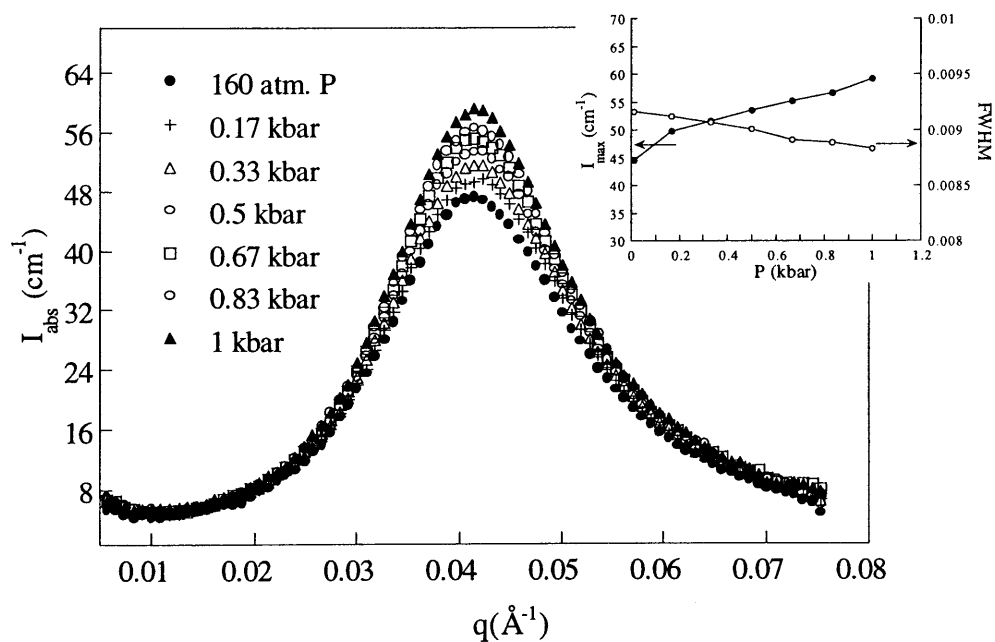
Figure III.23: Scattering intensity profile for 27.6K PS_{d8}-*b*-PMMA at 160°C and indicated pressures

III.2.3. Summary

The effect of pressure on the phase behavior of the styrene/alkyl methacrylate

block copolymers studied in this chapter is summarized in Table III.3 where the type of

phase behavior, the sign of ΔV_{mix} (change in volume upon segmental mixing or

disordering of the block copolymer) and the pressure coefficient of the ordering transition

dT_{ODT}/dP are given.

TABLE III.2: PRESSURE COEFFICIENTS OF PS-b-PnAMA

Copolymer	Type of behavior	sign of ΔV_{mix}	Pressure coefficient dT/dP (°C/kbar)
PS-b-PLMA	UDOT	+	~ 13
PS-b-POMA	UDOT	−	~ -5
PS-b-PHMA	UDOT	−	~ -60
PS$_{d8}$-b-PBMA	LDOT	−	~ 147
PS-b-PPMA	LDOT	−	~ 90
PS-b-PEMA	LDOT	−	~ 100
PS-b-PMMA	UDOT	+	~ 23

These results, combined with those obtained as a function of temperature, point to

a distinct *linkage between packing and energetics* which, for intermediate side chain

lengths, is favorable to mixing at low temperatures and leads to the LDOT. For

copolymers with longer alkyl side chains, on the other hand, the loss of compatibility at

low temperatures can be ascribed to a simultaneous increase in unfavorable interaction

energy and decrease in packing efficiency in the segmentally mixed state. This is evident

upon considering the steadily increasing enthalpic contribution to the interaction parameter χ (Figure III.7) and the change in sign of ΔV_{mix} with increasing n.

From a engineering standpoint, the large pressure coefficients of, not only the three LDOT-type systems, but also PS-*b*-PHMA, are particularly valuable. Indeed, in all four of these systems, pressure can be used effectively to force segmental miscibility and, hence, liquid-like rheological properties. The ability to molecularly engineer such pressure- and temperature-tunable thermodynamic and rheological behavior into new systems is the subject of the next two chapters of this thesis.

Chapter IV: A Predictive Tool for the Design of Block Copolymer Phase Behavior

IV.1. GC/LF Model Calculations

IV.1.1. Styrene/n-Alkyl Methacrylates

Although thermodynamic modeling of the complex phase behavior observed across the family of PS-*b*-P*n*AMA is reserved for the end of this thesis, simple group contribution/Lattice Fluid model calculations that qualitatively support the experimental findings reported in Chapter III are presented here. In the next section and in Chapter V, the use of these calculations as a predictive tool to *molecularly engineer* the phase behavior of new systems is presented.

Solubility parameters for each homopolymer used in this thesis were calculated using group contribution methods, according to Van Krevelen.[42] The details of these calculations are included in Appendix A.IV and the calculated δ for styrene and the series of alkyl methacrylates are given in Table A.IV.3. Figure IV.1 shows δ for the *n*-alkyl methacrylate homopolymers as a function of the number of hydrocarbons *n* in the alkyl side chain, ranging from $n = 1$ (PMMA) to $n = 12$ (PLMA). The value of δ for the methacrylate monotonically decreases with increasing alkyl side chain length, which is consistent with the reported decrease in the glass transition temperature[129], and indicates a progressive weakening of intermolecular interactions in this series homopolymers. An

intermediate value is obtained for polystyrene, however, which lies closest to that of

PBMA. This qualitatively supports the observation of a maximum in thermodynamic

compatibility (or minimum in $|\Delta\delta|$ or $\Delta\varepsilon$) between the styrene and the methacrylate

block for intermediate side chain lengths. For the particular formalism chosen here, the

solubility parameter analysis predicts the maximum to occur around PBMA (see inset of

Figure IV.1), while the results presented in Chapter III suggest PS/PPMA is the most

compatible system. However, the low accuracy of experimental values of δ, combined

with the strong sensitivity of calculated values on the particular formalism chosen,

complicate the use of this analysis as a quantitative predictive tool. Nevertheless, the

success of these calculations at capturing the main thermodynamic trends for this family

of materials is encouraging.
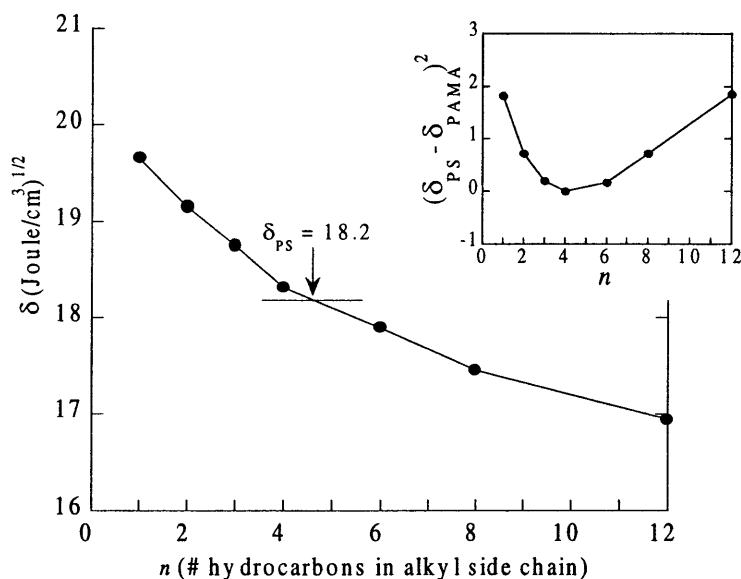
Figure IV.1: Calculated solubility parameters for poly n-alkyl methacrylates as a function of the # of hydrocarbons n in the alkyl side chain. The value for PS is indicated by the arrow. The inset represents the difference $(\delta_S-\delta_{AMA})^2$.

In fact, solubility parameters, having units of (energy/volume)$^{1/2}$, seem to precisely reflect the linkage between packing and energetics which emerged from the pressure and temperature studies presented in Chapter III. Such coupling should also be apparent in densities or *specific volumes*. Therefore, comparison of the styrene and n-alkyl methacrylate homopolymer specific volumes might shed additional light on the observed trend in phase behavior across the homologous copolymer series.

To this end, the Sanchez-Lacombe[44,66] lattice fluid (LF) model was used to predict the specific volume v_{spec} of each homopolymer as a function of temperature. Specific volume was chosen rather than segmental volume, because the former is normalized with respect to the repeating unit molecular weight, thereby reflecting better the degree of cohesion expected for a given chemistry. The LF equation of state in the long chain limit (equation I.17.b) was solved for each homopolymer for temperatures ranging from 100 to 200°C, using the equation of state parameters ρ^*, T^*, and P^* listed in Table A.IV.3 of Appendix A.IV. These were calculated for each homopolymer using the group contributions listed in Table A.IV.2.[88] Comparison with experimental PVT data was used, whenever possible, to test the accuracy of these calculations.[83] Reasonable to excellent agreement was obtained. The advantage of such analysis compared to the solubility parameter analysis presented above is its higher degree of accuracy, independent of the particular equation of state used.

Figure IV.2 represents the calculated v_{spec} for each homopolymer as a function of temperature. Again, it is seen that as the side chain length is increased from $n=1$ to $n=12$, the specific volume progresses from below (PMMA) to greatly above (PLMA) the values obtained for PS, while a close match is found for PPMA over the whole temperature

92

range. The similarity between the curves obtained for PS and PPMA is striking, although

a distinct difference in slope, and therefore in the *thermal expansion coefficients* of the

two components, is apparent. This testifies to differences in self-interaction energy and

packing efficiency for each of the components, although their resulting densities are very

similar. Such differences are ultimately the origin of the LDOT behavior in this system.
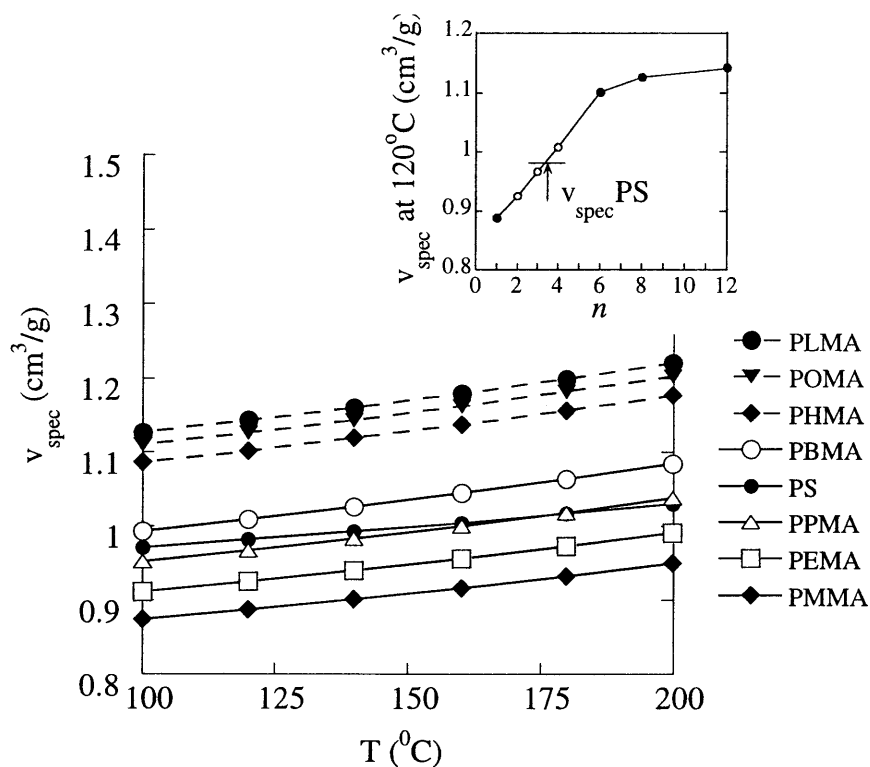
Figure IV.2: Calculated specific volumes for poly *n*-alkyl methacrylates and PS. The inset
shows the increase in v_{spec} with increasing side chain length at a fixed temperature of
120°C. The value for PS is indicated by the arrow.

In light of these results, the loss of thermodynamic compatibility for copolymers

with longer alkyl side chains can be rationalized in the following manner. First, the

magnitude of $\Delta\varepsilon$ increases with increasing number of hydrocarbons in the alkyl side

chain for $n \geq 6$, as indicated by the calculated solubility parameters. This correlates very

well with the increasing temperature-dependent portion of the fitted χ parameters in going from PS-b-PHMA to PS-b-PLMA. Additionally, the increasing mismatch in monomer structure reflected in a mismatch in specific volumes results in a decreasing ability to pack in the segmentally mixed state. This correlates very well with the observed change in sign for ΔV_{mix} from negative to positive with increasing side chain length. The group contribution calculations of v_{spec} and δ thus support a picture of increasing asymmetry in both monomer structure and self-interaction energy for $n>4$ which also emerged from the experimental investigation.

IV.1.2. Other styrene-based miscible blends

The solubility parameter δ and the specific volume v_{spec} are two homopolymer properties that reflect the degree of cohesion expected for a given chemistry. The calculations presented above further suggest that a close match in not only δ *but also* *v$_{spec}$* leads to thermodynamic compatibility of two weakly interacting homopolymers and the LDOT/LCST at high temperatures. In an attempt to confront this observation with existing literature on polymer blend compatibility, δ and v_{spec} were calculated for other homopolymers known to be miscible with polystyrene and exhibit the LCST. These systems include: PS/poly vinyl methyl ether (PS/PVME)[94,96-102,130], PS/poly cyclohexyl methacrylate (PS/PCHMA)[131-133], PS/poly cyclohexyl acrylate (PS/PCHA)[134,135] and PS/poly-*para*-phenylene oxide (PS/PPO).[103,104] The calculated δ and EOS parameters for these homopolymers can be found in Table A.IV.4 of Appendix A.IV. In fact, it is found that the same conclusions hold for these systems as well. The solubility parameters of

these four homopolymers (18.5, 18.7, 18.2 and 18.8, respectively) are close to that of PS

(18.2), while their predicted specific volumes fall within the limits of PEMA to PBMA,

as shown in Figure IV.3. Moreover, it is well known that while PVME is miscible with

PS, replacing the methyl side group by an ethyl or bulkier isobutyl group, yielding poly

vinyl ethyl ether (PVEE) and poly vinyl isobutyl ether (PVIBE), respectively, leads to

thermodynamic incompatibility and the UCST.[102,136] This trend is also successfully

captured by the GC/EOS calculations since they predict much lower values of the

solubility parameter for these ethers (17.2 and 16.55 respectively) combined with specific

volumes that exceed by far that of PBMA, as can be seen on Figure IV.3.
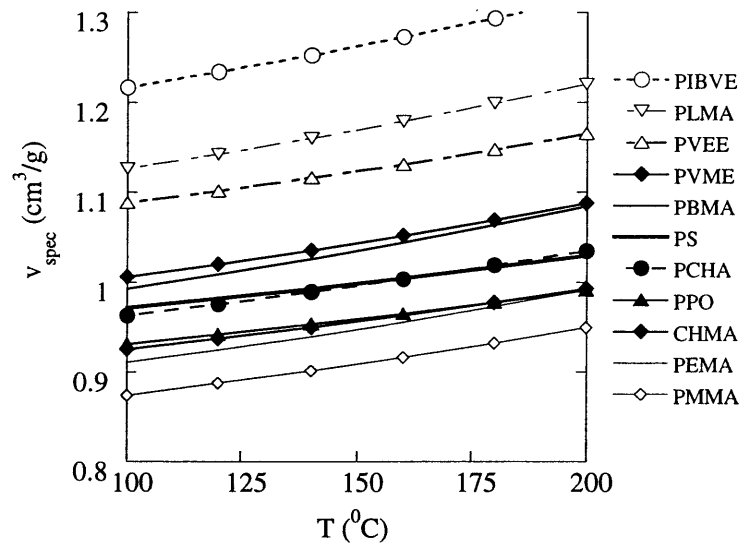
Figure IV.3: Calculated specific volumes of PVME (δ=18.5), PVEE (δ=17.2), PVIBE (δ=16.55), PCHMA(δ=18.7), PCHA (δ=18.2), PPO (δ=18.8) and PS (δ=18.2). For comparison, the values obtained for PMMA, PEMA, PBMA and PLMA are also shown.

IV.2. Molecular Design of LDOT in PS-*B*-PnAMA

IV.2.1. Anionically prepared PS-*b*-P(MMA-*r*-LMA)

The success of the group contribution calculations in capturing the general trends in phase behavior for the styrene/n-alkyl methacrylate family as well as other known miscible pairs inspired the following test of their predictive capability. A new styrene-methacrylate block copolymer that would exhibit the LDOT was designed and synthesized, whereby the methacrylate block is a random copolymer of two methacrylates that are individually immiscible with PS and also mutually immiscible, namely, MMA and LMA. It was indeed expected that the combination of a highly cohesive monomer such as MMA with a much more weakly cohesive one such as PLMA might result in a polymer with intermediate properties closer to those of PS. The composition of the random methacrylate block, denoted P(MMA-*r*-LMA), was selected by matching the specific volume and solubility parameter of the random copolymer to that of polystyrene based on the group contribution/LF EOS calculations. In keeping with the intrinsic additivity assumption of group contribution models, the random copolymer sequence distribution was neglected. Hence, the random copolymer was treated as a regular homopolymer with a repeat unit consisting of x moles of MMA and $(1-x)$ moles of LMA. A close match in δ and v_{spec}, i.e., within the bounds of EMA to BMA, can be obtained for compositions ranging from 92 to 72.5 mol% MMA (**82 to 51 wt%**). This is shown in Figure IV.4 where v_{spec} and δ (inset) are given for various

compositions of MMA in P(MMA-r-LMA). For the present exercise, a composition of

74 mol% MMA (53 wt%) was chosen, yielding a δ of 18.25 $(\text{J/cm}^3)^{1/2}$ and a v_{spec} at 120°C

of 1.0021 cm^3/g. The resulting random copolymer block is expected to have properties

similar to PBMA (δ = 18.3 $(\text{J/cm}^3)^{1/2}$, v_{spec} at 120°C = 0.99 cm^3/g). Note that the same

composition serves to match both δ and v_{spec}. The new block copolymer, denoted PS-b-

P(MMA-r-LMA), was synthesized anionically and characterized as described in Chapter

II, and has a total molecular weight of 80,000 g/mol (80K), a PDI of 1.05 and contains

50wt% of PS.
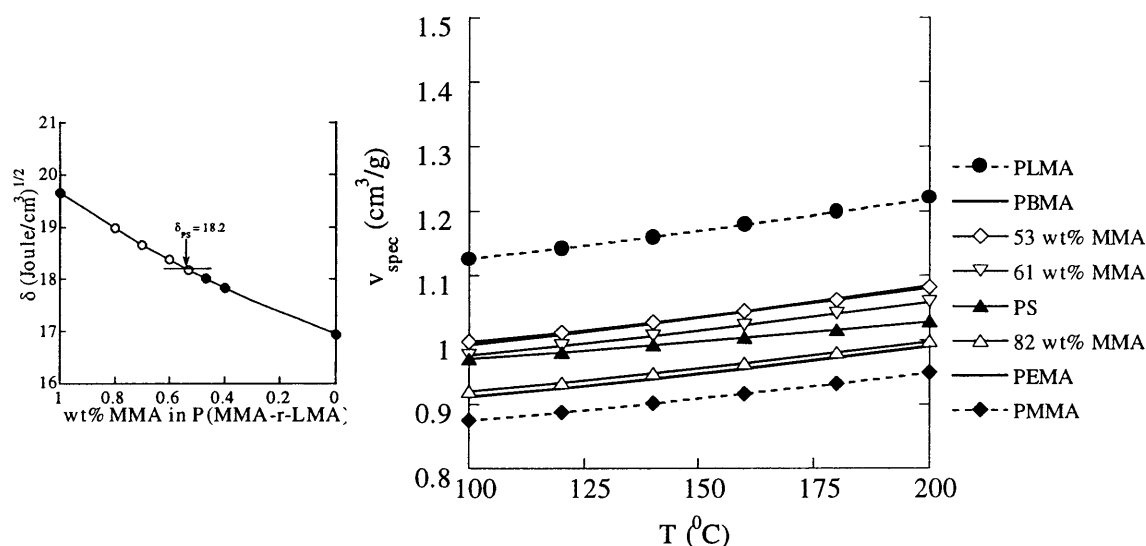
Figure IV.4: Calculated δ (left) and v_{spec} (right) of P(MMA-r-LMA)

for various compositions.

SANS profiles obtained for 80K PS-b-P(MMA-r-LMA) are shown in Figure IV.5.

Clearly, this material is in the disordered state for temperatures below 160°C, as

evidenced by the broad scattering maximum around q=0.022 Å^{-1}. Between 160 and

175°C, the peak intensifies and sharpens, indicating the onset of order and, hence, the

presence of a **LDOT** for this block copolymer. This coincides remarkably well with 85K

PS_{d8}-b-PBMA, which orders at 155°C.
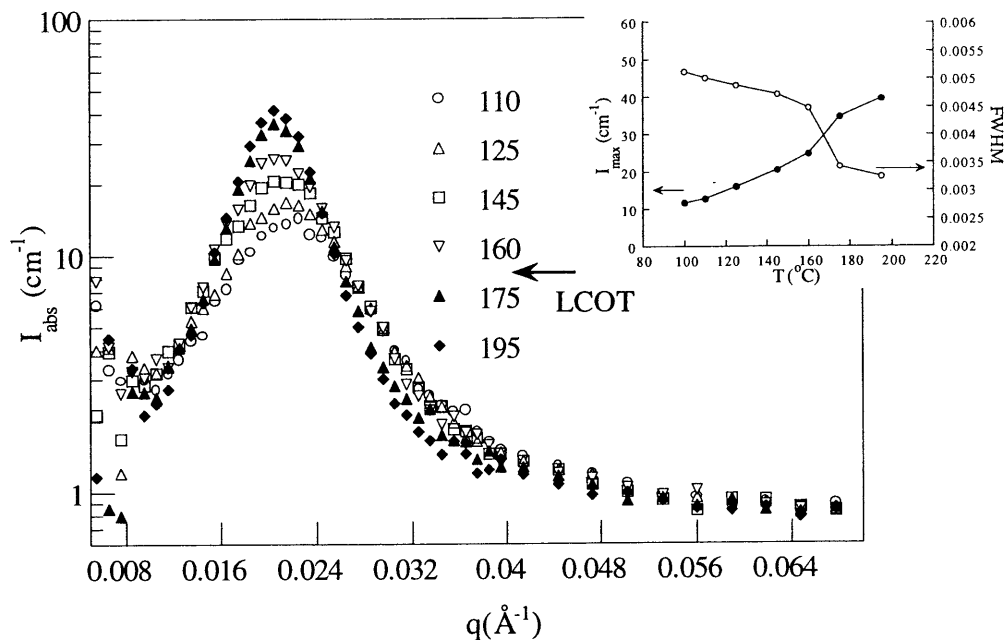
Figure IV.5: Scattering intensity profile for 80K PS-b-P(MMA-r-LMA) at indicated temperatures

The similarity in phase behavior for these two materials is further detected in the effect of pressure on the LDOT of this new block copolymer. Figure IV.6 shows the scattering profile as a function of pressure at a temperature of 165°C, at which the system is microphase separated. At this temperature, the application of as little as 0.17 kbar is sufficient to drive the system into the segmentally mixed state, as evidenced by the distinct decrease in peak intensity and increase in FWHM between atmospheric pressure and 0.17 kbar (see inset of Figure IV.6). Data obtained as a function of pressure at various temperatures yield a strong pressure coefficient of ~ **150°C/kbar** for PS-b-P(MMA-r-LMA), which can be used to construct the master plots for I_{max} and FWHM

shown in Figure IV.7. This coefficient is very similar to that obtained for PS-*b*-PBMA

and further confirms the similarity in phase behavior for these two materials. On the

other hand, the contrast between the phase behavior of PS-*b*-P(MMA-*r*-LMA) and that of

both PS-*b*-PMMA and PS-*b*-PLMA, which only exhibit the UDOT, is indisputable.
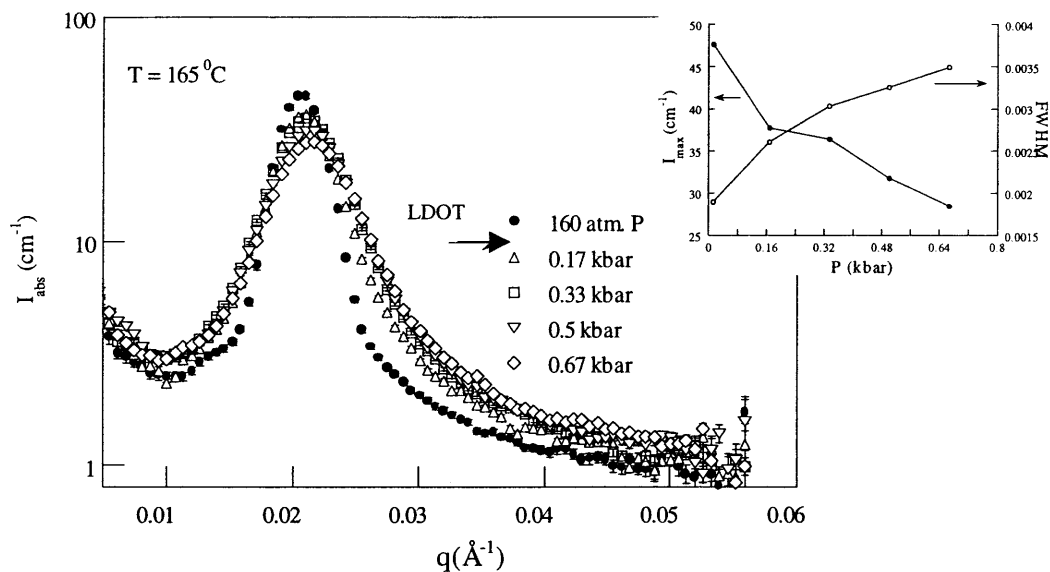
Figure IV.6: Scattering intensity profile for 80K PS-*b*-P(MMA-*r*-LMA) at 165°C
and indicated pressures
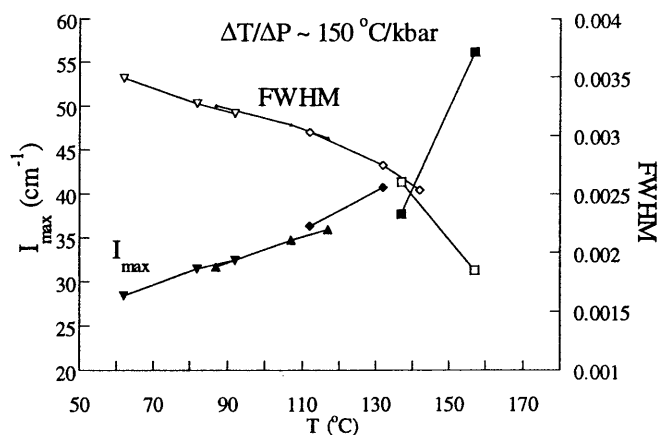
Figure IV.7: Master curves for Imax and FWHM of 80K PS-*b*-P(MMA-*r*-LMA)
at atmospheric pressure

Thus, by preparing the methacrylate block as a random sequence of *short* and

long alkyl side chain methacrylates, a new system can be designed which exhibits a

phase behavior similar to that obtained for block copolymers with *intermediate* side

chain methacrylates, namely, the LDOT and the strong pressure sensitivity which ensues.

This exercise, illustrated in Figure IV.8, suggests a simple, semi-quantitative approach to

designing the phase behavior of weakly interacting block copolymers such as

styrene/alkyl methacrylates.
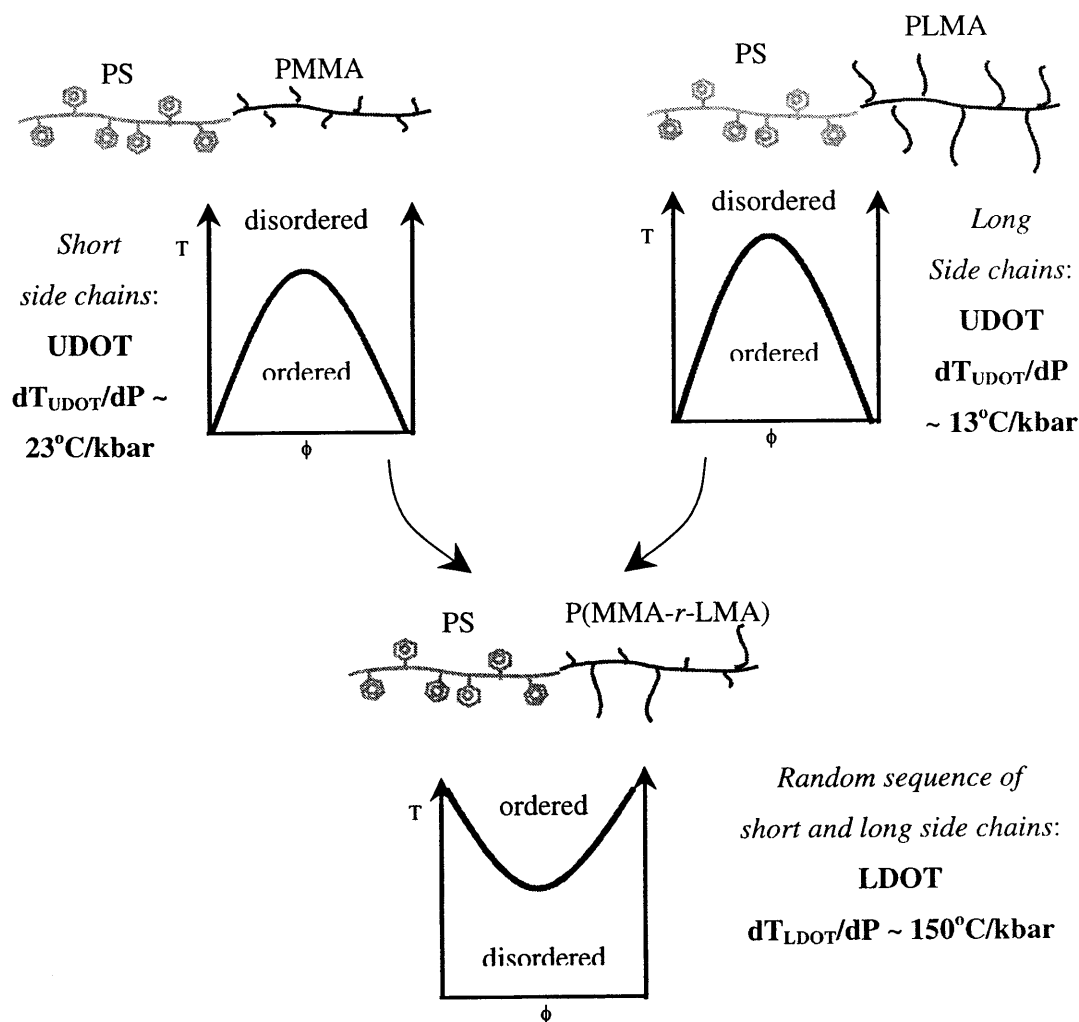
Figure IV.8: Molecular design of LDOT in PS-*b*-P(MMA-*r*-LMA)

IV.2.2. Analogy to PMMA/SAN miscible blends

In fact, a similar mechanism of mixing can be invoked to explain the widely known compatibilization of PS and PMMA through the copolymerization of styrene with acrylonitrile (AN)[137-140], methacrylonitrile (MAN)[141,142] or maleic anhydride (MAnh).[128] In all of these systems, the random copolymerization of S, which has a lower δ and larger v_{spec} than PMMA, with a more strongly cohesive and denser homopolymer such as AN (larger δ, smaller v_{spec}), results in copolymers with intermediate cohesive properties which are miscible with PMMA. This is illustrated for the PMMA/SAN system in Figure IV.9 where the solubility parameter and specific volumes of PMMA, PS, PAN and SAN are given for various compositions of the SAN copolymer. These were obtained from the group contribution/LF EOS calculations presented above and the parameters used for poly(acrylonitrile) (PAN) are given in Table A.IV.4. The compositional range over which PMMA/SAN blends are compatible and exhibit the LCST has been investigated experimentally by several authors and is reported to span 10 to 38wt% of AN. Our calculations suggest that this range corresponds to compositions for which the cohesive properties of PMMA can be matched with a combination of S and AN, thereby resulting in miscibility and the LCST as temperature increases. Curves for v_{spec} and δ entirely similar to those presented in Figure IV.9 for PMMA/SAN can be constructed for the PMMA/SMAN and PMMA/SMAnh systems. The simple predictive tool for the molecular design of miscibility in blends and block copolymers presented here can thus be generalized to other weakly interacting systems than styrene/n-alkyl methacrylates.

101
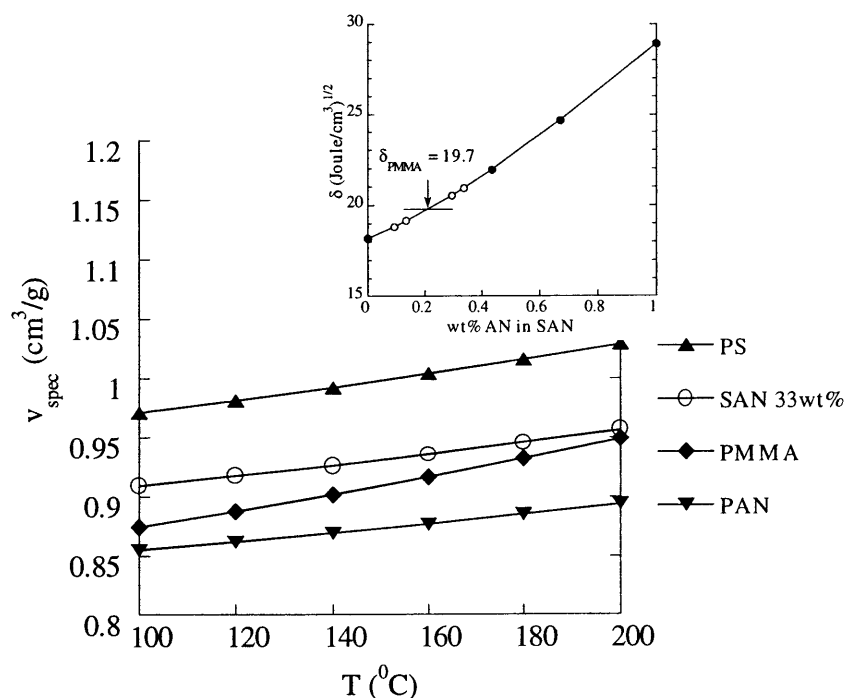
Figure IV.9: Calculated specific volumes of PS, PAN, PMMA and SAN

containing 33 wt% AN. The inset shows δ_{SAN} as a function of composition.

δ_{PMMA} is indicated by the arrow.

IV.2.3. A quantitative prediction of the miscibility window for PS-

b-P(MMA-r-LMA)

The group contribution/LF EOS calculations applied to PS-b-P(MMA-r-LMA)

indicate that a close match with the cohesive properties of PS can be obtained for

compositions ranging from **82 to 51 wt%** MMA in the methacrylate block. In an attempt

to appraise the quantitative use of this predictive tool, several additional block

copolymers between styrene and P(MMA-r-LMA) were prepared, with various amounts

of MMA in the methacrylate block. To further illustrate how the predictive tool developed in this chapter could be used in combination with more versatile and industrially amenable synthesis methods than anionic polymerization, these new block copolymers were prepared by ATRP as described in section II.1.2.b.

To confirm the ability of ATRP to produce block copolymers with phase behaviors similar to those observed for anionically synthesized materials, a control PS-*b*-P(MMA-*r*-LMA) was synthesized first, where the methacrylate block had the same composition as the anionic material studied in section IV.2.1, namely, 53 wt% MMA. Indeed, despite the increasing interest that ATRP has gained over the last 4 years, little information has been published regarding the resulting properties of block copolymers prepared in this manner. However, some important differences between ATRP and anionic polymerization that might affect phase behavior can be readily identified.

Firstly, since ATRP is a free radical polymerization method, differences in the monomer addition mechanisms and resulting tacticities can be expected which might alter thermodynamics. Secondly, ATRP block copolymers are rarely perfectly pure since removal of the transition metal halide is very difficult when the monomers used display some affinity for this catalyst. These impurities, even if present in small amounts, might affect the thermodynamics in block copolymers comprising monomers such as methacrylates, which tend to form complexes with these metallic salts. Thirdly, and perhaps most importantly, while anionically prepared block copolymers typically have small polydispersity indices (PDI) of ~1.01-1.05, the same materials lose their narrow molecular weight distribution when prepared by ATRP since the latter method is not truly living. This polydispersity in chain length further leads to compositional

polydispersity when block copolymers are prepared, since the first block has, at best,

PDI's of ~ 1.1-1.4.

Figure IV.10 shows the GPC traces of ATRP P(MMA-*r*-LMA) homopolymer

containing 53 wt% of MMA and the PS-*b*-P(MMA-r-LMA) block copolymer obtained

upon extending this material with styrene monomer. The successful preparation of a

block copolymer is evident upon considering the shift in peak position in going from the

methacrylate homopolymer to the block copolymer. Although quite broad (PDI ~ 1.315),

the molecular weight distribution of the copolymer is monomodal, precluding the

presence of substantial unreacted P(MMA-*r*-LMA) homopolymer. The average

composition of this material, as determined by NMR, is 60 wt% PS, and 53wt% MMA

within the methacrylate block. A total molecular weight of ~43,000 g/mol was extracted

from the NMR data and the molecular weight of the P(MMA-*r*-LMA) first block

determined with respect to PMMA standards (20,000 g/mol).

PS-b-P(MMA-r-LMA)
Mn ~ 43,000 g/mol
PDI = 1.315

P(MMA-r-LMA)
Mn ~ 20,000 g/mol
PDI = 1.18

elution volume (ml)
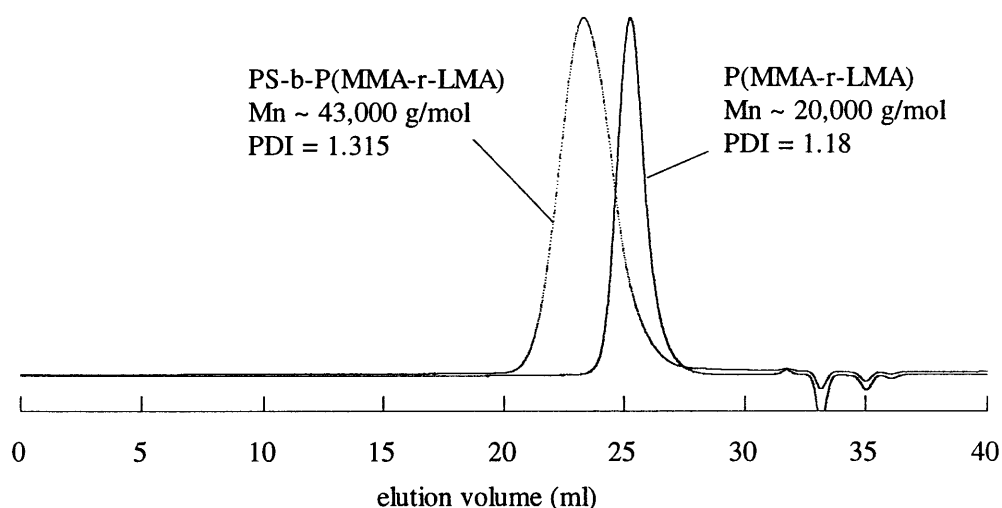
Figure IV.10: GPC trace for 43K PS-*b*-P(MMA-*r*-LMA) (ATRP)

Figure IV.11 shows the storage (G') and loss (G'') moduli of this block copolymer as a function of reduced frequency at various temperatures, time/temperature superimposed about a reference temperature of 150°C. This block copolymer is in the disordered state in the temperature range investigated (150-200°C), as evidenced by the low-frequency scaling of $G' \sim \omega^2$ and $G'' \sim \omega$. Moreover, the scattering data shown in Figure IV.12 indicate that this block copolymer indeed displays the LDOT-type phase behavior, since the peak intensity I_{max} increases and the FWHM decreases monotonically with increasing temperature (see inset of Figure IV.12). Hence, although the LDOT lies outside the experimental temperature range for this lower molecular weight material (43K versus 80K for the anionic diblock), these results indicate that ATRP can be successfully used to prepare block copolymers that behave similarly to their anionic counterparts.
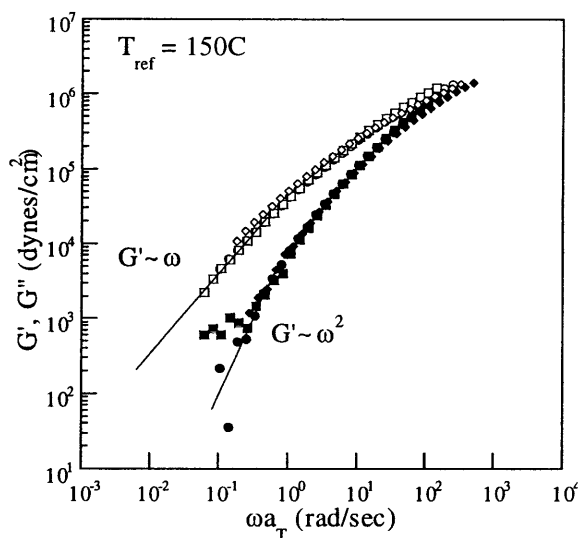
Figure IV.11: Master curves for G' and G'' for 43K
PS-*b*-P(MMA-*r*-LMA) (ATRP)
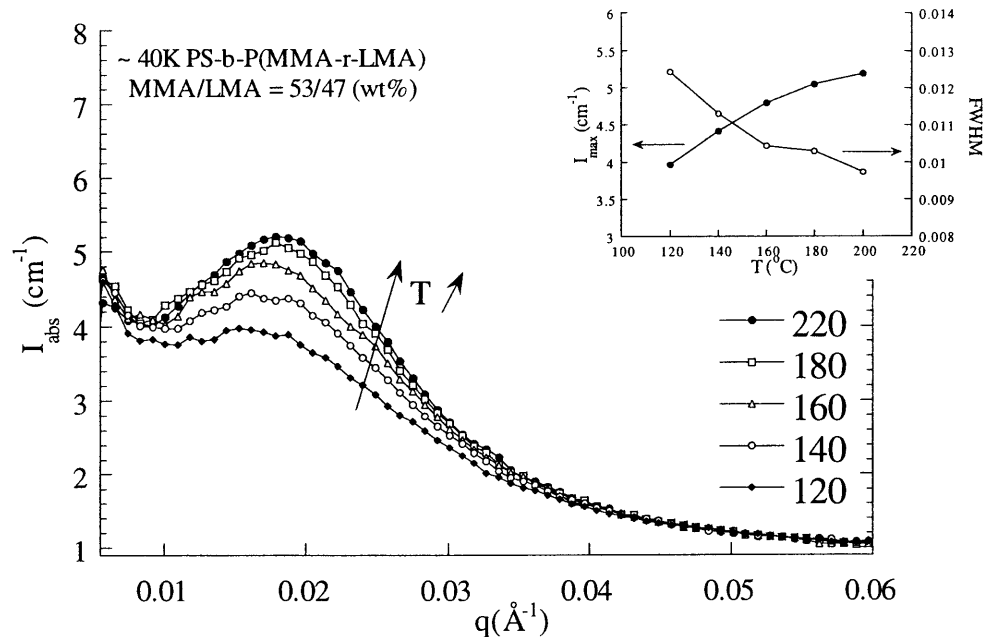
Figure IV.12: Scattering intensity profile for

43KPS-*b*-P(MMA-*r*-LMA) (ATRP)

However, an important observation to be made upon further inspection of the

scattering data presented in Figure IV.12 is the gradual increase in $q*$ as temperature

increases, which is in contrast to what is typically observed for anionically prepared

monodisperse block copolymers. Indeed, typically, $q*$, which is inversely proportional to

the preferred length scale of the local concentration fluctuations, decreases as a block

copolymer becomes less compatible, due to a gradual stretching of the copolymer blocks

away from their junction points upon approaching the ordering transition.[4,143] Here, the

opposite is observed, namely, the characteristic length scale of the local concentration

fluctuations decreases ($q*$ increases) as the strength of these fluctuations increases (I_{max}

increases). This is illustrated in Figure IV.13.a where $q*$ and I_{max}, as obtained from a

gaussian fit to the scattering data, are given as a function of temperature for this ATRP

PS-b-P(MMA-r-LMA). For comparison, the trend observed for anionically prepared PS-b-P(MMA-r-LMA) is given in Figure IV.13.b.

(a)　　　　　　　　　　　　　(b)
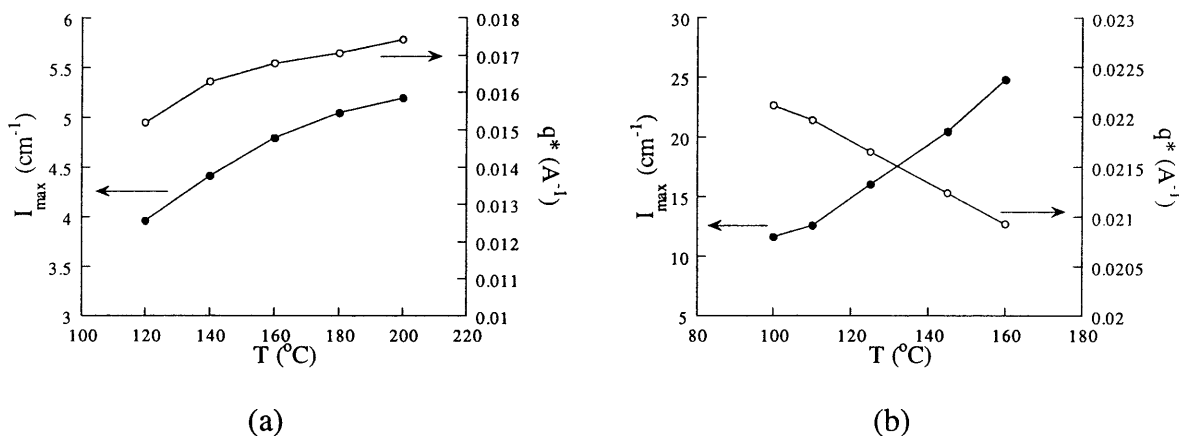
Figure IV.13: Variation of scattering peak position q^* with temperature for (a) 43K PS-b-P(MMA-r-LMA) (ATRP) and (b) 80K PS-b-P(MMA-r-LMA) (anionic)

In order to explain the anomalous shift in peak position for the ATRP block copolymer, the molecular weight and compositional polydispersity characterizing such materials must be invoked. Indeed, at low temperatures away from the LDOT, the longest copolymer chains as well as those closer to the symmetric composition are expected to undergo the strongest local concentration fluctuations since they are, at that temperature, closer to the microphase separation condition. These chains thus dictate the shape of the scattering profile at low temperature. However, as temperature increases, the shorter or more asymmetric copolymer chains also start approaching the microphase separation condition, leading to a shift of the correlation hole peak to the left, i.e., to a smaller length scale of average fluctuations . It is important to note, however, that the

system does not macrophase separate at any of the temperatures investigated, since this would lead to a strong increase in the low q scattering which is not observed here.[144] Hence, the scattering maximum observed for this polydisperse block copolymer in the disordered state can be thought of as an average correlation hole peak that, at temperatures far below the ordering transition, weights more strongly the longest copolymer chains. As temperature increases, the contribution of the shorter chains to this scattering peak increases, thus leading to a progressive shift of its position to larger $q*$ values. Ultimately, at the microphase separation transition (not observed in Figure IV.12) the system adopts an averaged domain spacing dictated by the overall entropic frustration of the distribution of copolymer chains as well as the interfacial area between the two dissimilar blocks. An analogous trend in peak position, although in the microphase separated state, was recently reported by Yamaguchi *et al.* for binary blends of two monodisperse block copolymers of different molecular weight and chain composition.[144]

Despite the effect described above, which can be reasonably ascribed to polydispersity, the overall similarity in phase behavior between PS-*b*-P(MMA-*r*-LMA) prepared by ATRP and anionic routes is manifest. A drastically different phase behavior was observed, however, upon decreasing the MMA content of the methacrylate random block from 53 to 47 wt%. Figure IV.14 shows the scattering intensity profile obtained for ~75K ATRP PS-*b*-P(MMA-*r*-LMA) where the methacrylate block contains only 47 wt% of MMA, while the total block copolymer, with a PDI of ~ 1.34, contains 58 wt% of PS. The distinct decrease in scattering intensity as temperature increases indicates that this block copolymer exhibits **UDOT**-type phase behavior. Moreover, this block

copolymer is actually found to undergo an order/disorder transition between 115 and 135°C, as evidenced by the discontinuous increase in peak width FWHM and decrease in peak intensity I_{max} (see inset of Figure IV.14). These results, summarized in Table IV.1, point to an extreme sensitivity of the phase behavior of PS-*b*-P(MMA-*r*-LMA) on the MMA content of the methacrylate block which, in fact, precisely mirrors the strong influence of the alkyl side chain length of the methacrylate block on the phase behavior of PS-*b*-PnAMA presented in Chapter III. They further indicate that, for this particular family of weakly interacting block copolymers, the predictive tool based on simple group contribution/LF EOS calculations presented above can be used quantitatively to control bulk thermodynamics and resulting rheological properties.
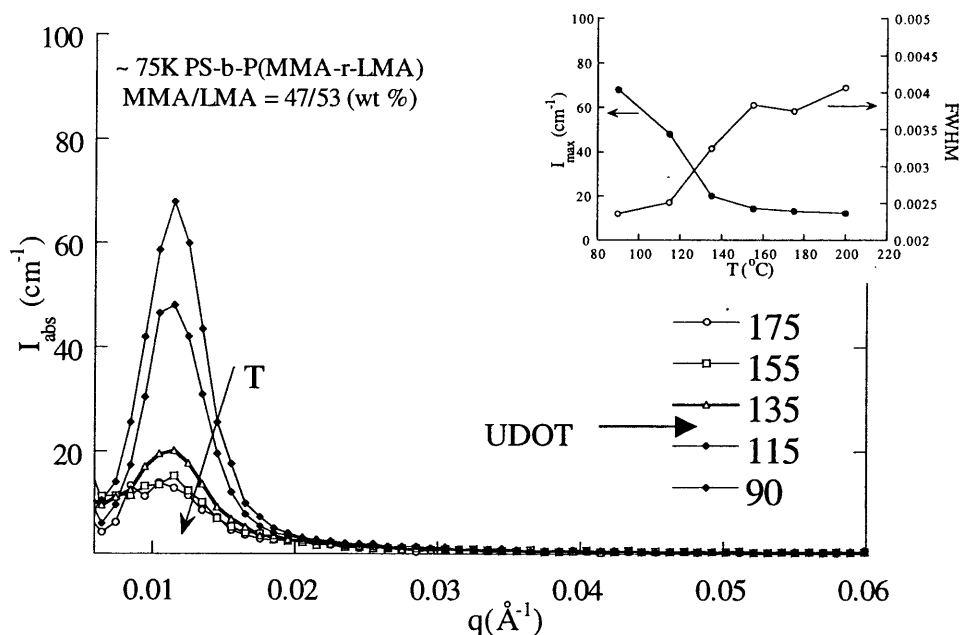
Figure IV.14: Scattering intensity profile for 75K PS-*b*-P(MMA-*r*-LMA)

TABLE IV.1. PHASE BEHAVIOR OF PS-*B*-P(MMA-*R*-LMA)

copolymer	MMA:LMA (wt %)	type of behavior
80K PS-*b*-P(MMA-r-LMA) (anionic)	~ 53:47	LDOT ~ 160°C
43K PS-*b*-P(MMA-r-LMA) (ATRP)	~ 53:47	LDOT > 220°C
75K PS-*b*-P(MMA-r-LMA) (ATRP)	~ 47:53	UDOT ~ 120°C

IV.3. DEPARTURES FROM THE GC/LF EOS CALCULATIONS

IV.3.1. Polyolefin blends and the packing length

The experimental results presented in Chapter III for the series of styrene/n-alkyl methacrylate block copolymers point to a direct relation between packing and energetics, which is further supported by the GC/LF EOS calculations presented in this Chapter. These calculations suggest that two weakly interacting systems with similar cohesive properties, represented by their solubility parameter and density, should be miscible. In fact, similar effects have been observed experimentally[53-60] and predicted theoretically[64,65,71,73] for even the simplest polymer blends based entirely on polyolefins. In these systems where the intersegmental interactions are restricted to very weak VDW (dispersive) forces, any asymmetry in monomer structure, and the local packing constraints which ensue, has an effect on blend compatibility. Therefore, only

110

components with very similar degrees of branching form miscible blends, while those with increasing structural asymmetries are characterized by large experimentally determined χ parameters.[46,60]

While these conclusions seem to relate closely to those drawn so far in this thesis, different requirements on what is referred to as "local monomer structure" can be identified. For the systems investigated in this thesis, wherein segmental interactions are not purely dispersive but can also be of the dipole/induced dipole type, it is found that solubility parameters and densities are the relevant parameters reflecting the similarity in local structure and energetics necessary for mixing. However, in blends consisting purely of polyolefins, some systems with matching densities and solubility parameters are known experimentally to form immiscible pairs. Perhaps the most compelling example is the miscibility of isotatic or atactic polypropylene (PP) with several matching copolymers of ethylene and α-olefins such as butene or hexene, while syndiotactic PP is immiscible with the same copolymers.[145] Moreover, the isotactic and atactic versions of PP are mutually miscible, while neither is miscible with its syndiotactic counterpart.[146] These observations clearly deviate from the trend identified in this thesis, since the three isomers of PP have similar predicted (based on GC/EOS) and measured[58,146] δ and v_{spec} values. However, they differ strongly in their backbone stiffness, characterized by the Flory characteristic ratio c_∞, defined as follows[37]:

$$c_\infty = \frac{\langle R^2 \rangle_o}{N_{bonds} l^2} \quad \text{or} \quad \langle R^2 \rangle_o = c_\infty N_{bonds} l^2 \tag{IV.1}$$

where $\langle R^2 \rangle_o$ is the unperturbed mean-square end-to-end distance of a polymer coil containing N_{bonds} backbone bonds of length l. Hence, the characteristic ratio c_∞ is a

measure of how extended a polymer coil is compared to a freely jointed chain of N_{bonds}

elements of length l. Alternatively, the chain dimensions and measure of chain flexibility

can also be expressed in terms of the statistical segment length a, which is related to c_∞:

$$\left\langle R^2 \right\rangle_o = c_\infty N_{bonds} l^2 = Na^2 \qquad \text{(IV.2)}$$

where N is the number of statistical segments, typically defined as the number of repeat

units or degree of polymerization, and a is the statistical length of the repeat unit. For

vinyl monomers, each repeat unit contains 2 backbone bonds and $N = 2N_{bonds}$ which leads

to:

$$a^2 = 2c_\infty l^2 \qquad \text{(IV.3)}$$

While c_∞ for the isotactic and atactic isomers of PP is about 6.0 ($a \approx 5.3$ Å), syndiotactic

PP is a much stiffer chain with a characteristic ratio of about 9.3 ($a \approx 6.6$ Å).[146] These

observations thus points to an additional requirement for miscibility in these purely van

der Waals systems besides matching solubility parameters and densities, namely, a

similarity in chain aspect ratio or backbone stiffness.

A molecular parameter that appears to captures these differences was introduced

by Witten, Milner and Wang, namely the packing length p.[147] The packing length is

defined as the total volume occupied by a chain, $V = \dfrac{M / N_{av}}{\rho}$, divided by its mean-

square end-to-end distance $\left\langle R^2 \right\rangle_o$:

$$p = \frac{M / N_{av}}{(\left\langle R^2 \right\rangle_o \rho)} \qquad \text{(IV.4)}$$

where M is the chain molecular weight (g/mol), ρ is the polymer density (g/cm^3) and N_{av}

is Avogadro's number. Since M is given by the number of segments N multiplied by the

112

segment molecular weight M_u and $\left\langle R^2 \right\rangle_o$ is given by Na^2, an alternative expression for p can be derived:

$$p = \frac{NM_u / N_{av}}{(Na^2 \rho)} = \frac{M_u / N_{av}}{a^2 \rho} \qquad (IV.5)$$

Equation IV.5 clearly shows how the packing length p captures the details of monomer structure, governed by the monomer volume $v_u = \dfrac{M_u / N_{av}}{\rho}$ and its statistical length a.

One can thus think of a polymer chain as being made up of freely jointed cylinders of diameter d, volume v_u and length a. Given this model of the polymer chain, the packing length p is thus related to the monomer aspect ratio (d/a) and length a as follows:

$$p = \frac{M_u / N_{av}}{a^2 \rho} = \frac{v_u}{a^2} = \frac{a \pi d^2 / 4}{a^2} \approx \left(\frac{d}{a}\right)^2 a \qquad (IV.6)$$

Polymers made up of long and/or skinny monomers, such as linear PE, are thus characterized by a small packing length, while fat repeat units, such those of branched polymers, have large packing lengths.[125,148,149]

Isotatic and atactic PP have very similar packing lengths (3.24 and 3.12 Å respectively), while the syndiotactic isomer has a much smaller packing length of 2.12 Å. While these differences are related to variations in the effective backbone stiffness (different c_∞) for these three isomers of PP, their direct consequence on blend miscibility arises from differences in the local intermolecular packing of the two components in the blend. These differences in packing in turn affect the enthalpic interactions between the hydrocarbon units in the mixed state and hence miscibility.

More generally, it has been shown that, for the most part, when the packing lengths of two polyolefins are nearly identical, miscibility is observed.[148] This correlation

is further supported by the recent PRISM calculations carried out by Schweizer and

Singh.[72] These calculations indeed show that in polyolefins, where segmental

interactions ε_{ij} are very small, local intermolecular packing and, hence, the blend

cohesive energy density strongly depend on the chain aspect ratio. This translates

mathematically into an inverse proportionality relationship between the experimentally

determined solubility parameter (based on SANS experiments on several polyolefin

blends known to mix regularly) and the packing length p:

$$\delta_{SANS} \propto (1/p)^{1/2} \propto \left(1 \middle/ \frac{M_u}{\rho a^2} \right)^{1/2} \tag{IV.7}$$

This relation, which appears to be verified experimentally for a limited series of saturated

polyolefins[148], points to a dependence of the solubility parameter of these polymers on not

only the density and monomer molecular weight, but also c_∞ or a. The dependence of

the cohesive energy density (δ^2) on polymer density ρ and monomer molecular weight

M_u is natural since:

$$\delta = \left(\frac{E_{coh}}{V_m} \right)^{1/2} \tag{IV.8}$$

where E_{coh} is the energy required to vaporize a mole of polymer chains (J/mol) and V_m is

the molar volume of the polymer (cm^3/mol). E_{coh} is related to the molar segmental

interaction energy ε (J/mol) and the degree of polymerization as follows:

$$E_{coh} = -\frac{1}{2} N z \varepsilon \tag{IV.9}$$

where N is the number of segments (or repeat units) in the polymer chain and z is the

number of nearest neighbors of a segment. The molar volume, on the other hand, is given

by:

$$V_m = \frac{M}{\rho} = \frac{NM_u}{\rho} \qquad\qquad\qquad\qquad (IV.10)$$

and, hence, δ reads:

$$\delta = \left(-\frac{1}{2}\frac{Nz\varepsilon}{NM_u}\rho \right)^{1/2} = \left(-\frac{1}{2}\frac{z\varepsilon\rho}{M_u} \right)^{1/2} \qquad\qquad (IV.11)$$

The proportionality expressed in equation IV.7, compared to equation IV.11, thus points

to an additional dependence of the experimentally determined δ_{SANS} for polyolefins on

the statistical segment length a, besides the parameters which naturally influence the

cohesive energy. However, it is important to note that, for the polyolefins satisfying

equation IV.7, c_∞ and, hence, a are a direct function of M_u.[148] Indeed, from the data

presented by the authors, the following approximate scaling can be extracted:

$$\langle R^2 \rangle_o / M = c_\infty l^2 / M_u \propto \frac{1}{M_u^\nu} \qquad\qquad\qquad (IV.12)$$

where M and M_u are in g/mol and the exponent ν is approximately 1.5. Upon inserting

this relationship between coil dimensions and repeat unit molecular weight for those

polyolefins into equation IV.4, the packing length becomes:

$$p = \frac{M}{\langle R^2 \rangle_o \rho} \propto \frac{M_u^\nu}{\rho} \qquad\qquad\qquad (IV.13)$$

and equation IV.7 then simply expresses a relationship comparable to that given by

equation IV.11 and expected based on the definition of cohesive energy.

While the concept of matching packing lengths presented above seems to hold for

several saturated polyolefins, a remarkable exception to this trend was found for systems

involving polyisobutylene (PIB). Indeed, it was recently found that PIB is highly

compatible with head-to-head PP (hhPP), while it is immiscible with regular PP (atactic

115

or isotactic).[56] Moreover, all the miscible blends containing PIB where found to undergo phase separation upon heating through a LCST, in contrast with most of the other polyolefin blends, which exhibit the UCST. The packing lengths of PIB, hhPP and PP are ~3.1-3.5, ~2.8 and 3.2 Å, respectively. Hence, based on the packing length criterion, a higher degree of thermodynamic compatibility would be expected for PIB/PP blends. However, PVT measurements on these materials further indicate that hhPP has a higher density and solubility parameter than PP, in fact, closer to those of PIB.[58] This indicates that, while the packing length criterion does not apply for blends of PIB and hhPP, a similarity in their cohesive properties is still found. Similar conclusions can be further drawn for unsaturated polyolefins. Indeed, while polyisoprene (PI) and polybutadiene (PB) have similar densities and solubility parameters, their packing lengths strongly differ (3.2 and 2.29 Å respectively)[148] and, yet, their blends and block copolymers are miscible and exhibit the LCST/LDOT.[150] Hence, for these unsaturated polyolefins, a similarity in packing length no longer seems to correlate with miscibility.

The lack of such correlation is further found for systems that are not purely dispersive. For example, polystyrene and poly vinyl methyl ether (PVME) have very dissimilar packing lengths (4 and 2.72 Å respectively[148]) but similar solubility parameters and densities, and their miscibility in the melt has been extensively reported. Moreover, while the effect of tacticity on miscibility in this system has been investigated by several authors,[100,101] it is, in magnitude, modest in comparison with blends of PP. Finally, while the small changes in local packing and cohesive energy density resulting from deuteration of one of the two components profoundly affect miscibility in polyolefins,[57] their effect on miscibility in systems such as PS/PVME or PS/PBMA are minor. Thus, as the

strength of intersegmental interactions increases, the stringent condition of complete similarity in the details of monomer structure found for polyolefins is progressively relaxed. Instead, more macroscopic parameters such as the density and the solubility parameter seem sufficient to capture the thermodynamic trends in these systems.

IV.3.2. Specific interactions

Besides certain polyolefins, a second category of blends was identified which does not seem to follow the miscibility criterion identified in this thesis for styrene-based systems. Examples include blends of PMMA and polyvinylidene fluoride (PVDF), as well as blends of methacrylates or acrylates and halogenated vinyl polymers such as PVC.[151-153] The well known miscibility of these systems has been attributed to strong specific interactions between the polar groups of these monomers. For such systems characterized by stronger interactions, i.e. dipole/dipole or even H-bond interactions, miscibility no longer seems to require a close match in density or solubility parameter. This is evident upon considering the calculated v_{spec} and δ of these homopolymers, shown in Figure IV.15. Clearly, PVC, with a δ of 21.73 $(J/cm^3)^{1/2}$ and a much lower v_{spec} (higher density) than PMMA, does not match at all several of the methacrylates with which it is reported miscible, namely, PMMA to PHMA ($n=1$ to $n=6$). PMMA/PVDF similarly lack any trend of close match in cohesive properties (Figure IV.15). Hence, for these systems characterized by increasingly energetically favorable interactions, compared to polyolefins and styrene-based systems, the requirement of similarity in monomer structure and cohesive energy density appears to be further relaxed. This is not

surprising, however, since the main driving force for miscibility in these systems is

believed to be a *negative enthalpy of mixing* ($\Delta\varepsilon < 0$), rather than favorable packing in

the segmentally mixed state ($\Delta\varepsilon \geq 0$ but small and $\Delta V_{mix} < 0$).

	δ
PHMA	17.9
PBMA	18.3
PPMA	18.7
PEMA	19.2
PMMA	19.7
PVC	21.7
PVDF	?
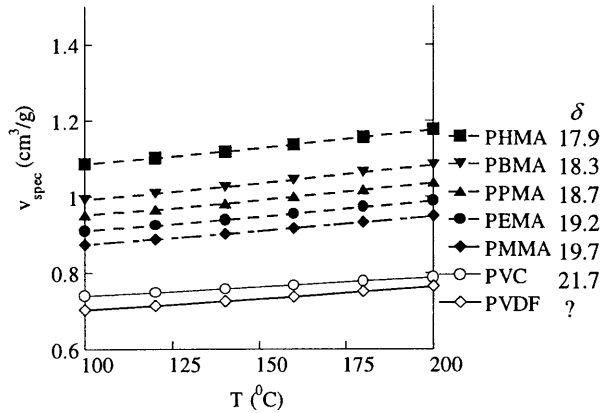
Figure IV.15: Calculated v_{spec} for the PnAMA/PVC and PMMA/PVDF pairs

IV.3.3. Summary

Based on these observations and those presented in section IV.3.1, two regimes

are thus identified for which matching δ and v_{spec} is not necessarily a sufficient or valid

criterion for miscibility. These correspond to purely VDW systems and, at the other end

of the spectrum, strongly interacting systems. In the former, segmental interactions are

very weak and miscibility entirely relies on local details of monomer structure and

segment packing. This appears to result in an additional requirement for miscibility

besides matching cohesive properties, namely, a similarity in backbone flexibility. In the

latter, thermodynamic compatibility results from favorable enthalpic interactions and is,

therefore, less dependent on the cohesive properties. Intermediate to these two extremes

are the styrene-based systems investigated in this thesis and others reported in the

literature. This is summarized graphically in Figure IV.16, where various systems have

been ranked according to the type of segmental interactions that prevail, namely, dispersive, dipole/induced dipole, dipole/dipole and H-bond interactions. The left end corresponds to purely VDW systems, while blends with specific interactions are found on the right side. The factors governing miscibility in each of the three regimes shown in Figure IV.16 are also listed. Hence, the criterion of matching δ and v_{spec} identified in this thesis seems to hold best for non-purely VDW weakly interacting systems. However, its zone of influence has been extended to purely VWD systems. Indeed, while there are some examples of immiscible polyolefin pairs with matching δs and v_{spec}'s but dissimilar packing lengths, no miscible blend could be found that consists of two polyolefins with very dissimilar δs and v_{spec}'s but similar packing lengths. Hence, in these VDW polymer blends, a similarity in δ and v_{spec} is apparently a necessary but not sufficient criterion for miscibility.

Increasing strength of segmental interactions
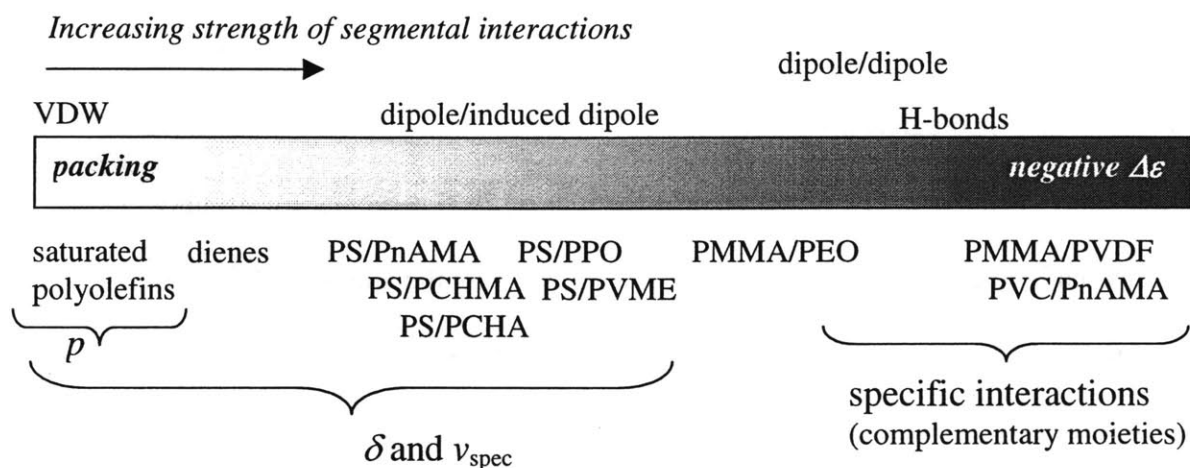
Figure IV.16: Spectrum of miscible polymer pairs and molecular parameters governing thermodynamic compatibility

119

CHAPTER V: NEW "*BAROPLASTIC*" ELASTOMERS AND ADHESIVES BASED ON STYRENE AND ALKYL ACRYLATES

In this chapter, the predictive tool for the design of miscibility into weakly interacting systems presented in Chapter IV is further applied to the molecular design of pressure- and temperature-tunable ordering transitions into attractive candidate thermoplastic elastomers and adhesives based on styrene and alkyl acrylates. Alkyl acrylates with low glass transition temperature ($T_g < 0^{\circ}C$), such as polyethylacrylate (PEA) and polybutylacrylate (PBA), are workhorses of the adhesives industry, often preferred over their polyolefin-based counterparts due to their greater stability (saturated backbone) and ability to wet a wider variety of surfaces, including polar ones such as glass, silicon etc.[9,154] Moreover, their block copolymerization with a stiffer second block such as polystyrene would result in thermoplastic elastomers with highly attractive adhesive and rheological properties, combining tackiness, adhesion and cohesive strength.[155] Unfortunately, living polymerizations of alkyl acrylates are strongly hampered by the termination reaction involving nucleophilic attack by the α-carbon.[117] So far, the preparation of block copolymers comprising an acrylate homopolymer has therefore been, at best, very limited. However, these materials can, for the first time, be readily prepared using more flexible controlled "living" free radical synthesis methods such as ATRP, described in Chapter II. The preparation of such materials and the possibility of designing their phase behavior and resulting rheological properties using the group contribution/LF EOS calculations described in Chapter IV is presented here.

V.1. GC/LF EOS CALCULATIONS FOR STYRENE/N-ALKYL

ACRYLATES

Figure V.1 shows the solubility parameter δ as a function of alkyl side chain

length (n) for a series of poly(n-alkyl acrylate) homopolymers (PnAA), while the value

for PS is indicated by the arrow. For comparison, the values obtained for the

corresponding methacrylates (PnAMA) are also given. Although systematically higher,

the values of δ for the acrylates are found to follow a trend similar to that observed for

the methacrylates. Indeed, it is again found that, upon increasing the side chain length, δ

for the acrylate homopolymer progresses from above (poly methyl acrylate = PMA) to

greatly below (poly lauryl acrylate = PLA) δ for PS, while a close match is obtained, this

time between $n=4$ and $n=6$. Likewise, the specific volume v_{spec} of the acrylates shown in

Figure V.2 is found to progress from below (PMA) to above (PLA) that of PS, while a

close match is obtained for $n=3$. The parallelism between the curves for δ and v_{spec}

obtained for the acrylates and those obtained for the methacrylates is manifest, suggesting

that a similar trend in phase behavior as a function of alkyl side chain length might be

expected for this new family of block copolymers. Indeed, based on the GC/EOS

calculations presented in Figures V.1 and V.2, one would expect thermodynamic

incompatibility and the UDOT for block copolymers containing short ($n=1$, PMA) and

long ($n>6$, PHA, POA, PLA) alkyl side chain methacrylates. For intermediate side chain

acrylates such as poly(butyl acrylate) (PBA), on the other hand, some degree of

121

thermodynamic compatibility and the LDOT might result from the closer mach of their

cohesive properties with those of PS.
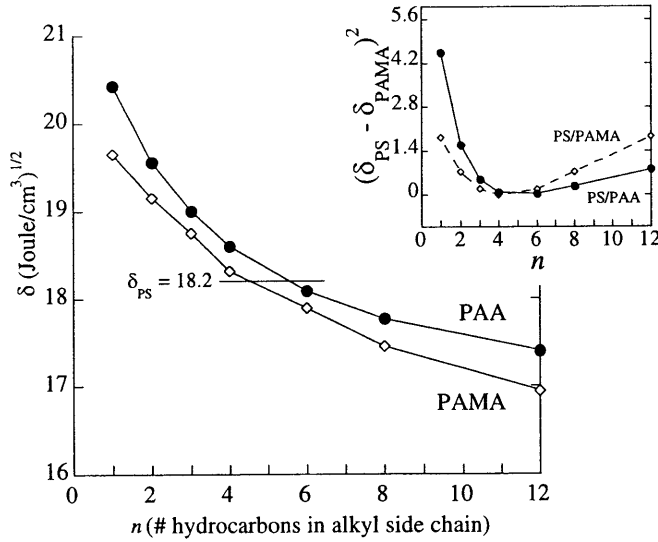
Figure V.1: δ for PnAA compared to PS and PnAMA
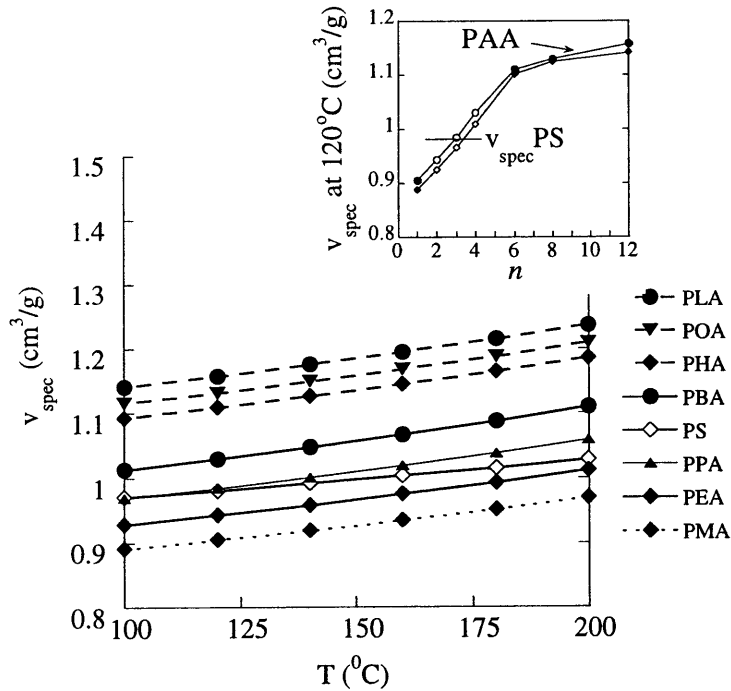
Figure V.2: v_{spec} for PnAA compared to PS and PnAMA

To verify this hypothesis, and perhaps identify new candidate *"baroplastic"* elastomers, a series of polystyrene-*block*-poly *n*-alkyl acrylates, denoted PS-*b*-PnAA, was

synthesized by ATRP and their phase behavior was characterized, for the first time, by dynamic rheological testing and SANS. These block copolymers are listed in Table V.1, along with their molecular characteristics. The characterization of their phase behavior as a function of temperature and pressure are the subject of the next two sections.

TABLE V.1: CHARACTERISTICS OF THE ATRP PS-*B*-PNAA

copolymer	M_n (kg/mol)	M_w/M_n	PS (wt %)	remarks
33K PS-*b*-PMA	33	1.32	65	-
65K PS-*b*-PHA	65	1.40	48	-
64K PS-*b*-PBA	64	1.31	53	-
100K PS-*b*-PBA	100	1.2	70	-

V.2. T-DEPENDENCE OF PHASE BEHAVIOR IN PS-B-PNAA

V.2.1. Copolymers with short (*n*=1) and long (*n*≥6) side chains

Figure V.3 shows the master curves for G' and G'' for 33K PS-*b*-PMA containing 65 wt% PS, time-temperature superimposed around a reference temperature of 150°C. Based on the scaling of the data at low frequencies, namely $G' \sim \omega^{0.85}$ and $G'' \sim \omega^{0.7}$, it appears that this block copolymer remains ordered throughout the experimental temperature range, even for this very low molecular weight.

Figure V.3: Master curves for

G' and G'' for

33K PS-b-PMA

$T_{ref} = 150C$

$G',\ G''\ (dynes/cm^2)$

$\omega a_T\ (rad/sec)$

G'

G''

$G'' \sim \omega^{0.7}$

$G' \sim \omega^{0.85}$

●	140
○	140
■	150
□	150
◆	160
◇	160
▲	170
△	170
▼	180
▽	180
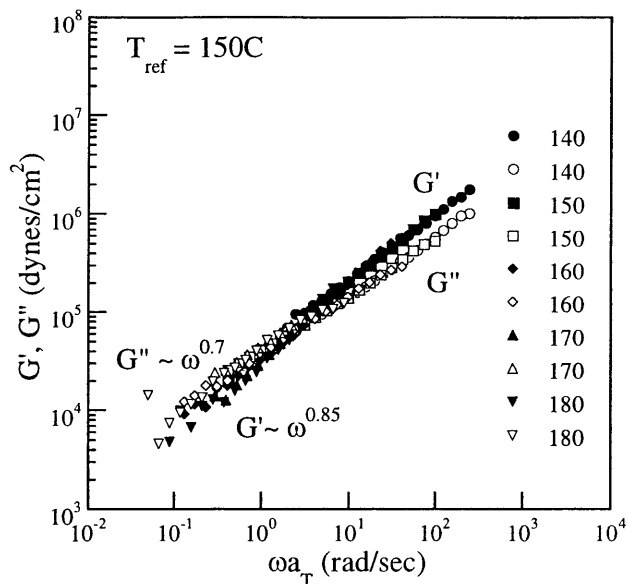
The stability of the ordered state for this block copolymer is further confirmed by the very sharp maximum of the scattering profile shown in Figure V.4. It is important to note that, although the scattering peak shown in Figure V.4 is very sharp at all temperatures, the total level of scattering for this block copolymer is very low. This apparent contradiction can be elucidated, however, upon considering that the 2-D scattering pattern for this material (not shown here) was highly anisotropic. This points to a large degree of alignment of the ordered microdomains for this melt-pressed diblock copolymer. Such tendency to align under the flow field developed upon melt-pressing in the fully molten state was observed for several of the block copolymers studied in this thesis and was found to result in preferential orientation of the lamellae in the sample plane. This preferential orientation, which is perpendicular to the incident neutron beam, can result in a dramatic lowering of the scattered intensity compared to an isotropic sample. The persistence of an anisotropic microstructure at all temperatures for 33K PS-b-PMA further confirms the stability of the ordered state for this low molecular weight

block copolymer. These results thus point to a large degree of thermodynamic incompatibility for PS-*b*-PMA, which was expected, based on the GC/EOS calculations presented above and the thermodynamic incompatibility reported for blends of the same components.[25] They further indicate a similarity between the phase behavior of this system and that reported for PS-*b*-PMMA, which is also ordered for similar molecular weights.[32]

Figure V.4: Scattering intensity profile for 33K PS-*b*-PMA
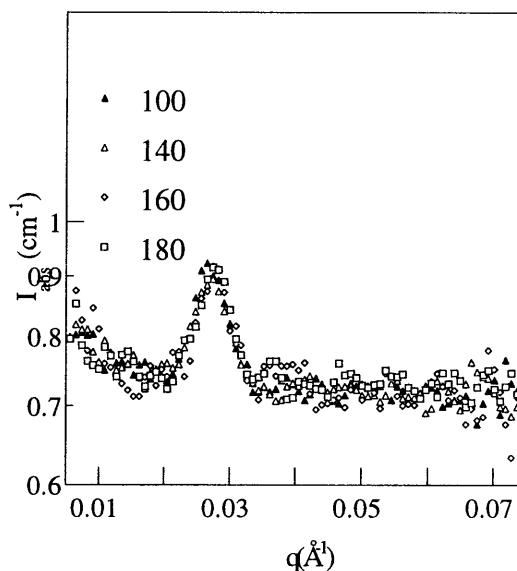
A similar degree of incompatibility was obtained for PS-*b*-PHA. Figure V.5 shows the scattering intensity profile as a function of temperature for 65K PS-*b*-PHA containing 48 wt% of PS. The two reflections observed at wave vectors $q \sim 0.0127$ Å^{-1} and $q \sim 0.024$ Å^{-1} for this material indicate the presence of an ordered state at all temperatures. Although the order/disorder transition lies outside the experimental temperature range for this molecular weight, this block copolymer exhibits a UDOT-type phase behavior, as evidenced by the monotonic decrease in peak intensity I_{max} and increase in FWHM of the first order reflection as temperature increases (see inset of Figure V.6). Based on these results and the GC/EOS calculations presented above,

UDOT-type phase behavior with even larger degrees of thermodynamic incompatibility can be reasonably expected for block copolymers formed from styrene and longer alkyl side chain acrylates, which were therefore not studied in this thesis.
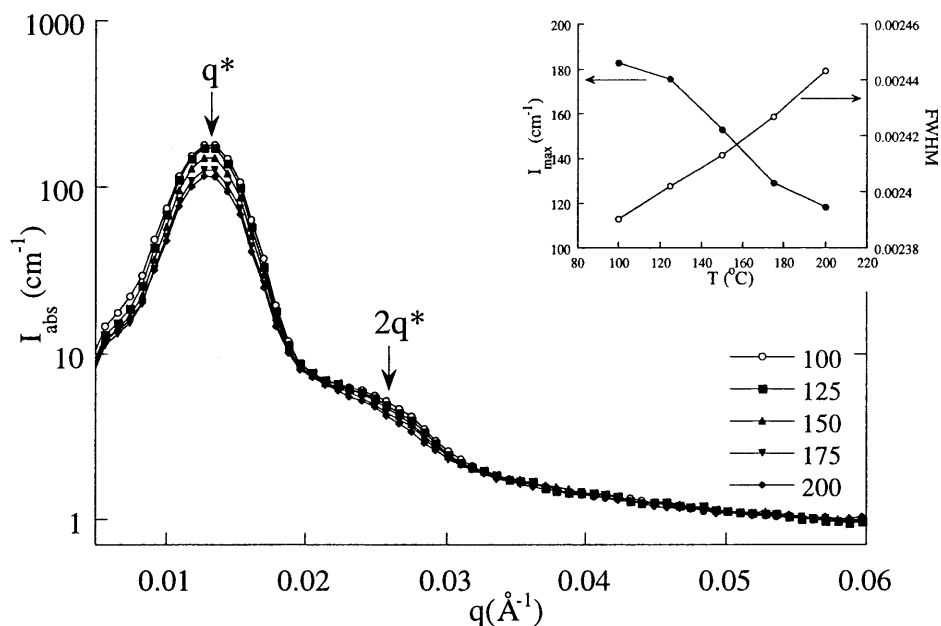
Figure V.5: Scattering intensity profile for 65K PS-*b*-PHA

V.2.2. Copolymers with intermediate side chains

In contrast to the materials presented above, a higher degree of thermodynamic compatibility and a phase behavior very much similar to that observed for PS-*b*-PBMA was found for PS-*b*-PBA. Figure V.6 shows the master curves for G' and G'' at a reference temperature of 150°C for 64K PS-*b*-PBA containing 53 wt% of PS. From the low frequency scaling of G' and G'', namely $G'' \sim \omega^1$ and $G' \sim \omega^2$, it is inferred that this block copolymer is disordered over the temperature range investigated (140-200°C). This

is in contrast to PS-*b*-PHA which, for similar molecular weight and composition, is

ordered throughout the temperature range. To identify the type of phase behavior,

namely UDOT versus LDOT, SANS measurements were performed on this block

copolymer.
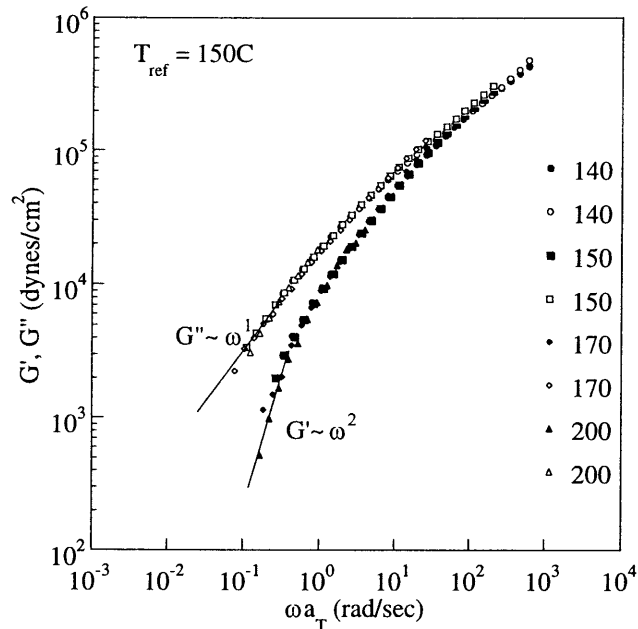
Figure V.6: Master curves for G' and G'' of 64K symmetric PS-*b*-PBA

Figure V.7 shows the scattering intensity profile for 64K PS-*b*-PBA, while the

inset shows the variation of the peak intensity I_{max} and peak width FWHM with

temperature. The disordered state apparent from dynamic rheological testing on this

block copolymer is further confirmed by the broad correlation hole scattering observed at

all temperatures. Moreover, although the magnitude of these changes is very small, I_{max}

and FWHM are found to monotonically decrease with increasing temperature, suggesting

a UDOT-type phase behavior for this block copolymer.
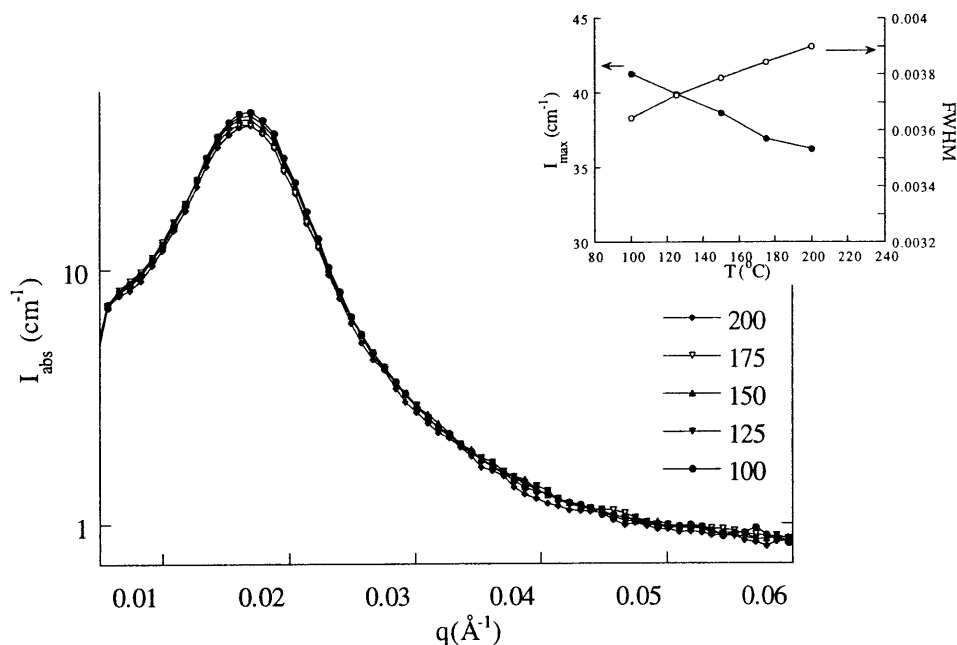
Figure V.7: Scattering intensity profile for 64K PS-*b*-PBA as a function of T

Such phase behavior is further suggested by the dynamic rheological data obtained on a higher molecular weight (100,000 g/mol) and asymmetric PS-*b*-PBA containing 70 wt% PS. Figure V.8 shows the master curves for G' and G'' at a reference temperature of 150°C for 100K PS-*b*-PBA. Clearly, horizontal frequency shifts of the data obtained at increasing temperatures do not result in good overlap with the data at 150°C for this material, indicating a change in structure over the temperature range investigated. Moreover, the progressive shift in the scaling of G' towards higher values as temperature increases, namely from ω^1 to $\omega^{1.5}$, suggests that this block copolymer is undergoing an UDOT between 150 and 180°C. At the highest temperature (180°C), the low frequency scaling of the storage and loss moduli, namely $G' \sim \omega^{1.5}$ and $G'' \sim \omega^{0.9}$,

approach that of a liquid-like homogeneous melt, although the value of 1.5 (instead of 2)

indicates that thermodynamic fluctuations are still strong.
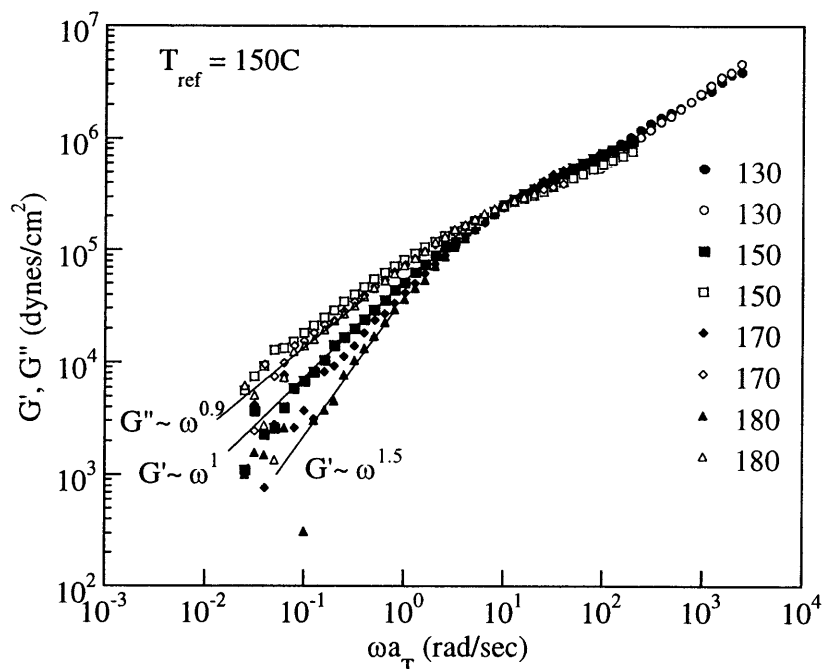
Figure V.8: Master curves for G' and G'' of asymmetric 100K PS-b-PBA

These results are further confirmed by the scattering intensity profiles for 100K

PS-b-PBA shown in Figure V.9, where the data have been shifted vertically and plotted

on a double logarithmic scale to emphasize higher order reflections in the ordered state.[150]

The segmentally mixed state of 100K PS-b-PBA observed at high temperatures with

dynamic rheological testing is further confirmed by the broad scattering maximum at q^*

~ 0.018 Å^{-1} and the absence of higher order reflections at temperatures above 160°C. At

120°C and 140°C, on the other hand, a clear second-order shoulder is observed at q_2^* ~

0.036 Å^{-1}, which is indicative of the periodic microphase separated state. Hence, from

the SANS data shown in Figure V.9, a UDOT is identified for this block copolymer, between 140 and 160°C.
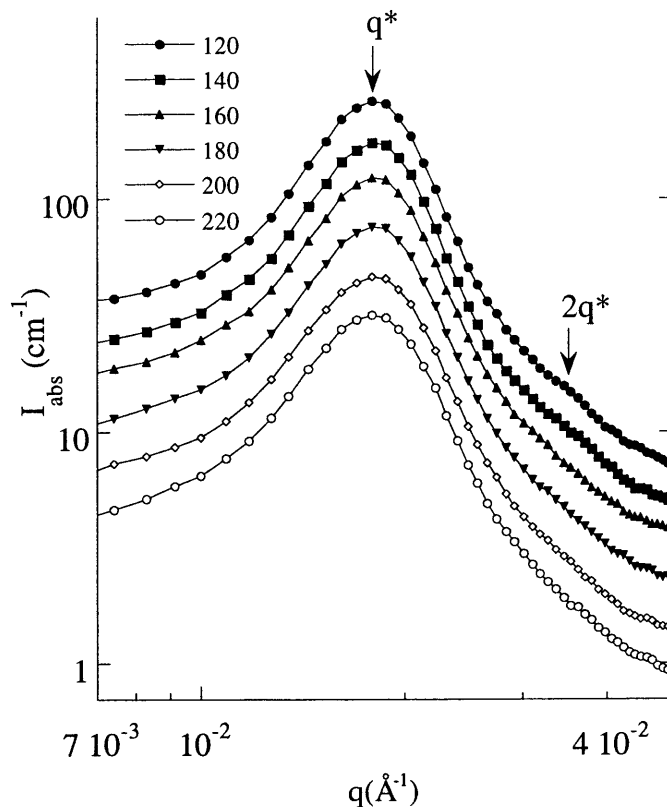
Figure V.9: Scattering intensity profile (log-log scale, data shifted) for 100K PS-b-PBA as a function of T

However, and perhaps more importantly, the peak intensity I_{max} of the first order reflection does not vary monotonically with temperature for this block copolymer, as shown on Figure V.10 where the scattering data is plotted on a linear scale. Indeed, between 120 and 180°C, I_{max} is found to decrease with increasing temperature (see inset of Figure V.10), which is consistent with the UDOT-type phase behavior found for this block copolymer and the lower molecular weight, symmetric 64K PS-b-PBA.

Conversely, as temperature is increased beyond 180°C, the peak intensity *increases* reversibly, suggesting a LDOT-type phase behavior at elevated temperatures for this block copolymer, although the actual transition is not observed in the temperature range investigated. This fully reversible thermodynamic trend is consistent with the phase diagram shown in Figure V.11, where both UDOT and LDOT branches are present. Two qualitative coexistence curves have been drawn, for 64K and 100K PS-*b*-BA, respectively, while the arrows indicate the temperature cycles to which these materials were subjected during the SANS experiments. For the lower molecular weight sample, the LDOT is expected to lie at a higher temperature and the thermodynamic fluctuations over the experimentally accessible temperature range are thus mainly governed by the UDOT-part of the phase diagram. However, as the block copolymer molecular weight increases, the simultaneous decrease in the LDOT and increase in the UDOT result in a coexistence curve such as that drawn for 100K PS-*b*-PBA. A similar phase diagram, resulting from the simultaneous occurrence of UDOT and LDOT phase behaviors, has also been reported for blends and block copolymers of PS-*b*-PBMA[22,93], therefore suggesting a similarity in the thermodynamics of these two systems.
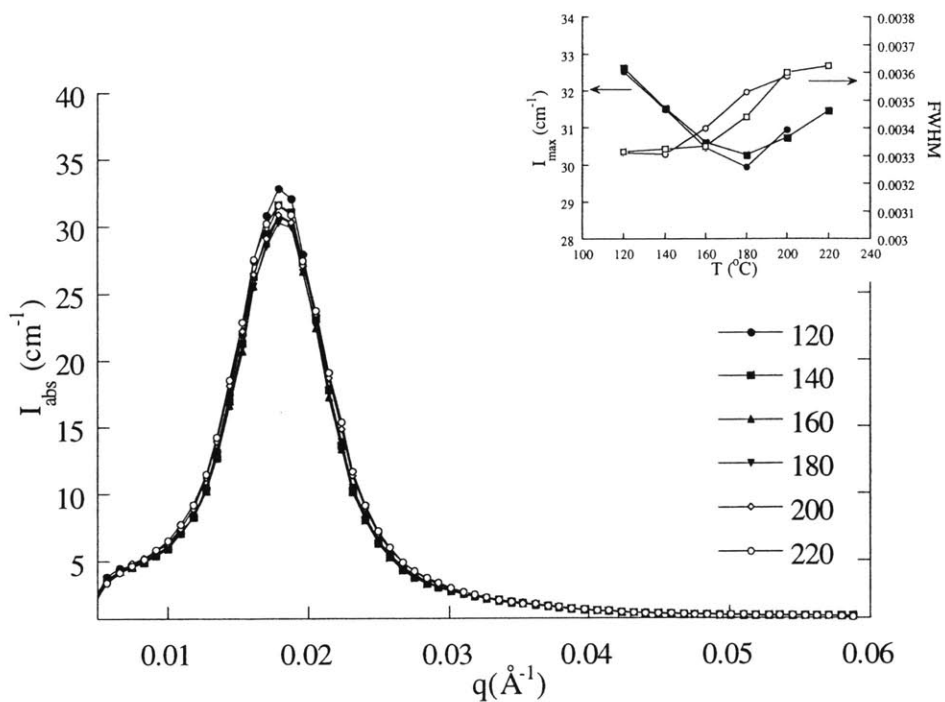
Figure V.10: Scattering intensity profile (linear scale, no shift) for 100K PS-*b*-PB. The inset shows the non-monotonic dependence if I_{max} with T and FWHM.
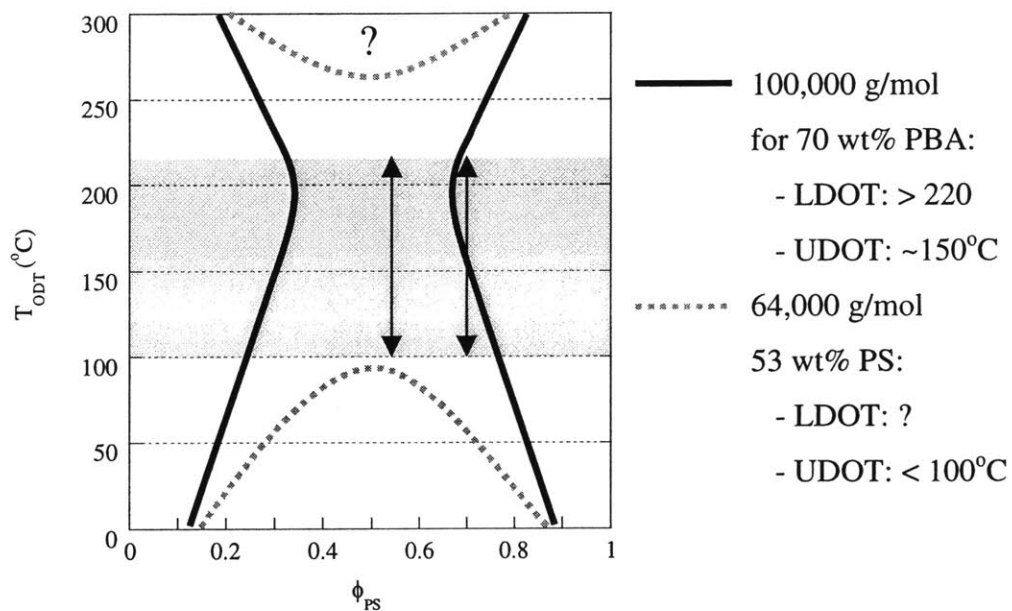
Figure V.11: Schematic phase diagram for PS-*b*-PBA

However, while the observed crossover temperature from UDOT to LDOT behavior lies below 100°C for the latter system (see Figure I.4, section I.3.1), a much higher value of ~ 190°C is obtained for 100K PS-*b*-PBA, implying a lower degree of thermodynamic compatibility for this material. This change does not need to be large, however, since it is well known that very small changes in the interaction parameter χ are sufficient to lead to strong variations in the UDOT of block copolymers.[4] Moreover, the very fact that PS-*b*-PBA exhibits both UDOT and LDOT trends precludes the possibility of a large χ parameter of enthalpic origin for this system, but rather points to a low enough exchange interaction energy $\Delta\varepsilon$ allowing for EOS effects to govern the phase behavior at elevated temperatures. Hence, the higher UDOT of PS-*b*-PBA compared to that of PS-*b*-PBMA seems to indicate a slight increase in the exchange segmental interaction energy $\Delta\varepsilon$ upon substituting the methyl group attached to the α-carbon of BMA by a H atom. Although this substitution does not seem to affect greatly the cohesive properties of the polymer (similar v_{spec} and δ for PBA and PBMA), it does result in differences in the local packing of the segments, which is reflected in the very low glass transition of PBA ($T_g = -54$°C) compared to that of PBMA ($T_g = 35$°C). This change in local segmental conformations further appears to slightly affect the strength of the segmental interactions between PBA and PS.

V.3. NEW STYRENE/ACRYLATE "BAROPLASTIC" ELASTOMERS

V.3.1. PS-b-PBA

From the results presented so far, it appears that the trend in thermodynamic compatibility for styrene/n-alkyl acrylate block copolymers is, as expected based on the GC/EOS calculations, roughly similar to that observed for PS-b-PnAMA. Indeed, for $n=1$ and $n \geq 6$, the copolymers exhibit strong degrees of incompatibility and UDOT behavior, while for PS-b-PBA, a phase behavior similar to that reported for PS-b-PBMA is obtained, with, however, higher UDOT temperatures for a given molecular weight. The presence of a LDOT at high temperatures for PS-b-PBA is an encouraging result, since it suggests that the strong pressure sensitivity characterizing the LDOT materials discussed so far in this thesis might be observed for this copolymer as well. To verify this hypothesis, the phase behavior of 100K PS-b-PBA was studied under hydrostatic pressure.

Figure V.12 shows the scattering intensity profile for 100K PS-b-PBA at 180°C and indicated pressures. It is found that as pressure increases, the scattering peak intensity I_{max} decreases monotonically, while the FWHM increases, indicating an increase in thermodynamic compatibility upon the application of pressure. This implies a negative ΔV_{mix} for PS-b-PBA, which is entirely consistent with the observation of a LDOT at elevated temperatures for this system. Moreover, from the data at 180°C and other temperatures, the master curves shown if Figure V.13 can be constructed for I_{max} and FWHM as described in section III.2.1, yielding an estimate of the pressure

coefficient dT/dP for this material of ~ **100°C/kbar**. Unfortunately, due to the upper

temperature limit of the pressure cell (190°C), the effect of pressure could only be probed

in the UDOT-region of the phase diagram of this block copolymer. Therefore, the master

plots for I_{max} and FWHM shown on Figure V.13 only display the UDOT-trend, namely a

decrease in I_{max} and an increase in FWHM with increasing temperature. Nevertheless,

the strong pressure coefficient of 100°C/kbar for PS-*b*-PBA demonstrates an important

concept of this chapter, namely that pressure-tunable phase behaviors can be designed

into new candidate *"baroplastic"* elastomers and adhesives based on styrene and low-T_g

acrylates.
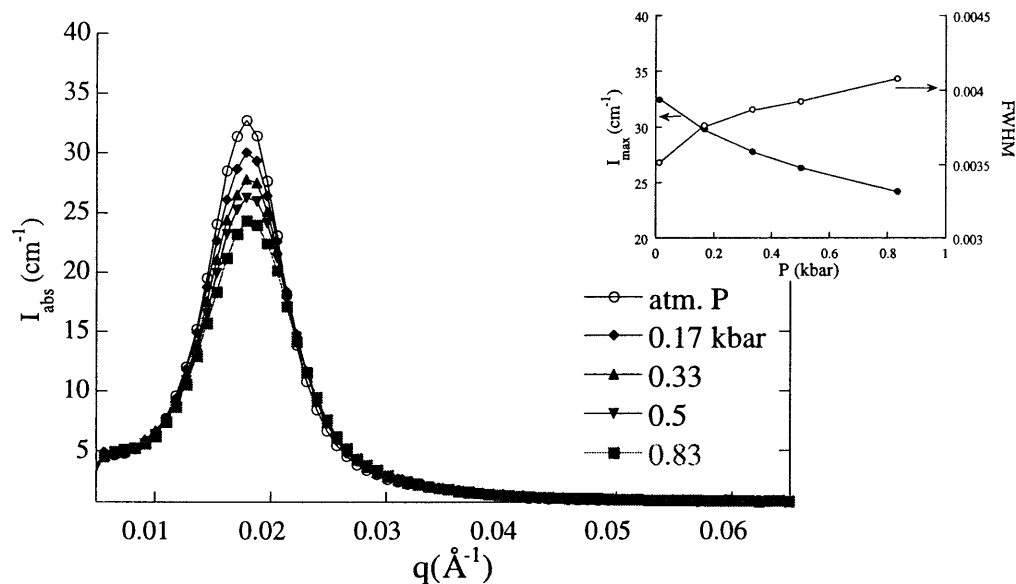
Figure V.12: Scattering intensity profile for 100K PS-*b*-PBA

at 180°C and indicated pressures

Figure V.13:
Master curves for
I_{max} and FWHM
for 100K PS-*b*-PBA
$(P_o=1 \text{ atm})$
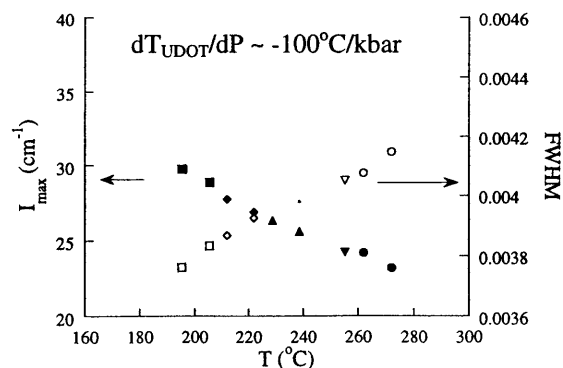
V.3.2. Molecularly designed PS-*b*-P(MA-*r*-LA)

To further illustrate how such pressure sensitivity could be designed into styrene/alkyl acrylate block copolymers, other materials were prepared, where the acrylate block consists of a random copolymer between two acrylates individually immiscible with PS and mutually immiscible, namely, methyl (MA) and lauryl acrylate (LA). Such copolymers, denoted PS-*b*-P(MA-*r*-LA), were designed in a similar fashion as the PS-*b*-P(MMA-*r*-LMA) block copolymers described in section IV.2, by matching δ and v_{spec} of the acrylate random copolymer to the values of PS. The characteristics of these block copolymers are given in Table V.2.

TABLE V.2: CHARACTERISTICS OF THE ATRP PS-*b*-P(MA-*r*-LA)

copolymer	M_n (kg/mol)	M_w/M_n	PS (wt %)	MA/LA (wt %)
PS-*b*-P(MA-*r*-LA) A	45	1.32	66	44/56
PS-*b*-P(MA-*r*-LA) B	50	1.31	54	52/48
PS-*b*-P(MA-*r*-LA) C	60	1.34	57	61/39

Similar to what was observed for PS-*b*-P(MMA-*r*-LMA), copolymerization of PS with a well matched P(MA-*r*-LA) was found to result in a significant increase in thermodynamic compatibility compared to PS-*b*-PMA. This is evident upon considering the master curves for G' and G'' shown in Figure V.14 for PS-*b*-P(MA-*r*-LA) B (see Table V.2). The low frequency scalings of $G' \sim \omega^2$ and $G'' \sim \omega$ imply a segmentally

136

mixed state for this block copolymer over the temperature range investigated (100-160°C). In contrast, 33K PS-*b*-PMA was ordered throughout the temperature range, pointing to a definite increase in thermodynamic compatibility for this new block copolymer.

Figure V.14: Master curves
for *G'* and *G"* for
PS-*b*-P(MA-*r*-LA)B
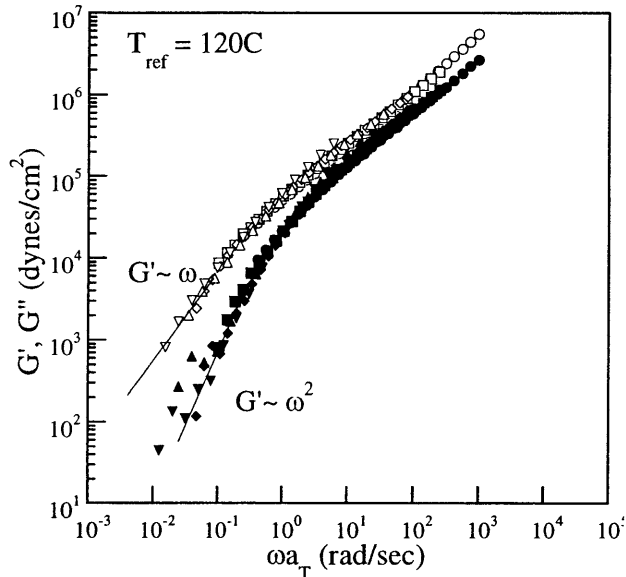
Unlike what was observed for PS-*b*-P(MMA-*r*-LMA), however, no composition could be identified which would display a LDOT. Instead, UDOT-trends similar to that shown in Figure V.16 for PS-*b*-P(MA-*r*-LA) B were observed for the three compositions investigated. However, based on the results obtained for PS-*b*-PBA, it appears that the UDOT of styrene/n-alkyl acrylate block copolymers is substantially higher than that of the corresponding styrene/n-alkyl methacrylate materials. This might explain why only the UDOT-part of the phase diagram is observed for the more symmetric (~50 wt% PS) and lower molecular weight (all ~ 50,000 g/mol) block copolymers investigated here.

Figure V.15:
Scattering intensity
profile for
PS-*b*-P(MA-*r*-LA)B
at indicated T
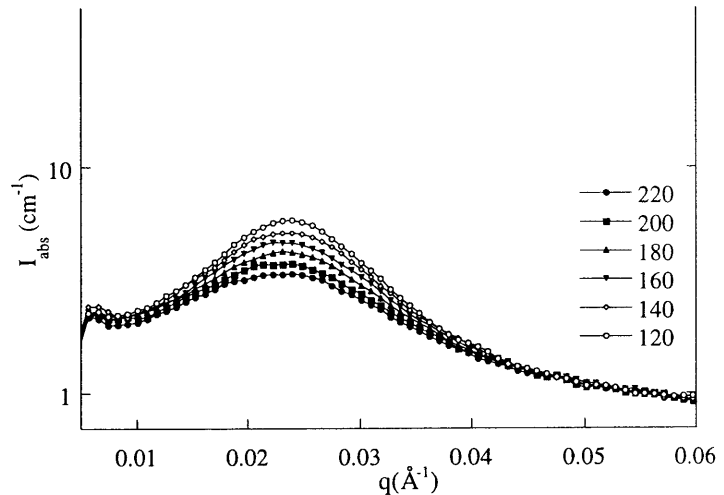
Nevertheless, based on the results obtained for PS-*b*-PBA, it was expected that

PS-*b*-P(MA-*r*-LA) would also display a strong pressure sensitivity. Figure V.16 shows

the effect of pressure at 120°C on 50K PS-*b*-P(MA-*r*-LA) where the acrylate block

contains 52 wt% of MA. The monotonic decrease in peak intensity I_{max} and increase in

peak FWHM with increasing pressure, shown on the inset of Figure V.16, imply a ΔV_{mix}

< 0 for this material. To quantify the effect of pressure on this material, master plots for

I_{max} and FWHM shown in Figure V.17 were again constructed, yielding a dT/dP of -

90°C/kbar. Hence, although this block copolymer displays a UDOT-type phase behavior

over the temperature range investigated, strong pressure coefficients are again obtained,

which resemble those extracted for LDOT-type block copolymers.

Figure V.16:
Scattering intensity
profile at 120°C
as a function of P
for PS-*b*-P(MA-*r*-LA)B

○   atm P

◆   0.017 kbar

△   0.034

▼   0.067
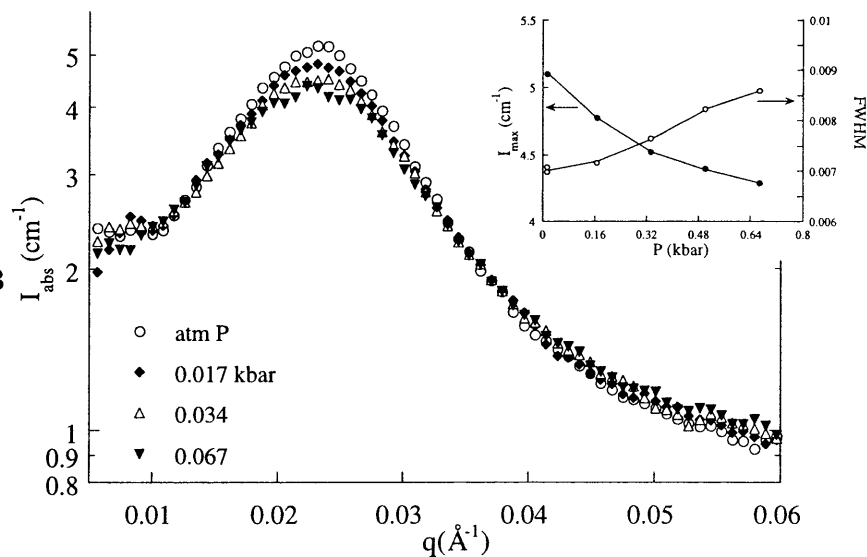
Figure V.17:
Master curves for
I_{max} and FWHM for
PS-*b*-P(MA-*r*-LA)B
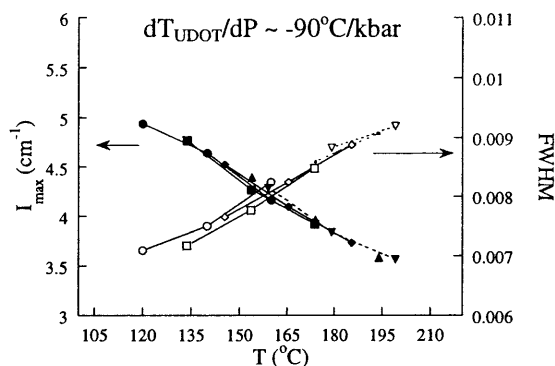
This result amply demonstrates how new baroplastic elastomers can be designed

to exhibit strong pressure sensitivity. Together with the results obtained for PS-*b*-PHMA

(dT_{UDOT}/dP = -60°C/kbar, see Table III.3 of Chapter III), they further show that **UDOT-**

type block copolymers can also be characterized by ***large pressure coefficients***. To our

knowledge, it is the first time that pressure coefficients of this magnitude are reported for

such materials. From an application standpoint, the results presented in this chapter

demonstrate how industrially amenable synthetic routes such as ATRP can be

successfully combined with the molecular design tool identified in this thesis to impart

pressure and temperature-tunable phase behavior into new acrylic block copolymers of commercial relevance. What may be less appreciated is that, in this manner, elastomeric block copolymers exhibiting strong pressure coefficients could be designed wherein the hard block has a $T_g \sim 40$ to $60^{\circ}C$. Such materials have extremely attractive rheological properties. Indeed, at room temperature, they exhibit elastomeric properties, while under the application of high pressure and at temperatures hardly exceeding RT, they can be processed from the melt (liquid segmentally mixed state).

CHAPTER VI: A COMPRESSIBLE FREE ENERGY

EXPRESSION

The results presented in this thesis have unveiled a systematic trend in phase behavior across two families of block copolymer materials, styrene/*n*-alkyl methacrylates and styrene/*n*-alkyl acrylates. Macroscopic parameters were proposed, namely the solubility parameters and densities of the homopolymer melts, which seem to capture these trends as well as those reported for other known miscible pairs almost in a predictive manner. Based on these findings, a tool for the molecular design of miscibility into new systems was identified, which was successfully used to induce "baroplastic" behavior into new acrylic elastomers or adhesives presented in Chapter V. All these observations further reveal a systematic dependence of phase behavior on pure component properties that can be measured or computed quite accurately.

Unfortunately, while the tool identified and utilized in this thesis successfully predicts whether or not miscibility will be encountered for a given polymer pair, it does not allow one to predict the type of phase diagram to be expected, namely, UCST/UDOT versus LCST/LDOT. In an attempt to address this last need, a simplified free energy expression is derived here for compressible mixtures of two homopolymers A and B. Given the similarity in phase behavior for block copolymers and the corresponding homopolymer blends, its extension to block copolymers is straightforward and will not be discussed here. The ability of the model to predict phase diagrams for the homopolymer pairs investigated in this thesis and others reported in the literature is discussed.

The change in Gibbs free energy on mixing, ΔG_{mix}, is the difference between the free energy of the mixture G^{mixt} and that of the pure components G^{pure}. For a compressible mixture accompanied by a finite change in volume upon mixing, $\Delta V_{mix} \neq 0$, the change in free energy consists of three terms: a change in internal energy ΔE_{mix}, in volume ΔV_{mix} and in entropy ΔS_{mix}:

$$\begin{aligned} \Delta G_{mix} &= \Delta E_{mix} + P\Delta V_{mix} - T\Delta S_{mix} \\ &= (E^{mixt} - E^{pure}) + P(V^{mixt} - V^{pure}) - T(S^{mixt} - S^{pure}) \end{aligned} \tag{VI.1}$$

A phenomenological expression for each of these contributions is provided below.

VI.1. ENTROPY CHANGE UPON MIXING: ΔS_{MIX}

As pointed out by Flory[37], the change in configurational entropy upon mixing for a compressible 2-component (A and B) polymer solution or mixture should scale as the logarithms of the ratios of the free volume available in the mixture, $V_{f,m}$, and that in the pure components, $V_{f,A}$ and $V_{f,B}$:

$$\Delta S_{mix} / R = n_A \ln\left(\frac{V_{f,m}}{V_{f,A}}\right) + n_B \ln\left(\frac{V_{f,m}}{V_{f,B}}\right) \tag{VI.2}$$

where n_i is the number of chains of component i in the system.

The free volume of component i, $V_{f,i}$, is defined as the difference between the total volume V_i at temperature T and pressure P and the excluded or hard core (occupied) volume $V_{hc,i}$:

$$V_{f,i} = V_i - V_{hc,i} = V_i - n_i N_i v_i \tag{VI.3}$$

$$V_{f,m} = V - V_{hc,A} - V_{hc,B} = V - n_A N_A v_A - n_B N_B v_B \tag{VI.4}$$

142

since each chain of component i contains N_i segments of hard core volume v_i (g/mol).

According to the definition of reduced properties typically used in EOS theories[66,83], V-$V_{hc,A}$-$V_{hc,B}$, V_A-$V_{hc,A}$ and V_B-$V_{hc,B}$ are related to the reduced densities $\tilde{\rho}$, $\tilde{\rho}_A$ and $\tilde{\rho}_B$, respectively, defined as the hard core volume ($V_{hc,i}$) divided by the total volume (V_i):

$$\tilde{\rho}_i = \frac{\rho_i}{\rho_i^*} = \left(\frac{V_{hc,i}}{V_i}\right) = \frac{n_i N_i v_i}{V_i} \tag{VI.5}$$

$$\tilde{\rho} = \frac{\rho}{\rho^*} = \left(\frac{V_{hc,A} + V_{hc,B}}{V}\right) = \frac{n_A N_A v_A + n_B N_B v_B}{V} \tag{VI.6}$$

where $\rho_i^* = \dfrac{M_i}{v_i}$ and ρ^* are the hard core densities of component i (known) and the

mixture (unknown) respectively. Hence:

$$V - V_{hc,A} - V_{hc,B} = (1 - \tilde{\rho})V \tag{VI.7}$$

$$V_i - V_{hc,i} = (1 - \tilde{\rho}_i)V_i \tag{VI.8}$$

and equation VI.2 becomes:

$$\Delta S_{mix} / R = n_A \ln\left(\frac{(1 - \tilde{\rho})V}{(1 - \tilde{\rho}_A)V_A}\right) + n_B \ln\left(\frac{(1 - \tilde{\rho})V}{(1 - \tilde{\rho}_B)V_B}\right) \tag{VI.9}$$

or

$$\Delta S_{mix} / R = -[n_A \ln\phi_A + n_B \ln\phi_B] + \left[n_A \ln\left(\frac{1 - \tilde{\rho}}{1 - \tilde{\rho}_A}\right) + n_B \ln\left(\frac{1 - \tilde{\rho}}{1 - \tilde{\rho}_B}\right)\right] \tag{VI.10}$$

where ϕ_i is the volume fraction of component i defined as $V_i/(V_A+V_B)$. In equation

(VI.10), we have made use of the approximation $\phi_i \sim V_i/V$, since $V_A + V_B$ differs from V

only by the small quantity ΔV_{mix}. Indeed, in macromolecular mixtures, it is well known

that the magnitude of the fractional volume change upon mixing, $\Delta V_{mix}/V$, is minute[156],

typically $\sim o(10^{-4})$, and the approximation $\phi_i = V_i/(V_A+V_B) \sim V_i/V$ is thus justified.

Alternatively, one can arrive at an expression entirely similar to that given in equation VI.10, using a phenomenological van der Waals equation of state for non-ideal gases:

$$(P + \frac{a}{V^2})(V - b) = nRT \tag{VI.11}$$

and equating the parameter b to the hard core volume V_{hc}. This alternative derivation is given in Appendix A.VI.1.

Equation (VI.10) gives a simple expression for the configurational entropy gain upon mixing for a binary compressible mixture. It consists of two terms: the classical (incompressible) combinatorial entropy which scales with the logarithms of the volume fraction of each component, and a second term which arises from compressibility and is related to the difference in free volume between the mixture and the pure components.

Hence, if component i undergoes a contraction upon mixing, in which case $\dfrac{1-\tilde{\rho}}{1-\tilde{\rho}_i} < 1$,

this will contribute a negative term to the entropy of mixing which destabilizes the mixture in comparison to the incompressible limit. In general, each component of the polymer mixture is expected to undergo opposite trends, namely, if one undergoes a reduction, the other will undergo an increase in free volume. This results from the fact that deviations from a simple volume average ($\tilde{\rho} = \phi_A\tilde{\rho}_A + \phi_B\tilde{\rho}_B$) for the reduced density of macromolecular mixtures are very small. Indeed,

$$\tilde{\rho} = \frac{V_{hc,A} + V_{hc,B}}{V} = \frac{V_{hc,A} + V_{hc,B}}{V_A + V_B + \Delta V_{mix}} = \frac{V_{hc,A}}{V_A}\left(\frac{V_A}{V_A + V_B + \Delta V_{mix}}\right) + \frac{V_{hc,B}}{V_B}\left(\frac{V_B}{V_A + V_B + \Delta V_{mix}}\right)$$

144

$$= \tilde{\rho}_A \left(\frac{V_A}{V_A + V_B + \Delta V_{mix}} \right) + \tilde{\rho}_B \left(\frac{V_B}{V_A + V_B + \Delta V_{mix}} \right) \qquad \text{(VI.12)}$$

However, since ΔV_{mix} is very small compared to $V_A + V_B$, one can expand the above

expression around $\Delta V_{mix} \to 0$, yielding, to first order:

$$\tilde{\rho} = \tilde{\rho}_A \frac{V_A}{V_A + V_B} \left[1 - \frac{\Delta V_{mix}}{V_A + V_B} \right] + \tilde{\rho}_B \frac{V_B}{V_A + V_B} \left[1 - \frac{\Delta V_{mix}}{V_A + V_B} \right]$$

$$= \left(\phi_A \tilde{\rho}_A + \phi_B \tilde{\rho}_B \right) \left[1 - \frac{\Delta V_{mix}}{V_A + V_B} \right] \qquad \text{(VI.13)}$$

VI.2. INTERNAL ENERGY CHANGE UPON MIXING: ΔE_{MIX}

The internal energy in the pure state is the total interaction energy of the pure

components and is obtained by counting the number of pair-wise interactions of type A-A

and B-B:

$$E^{pure} = \frac{1}{2} \tilde{\rho}_A (n_A N_A z \varepsilon_{AA}) + \frac{1}{2} \tilde{\rho}_B (n_B N_B z \varepsilon_{BB}) \qquad \text{(VI.14)}$$

where ε_{ii} is the attractive (negative) molar segmental interaction energy of the i-i pair and

z is the number of nearest neighbors in the pure melts. The factors $\tilde{\rho}_i$ simply arise from

the reduced probability of interacting with a nearest neighbor in a mixture with free

volume.

Likewise, the free energy of the mixed state, **assuming equivalent z's for the**

mixture and the pure components, will be given by:

145

$$E^{mixt} = \frac{1}{2}(n_A N_A z \varepsilon_{AA}) f_A \tilde{\rho} + \frac{1}{2}(n_B N_B z \varepsilon_{BB}) f_B \tilde{\rho} + \frac{1}{2}(n_A N_A z \varepsilon_{AB}) f_B \tilde{\rho} + \frac{1}{2}(n_B N_B z \varepsilon_{AB}) f_A \tilde{\rho}$$

$$= \frac{1}{2}(n_A N_A z \varepsilon_{AA}) f_A \tilde{\rho} + \frac{1}{2}(n_B N_B z \varepsilon_{BB}) f_B \tilde{\rho} + (n_B N_B z \varepsilon_{AB}) f_A \tilde{\rho}$$

$$(VI.15)$$

where f_i is the segment fraction of component i

$$f_i = \frac{n_i N_i}{n_A N_A + n_B N_B}$$

$$(VI.16)$$

and $f_A n_B N_B = f_B n_A N_A$.

Hence, ΔE_{mix} is given by:

$$\Delta E_{mix} = E^{mixt} - E^{pure}$$

$$(VI.17)$$

$$= \frac{1}{2} n_A N_A z \varepsilon_{AA} [f_A \tilde{\rho} - \tilde{\rho}_A] + \frac{1}{2} n_B N_B z \varepsilon_{BB} [f_B \tilde{\rho} - \tilde{\rho}_B] + n_A N_A f_B \tilde{\rho} z \varepsilon_{AB}$$

which, using the relations $f_A = (1 - f_B)$ and $n_A N_A f_B = n_B N_B f_A$, can be rewritten as:

$$\Delta E_{mix} = \frac{1}{2}[n_A N_A z \varepsilon_{AA}(\tilde{\rho} - \tilde{\rho}_A) + n_B N_B z \varepsilon_{BB}(\tilde{\rho} - \tilde{\rho}_B)] + n_A N_A f_B \tilde{\rho} z \left[\varepsilon_{AB} - \frac{\varepsilon_{AA} + \varepsilon_{BB}}{2} \right]$$

or

$$\Delta E_{mix} = n_A N_A f_B (RT \chi^{FH}) \tilde{\rho} + \frac{1}{2}[n_A N_A z \varepsilon_{AA}(\tilde{\rho} - \tilde{\rho}_A) + n_B N_B z \varepsilon_{BB}(\tilde{\rho} - \tilde{\rho}_B)]$$

$$(VI.18)$$

where the definition

$$\chi^{FH} = \frac{z}{RT}\left(\varepsilon_{AB} - \frac{\varepsilon_{AA} + \varepsilon_{BB}}{2} \right)$$

$$(VI.19)$$

has been used.[37] Hence, similar to the change in entropy upon mixing, the expression for

the change in internal energy for the compressible mixture contains two terms:

146

1. The *classical exchange interaction energy term*, or "χ^{FH}" term, although *diluted* by a factor $\tilde{\rho}$, since the probability of interacting with a nearest neighbor of type i is not f_i but $f_i\tilde{\rho}$.

2. A second term simply arising from the fact that the self-interactions (ε_{ii}) will become either weakened or strengthened upon mixing, depending on the relative amount of free volume in the mixture compared to that in the pure components. Hence, if component i is characterized by a larger degree of free volume than the mixture, i.e., $(\tilde{\rho} - \tilde{\rho}_i) > 0$, the contraction this component will undergo is in fact *energetically favorable* from a standpoint of self-interactions.

VI.3. GIBBS FREE ENERGY CHANGE UPON MIXING: ΔG_{MIX}

The expressions derived above for ΔS_{mix} and ΔE_{mix} can now be used to compile the free energy expression for the compressible mixture:

$$\Delta G_{mix} = RT[n_A \ln\phi_A + n_B \ln\phi_B] - RT\left[n_A \ln\left(\frac{1-\tilde{\rho}}{1-\tilde{\rho}_A}\right) + n_B \ln\left(\frac{1-\tilde{\rho}}{1-\tilde{\rho}_B}\right)\right]$$

$$+ P\Delta V_{mix} \tag{VI.20}$$

$$+ n_A N_A f_B (RT\chi^{FH})\tilde{\rho} + \frac{1}{2}[n_A N_A z\varepsilon_{AA}(\tilde{\rho} - \tilde{\rho}_A) + n_B N_B z\varepsilon_{BB}(\tilde{\rho} - \tilde{\rho}_B)]$$

147

Equation (VI.20) can be further simplified as shown in Appendix A.VI.2, to yield

the following expression for $\Delta G_{mix}/V$, the change in free energy per unit volume, denoted

Δg_{mix}. In the following expression, the second entropy term of equation VI.20 and the

$P\Delta V_{mix}$ term were neglected, since it can be readily shown that they are orders of

magnitude smaller than the leading terms.

$$\Delta g_{mix} \approx RT\left[\frac{\phi_A\tilde{\rho}_A}{N_A v_A}\ln\varphi_A + \frac{\phi_B\tilde{\rho}_B}{N_B v_B}\ln\varphi_B\right] + \frac{\phi_A\tilde{\rho}_A}{v_A}f_B\tilde{\rho}(RT\chi^{FH}) + \phi_A\phi_B\left[(\tilde{\rho}_A - \tilde{\rho}_B)(\delta_A{}^2 - \delta_B{}^2)\right]$$

(VI.21.a)

In equation (VI.21), the first term is the classical combinatorial entropy of mixing,

while the second term is the classical F-H interaction energy term, diluted compared to

the incompressible limit. The third term, entropic in nature, arises from the very fact that

the mixture is compressible, thus accounting for equation of state effects. Note that this

extra term depends on the pure component properties only, namely the cohesive energy

density and fractional free volume, and more precisely how they differ between the two

components.

Upon assuming an average hard core segmental volume $v = (v_A v_B)^{1/2}$ in the

mixture, which is consistent with the assumption of equal z's made in deriving ΔE_{mix}, the

interaction energy term can be further simplified to:

$$\frac{\phi_A\tilde{\rho}_A}{v_A}f_B\tilde{\rho}(RT\chi^{FH}) \approx \phi_A\phi_B\tilde{\rho}_A\tilde{\rho}_B(RT\chi^{FH})/v$$

(VI.22)

Upon inserting this expression for the interaction term into equation VI.21, the following

simple expression for Δg_{mix} is obtained:

148

$$\Delta g_{mix} = RT\left[\frac{\phi_A \tilde{\rho}_A}{N_A v_A}\ln\varphi_A + \frac{\phi_B \tilde{\rho}_B}{N_B v_B}\ln\varphi_B\right] + \phi_A\phi_B\tilde{\rho}_A\tilde{\rho}_B(\frac{RT\chi^{FH}}{v}) + \phi_A\phi_B\left[(\tilde{\rho}_A - \tilde{\rho}_B)(\delta_A^{\ 2} - \delta_B^{\ 2})\right]$$

<div align="right">(VI.21.b)</div>

Taking the second derivative of this expression for Δg_{mix} with respect to composition and further assuming Berthelot's mixing rule and the Hildebrand solubility parameter formalism:

$$\chi^{FH} = v\frac{(\delta_{A_o} - \delta_{B_o})^2}{RT}$$

to express χ^{FH} as a function of the pure component hard core solubility parameters, δ_{i_o}, yields the following *stability criterion for the mixed state*:

$$\frac{\partial^2(\Delta g_{mix}/RT)}{\partial\phi_A^{\ 2}} = \frac{g_{\phi\phi}}{RT} = \left[\frac{\tilde{\rho}_A}{\phi_A N_A v_A} + \frac{\tilde{\rho}_B}{\phi_B N_B v_B}\right] - 2\frac{\tilde{\rho}_A\tilde{\rho}_B}{RT}(\delta_{A_o} - \delta_{B_o})^2 - \frac{2}{RT}\left[(\tilde{\rho}_A - \tilde{\rho}_B)(\delta_A^{\ 2} - \delta_B^{\ 2})\right] > 0$$

<div align="right">(VI.23)</div>

while at the spinodal, $g_{\phi\phi}$ is equal to 0.

VI.4. PHASE DIAGRAM PREDICTIONS

VI.4.1. Pure component properties

In the next sections, equation VI.23 is employed to predict phase diagrams for the various polymer pairs investigated in this thesis as well as others reported in the literature. To this end, the following pure component properties were determined from experimental PVT data[83] and GC calculations[42]:

<div align="center">149</div>

1. Pure component reduced densities as a function of T

2. Pure component solubility parameters as a function of T

3. Hard core (0K) segmental volumes v_i or, equivalently, hard core densities ρ_i^*

The reduced densities were obtained in the following manner. Experimental PVT data is available in the literature for many homopolymers over a certain temperature range (see for example reference 83 which reviews PVT properties for 56 homopolymers). These data were extrapolated to 0K, which is taken here as the hard core state. To this end, the following variation of density with temperature T (K) and at zero pressure was assumed:

$$\rho_i(T) = \rho_i^* \exp(-\alpha_i T) \tag{VI.24}$$

where a constant α_i (the melt state value) was used as a first approximation. This procedure, described in Appendix A.VI.3, yields v_i and ρ_i^*. The reduced density $\tilde{\rho}_i(T)$ is then given by the actual density $\rho_i(T)$ divided by ρ_i^*.

A similar approach was used to determine the temperature dependent solubility parameters. The values calculated according to van Krevelen at 25°C were extrapolated to other temperatures in the following manner:

$$\delta_i^2(T) = -\frac{1}{2}\frac{z\varepsilon_{ii}\rho_i(T)}{M_u^i} = \delta_i^2(298)\left(\frac{\rho_i(T)}{\rho_i(298)}\right) = \delta_i^2(298)\left(\frac{\tilde{\rho}_i(T)}{\tilde{\rho}_i(298)}\right) \tag{VI.25.a}$$

$$\delta_{i_o}^2 = \delta_i^2(298)\left(\frac{1}{\tilde{\rho}_i(298)}\right) \tag{VI.25.b}$$

The homopolymer values of $\alpha_i, \rho_i^*, \delta_{i_o}^2, \delta(298)$ and v_i used to compute the phase diagrams presented in the next sections are listed in Table A.VI.1 of Appendix A.VI.3.

VI.4.2. Styrene/methacrylate blends

VI.4.2.a. Phase diagrams

As described in Chapter III, PS was found to be miscible over a certain

temperature range with PEMA, PPMA and PBMA, and block copolymers of PS with

these components exhibit the LDOT. On the other hand, PMMA as well as methacrylates

with alkyl side chains longer than butyl are immiscible with PS and the corresponding

block copolymers exhibit the UDOT. Figure VI.1 gives the predicted phase diagrams for

6 styrene/methacrylate systems, namely, PS/PMMA (n=1), PS/PEMA (n=2), PS/PBMA

(n=4), PS/POMA (n=8), PS/PLMA (n=12) and PS/PCHMA (a well-known miscible

styrene/methacrylate system not investigated experimentally in this thesis). In computing

the phase diagrams of these blends, homopolymer molecular weights were chosen such

that the predicted spinodal temperature for a symmetric blend composition (50 wt% PS)

would fall within an experimentally accessible T-range.

As can be seen, equation VI.23 strongly captures the temperature-dependent

phase behavior of these polymer pairs. Hence, PS/PEMA, PS/PBMA and PS/PCHMA

are predicted to exhibit both the UCST and the LCST. However, for PMMA, POMA and

PLMA, high UCST temperatures are predicted even for very low molecular weights. It is

important to note that no adjustable parameters were used to compute the phase diagrams

shown in Figure VI.1, since Berthelot's mixing rule was assumed to calculate the

interaction parameters. The qualitative agreement between the calculated phase diagrams

and the experimentally observed phase behavior is excellent, implying that equation

VI.23 is predictive for these weakly interacting systems, which contrasts with other

compressible formalisms developed to date and discussed in section I.3.2 of Chapter I.

151
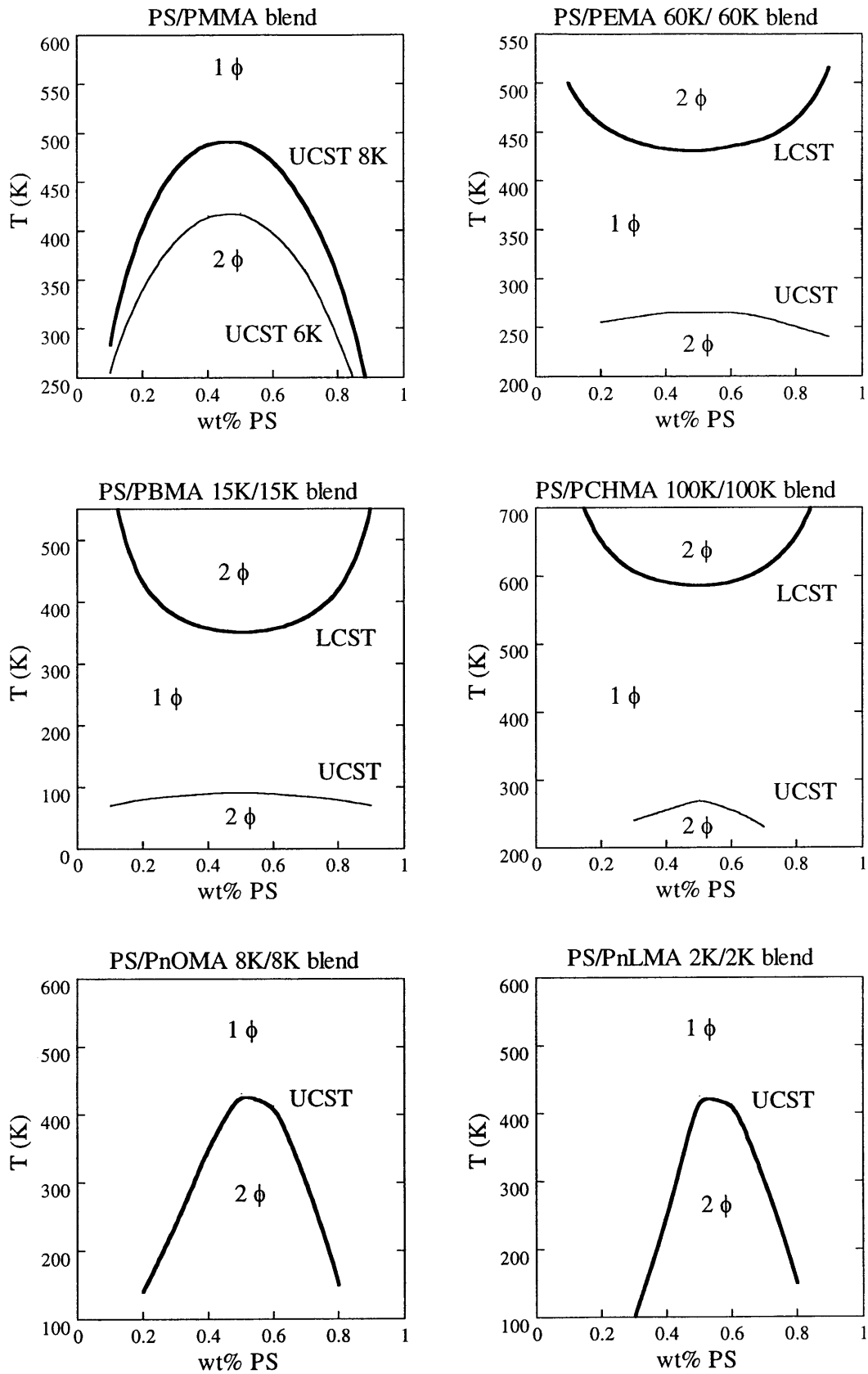
Figure VI.1: Predicted phase diagrams for styrene/methacrylate blends

More generally, equation VI.23 provides a simple molecular explanation for the LCST/LDOT. Indeed, it can be readily shown that, independent of the choice of reference (hard core) state, PS has a higher reduced density (lower fractional free volume) than all the methacrylates considered in this thesis, as well as the other homopolymers with which it is reported miscible. This is shown in Figure VI.2 where the reduced densities as obtained using the extrapolation procedure described above are plotted as a function of T for PS, PMMA, PBMA and PCHMA. On the other hand, the differences in cohesive energy densities are negative at 25°C for these methacrylates as well as those having linear alkyl side chains with $n<6$, since $\delta_{PnAMA} > \delta_{PS}$ for $n \leq 4$ and for PCHMA (see Tables A.IV.3 and 4). Hence, at low temperatures,

$$\left(\tilde{\rho}_{PS} - \tilde{\rho}_{PnAMA}\right)\left(\delta^2_{PS} - \delta^2_{PnAMA}\right) < 0 \tag{VI.26}$$

which favors mixing. This simply results from the fact that these more strongly cohesive methacrylates undergo a reduction in free volume upon segmental mixing with PS, thereby concentrating their self-interactions.

However, as temperature increases, the cohesive energy densities of the homopolymers decrease due to thermal expansion, as does $\tilde{\rho}_i$. The magnitude of these changes is related to the thermal expansion coefficient of each homopolymer α_i since:

$$\frac{d\tilde{\rho}_i}{dT} = \frac{1}{\rho_i^*}\frac{d\rho_i}{dT} = \frac{1}{\rho_i^*}\left(-\alpha_i\rho_i\right) \quad \text{or} \quad \frac{1}{\tilde{\rho}_i}\frac{d\tilde{\rho}_i}{dT} = -\alpha_i \tag{VI.27}$$

and

$$\frac{d\delta_i^2}{dT} = \frac{d\left(-\dfrac{1}{2}\dfrac{z\varepsilon_{ii}\rho_i}{M_u^i}\right)}{dT} = -\alpha_i\delta_i^2 \quad \text{or} \quad \frac{1}{\delta_i^2}\frac{d\delta_i^2}{dT} = -\alpha_i \tag{VI.28}$$

153
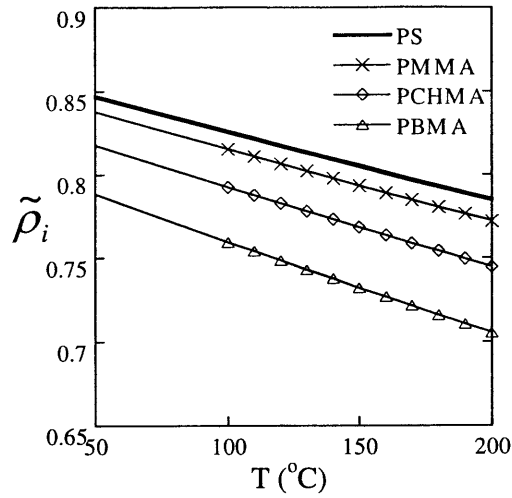
Figure VI.2: Reduced densities for PS, PMMA, PBMA and PCHMA

Hence, although both $\tilde{\rho}_i$ and δ_i^2 decrease with temperature, the term given in

equation (VI.26) will either decrease or increase in magnitude depending on whether the

thermal expansion coefficient of styrene is higher or lower than that of the methacrylate.

Upon examining the values of the thermal expansion coefficient of these materials, it is

found that α_{PS} (5.13×10^{-4} K^{-1}) is much lower than α_{PnAMA} (6 to 8×10^{-4} K^{-1}) except for

PMMA ($\sim 5.48 \times 10^{-4}$ K^{-1}).[79,83] Hence, the reduced densities and cohesive energy densities

of the methacrylates decrease with increasing T at a higher rate than those of PS. These

differences in thermal expansion coefficients of the pure components imply that there

will inevitably be a temperature at which δ^2_{PnAMA} becomes smaller than δ^2_{PS} and the term

in equation (VI.26) changes sign. As temperature further increases and this term

becomes more important than the combinatorial entropy of mixing, the system phase

separates through a LCST/LDOT. However, the necessary but not sufficient condition

for the LCST is that χ be sufficiently small, i.e. of comparable magnitude to the term

154

arising from compressibility (equation VI.26). Otherwise, the classical F-H interaction term dominates the free energy of mixing and the system only displays a UCST in the accessible temperature range, which is the case for PS/PMMA and other methacrylates with alkyl side chains longer than butyl. As discussed in Chapters IV and V of this thesis, the latter condition is met in weakly interacting systems for homopolymer pairs with matching cohesive properties, characterized by their solubility parameters and densities.

The second condition for the experimental observation of the LCST, i.e., at an experimentally accessible temperature, is that these matched homopolymers have sufficiently different thermal expansion coefficients. Indeed, if these parameters are too similar, the LCST lies at a temperature exceeding by far the degradation temperature of the polymer components. Such a difference in thermal expansion coefficients is precisely found for PS and, not only the methacrylates with which it is reported miscible, but also PVME, PPO and PCHA. For equal molecular weights, the temperature of the LCST for each of these polymer pairs strongly depends on the actual difference in thermal expansion coefficients and reduced densities (free volume) between the pure components. Indeed, the smaller this difference, the higher the LCST. Hence, for PCHMA, the values of these parameters are closer to those of PS than for the other methacrylates, which explains the higher observed[128,131-133] and predicted degree of thermodynamic compatibility and LCST temperature for this blend compared to PS/PBMA or PS/PEMA.

155

Although the primary terms of equations VI.21.b and 23 responsible for the LCST

originated from an expression for the change in internal energy upon mixing, it can be

shown that this phase separation transition is indeed entropically driven, in contrast to the

enthalpically driven UCST/UDOT. Using equations VI.21.b and VI.23, the total change

in entropy upon mixing per unit volume Δs_{mix} and its second derivative with respect to

composition $s_{\phi\phi}$, can be calculated:

$$\Delta s_{mix} = -\frac{\partial \Delta g_{mix}}{\partial T}\bigg|_{P,\phi_i} \tag{VI.29.a}$$

$$s_{\phi\phi} = \frac{\partial^2 \Delta s_{mix}}{\partial \phi^2}\bigg|_{T,P} = -\frac{\partial g_{\phi\phi}}{\partial T}\bigg|_{\phi,P} \tag{VI.29.b}$$

In equation VI.21 and VI.23, the following variables depend on temperature:

$$\tilde{\rho}_i(T) \approx \rho_i^* \exp(-\alpha_i T) \tag{VI.30.a}$$

$$\delta_i^{\,2}(T) \approx \delta_{i_o}^{\,2} \exp(-\alpha_i T) \tag{VI.30.b}$$

while the volume fractions can reasonably be treated as constant. Indeed, their minor

temperature dependence was found to have a negligible effect on the blend free energy.

Likewise, the change in enthalpy upon mixing per unit volume Δh_{mix} and its second

derivative with respect to composition $h_{\phi\phi}$ are readily obtained:

$$\Delta h_{mix} = \Delta g_{mix} + T\Delta s_{mix} = \Delta g_{mix} - T\frac{\partial \Delta g_{mix}}{\partial T}\bigg|_{P,\phi_i} \tag{VI.31.a}$$

$$h_{\phi\phi} = \frac{\partial^2 (\Delta h_{mix})}{\partial \phi^2}\bigg|_{T,P} = g_{\phi\phi} - T\frac{\partial g_{\phi\phi}}{\partial T}\bigg|_{\phi,P} \tag{VI.31.b}$$

The derivations of these thermodynamic quantities are given in Appendix A.VI.4.

For a system undergoing a UCST, $g_{\phi\phi}$ changes from negative to positive with

increasing temperature ($\dfrac{\partial g_{\phi\phi}}{\partial T} > 0$) and $s_{\phi\phi}$ and $h_{\phi\phi}$ are both < 0, which implies that Δh_{mix}

and Δs_{mix} are positive. Hence, phase separation upon cooling through a UCST is driven

by the unfavorable enthalpy of mixing. At the LCST, on the other hand, $g_{\phi\phi}$ changes

from positive to negative with increasing temperature ($\dfrac{\partial g_{\phi\phi}}{\partial T} < 0$) and $s_{\phi\phi}$ and $h_{\phi\phi}$ are both

> 0, which implies that Δh_{mix} and Δs_{mix} are negative. In this case, phase separation is thus

driven by an increase in the system entropy compared to the phase mixed state since Δs_{mix}

< 0. This is shown in Figure VI.3 where the changes in free energy, entropy and enthalpy

upon mixing and their second derivatives with respect to composition are given as a

function of temperature for a 60K/60K blend of PS/PEMA containing 50 wt% PS.
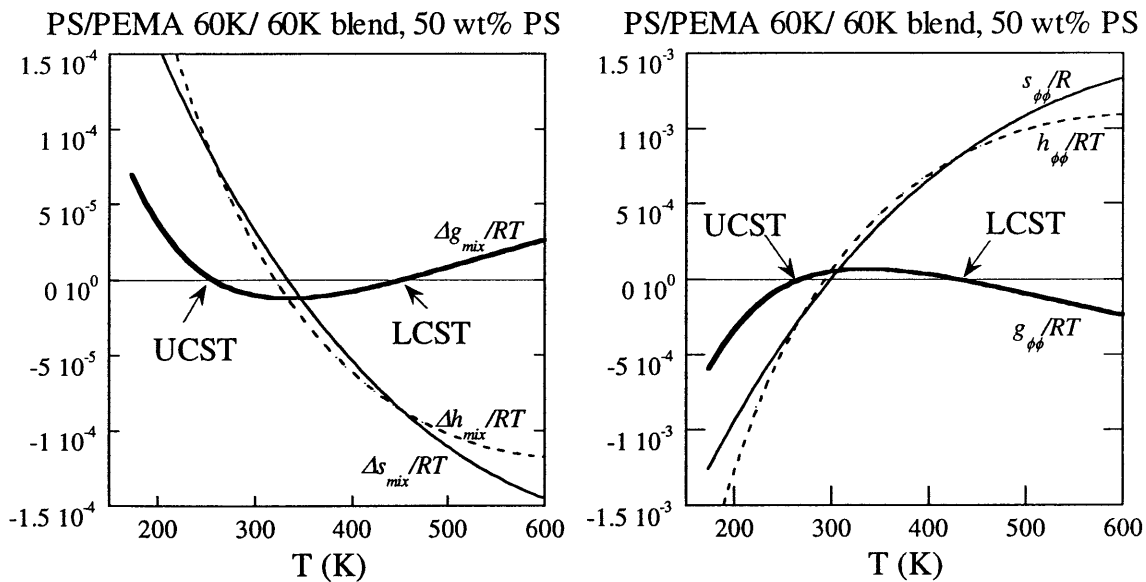
Figure VI.3: Changes in free energy, enthalpy and entropy upon mixing and their second
derivatives with respect to composition as a function of temperature.

VI.4.3. Polyolefin-based blends

Phase diagrams were also computed for styrene/butadiene and styrene/isoprene, two well-known immiscible polymer pairs. The predicted UCST's for very low molecular weight blends of these homopolymers (1.5K and 2K respectively) are shown in Figure VI.4. On the other hand, block copolymers of PB and PI were recently reported to be highly miscible and exhibit a LDOT at elevated temperature for very large molecular weights.[150] The predicted phase diagram for blends of these components is also shown. Again, the LCST/LDOT in this system arises from the lower thermal expansion coefficient and higher reduced density of PB ($\alpha = 5.67 \times 10^{-4}$ K^{-1}) compared to those of PI ($\alpha = 6.56 \times 10^{-4}$ K^{-1}), combined with the very small predicted χ for this polymer pair.

In fact, in light of these results, the "anomalous" LCST for most saturated polyolefin blends involving polyisobutylene (PIB) is entirely explicable.[56] Indeed, PIB is characterized by a very small thermal expansion coefficient in comparison to all the other saturated polyolefins ($\alpha_{PIB} \sim 5.65 \times 10^{-4}$ K^{-1} compared to $\sim 7 \times 10^{-4}$ K^{-1}), which provides the right conditions for LCST behavior in blends involving this homopolymer and other saturated polyolefins with matching solubility parameters and densities. The predicted phase diagrams for blends of PIB and two random copolymers of ethylene and butene, denoted P(E-r-B) and containing 66 and 97 wt% of butene, respectively, are also shown in Figure VI.4. While the former is miscible at room temperature and displays a LCST at $\sim 100°C$ for $\sim 80K$ homopolymers, the latter is macrophase separated at 25°C and higher temperatures even for molecular weights of $\sim 50K$.[56] These thermodynamic trends are

quantitatively captured by the fourth phase diagram of Figure VI.4, where the spinodals

of 70K and 13K blends of PIB/P(E-r-B)66 and PIB/P(E-r-B)97, respectively, are shown.
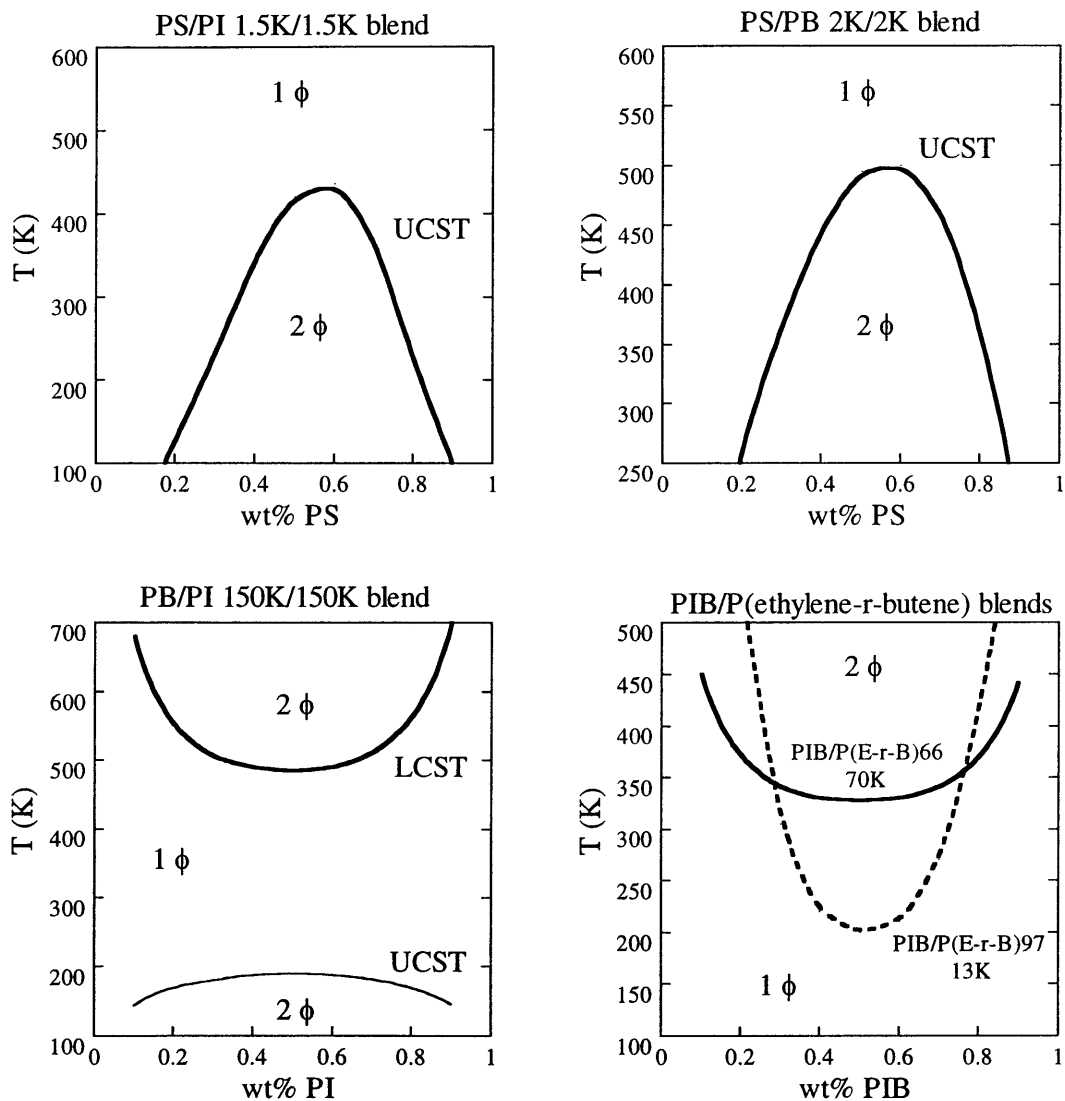
Figure VI.4: Predicted phase diagrams for PS/PI, PS/PB, PB/PI and PIB/P(E-r-B)

VI.4.4. Chemically similar homopolymer blends

Typically, miscibility is expected for blends of chemically similar homopolymers such as PS and P(α-methylstyrene) (PαMS), poly(alkyl methacrylates) and poly(alkyl acrylates) of similar degrees of branching, polybutadiene and polyisoprene, etc. However, both types of phase behavior (LCST or UCST) have been reported, depending on the particular polymer pair. Hence, blends of PS and PαMS display a low-T UCST even for large molecular weights[134,157], as do blends of PEMA and PEA, though with a much lower degree of thermodynamic compatibility.[158] The phase behavior of these two polymer pairs is correctly predicted by equation VI.23 and the phase diagrams shown in Figure VI.5 for 300K and 24K blends, respectively. On the other hand, as mentioned above, LCST/LDOT-type phase behavior was recently reported for the PB/PI pair, also successfully captured by equation VI.23 (see Figure VI.4). For this polymer pair, the LCST arises from a large difference in the pure component thermal expansion coefficients, which is absent in blends of PS and PαMS, and even more so in blends of PEA and PEMA. Indeed, the thermal expansion coefficients of PB and PI are 5.67 and 6.56 10^{-4} K^{-1}, those of PS and PαMS 5.13 and 5.76 10^{-4} K^{-1}, and those of PEA and PEMA 7.24 and 7.47 10^{-4} K^{-1}, respectively. For the latter two polymer pairs, the LCST should lie at increasingly high temperatures, thereby precluding its experimental observation.
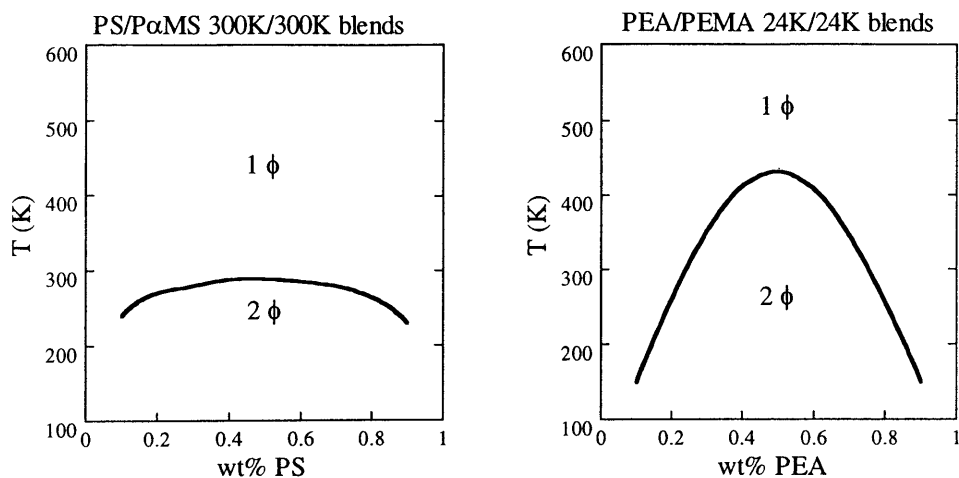
Figure VI.5: Predicted phase diagrams for PS/PαMS and PEA/PEMA.

VI.4.5. PMMA, PC and PCL-based blends

Finally, in this section, the phase diagrams of some other well-known miscible

pairs involving PMMA, polycarbonate (PC) and polycaprolactone (PCL) are presented.

Figure VI.6 shows the phase diagrams of three blends of PMMA and styrene/acrylonitrile

(SAN) random copolymers containing 6 (SAN6), 18 (SAN18) and 40 wt% acrylonitrile

(SAN40), respectively. The miscibility and LCST in these blends is restricted to SAN

copolymers containing 10 to 38 wt% AN.[137-140] Again, this is successfully predicted by

equation VI.23, since both PMMA/SAN6 and PMMA/SAN40 exhibit a UCST for low

molecular weights, while a 250K/250K PMMA/SAN18 blend is miscible and exhibits the

LCST. Similar miscibility windows spanning 8 to 28 wt% and ~15-25 wt% AN,

respectively, have been reported for blends of SAN/PCL[159,160] and SAN/PC.[161,162] These

trends are also successfully predicted, as seen in the phase diagrams shown in Figure

VI.6.

161
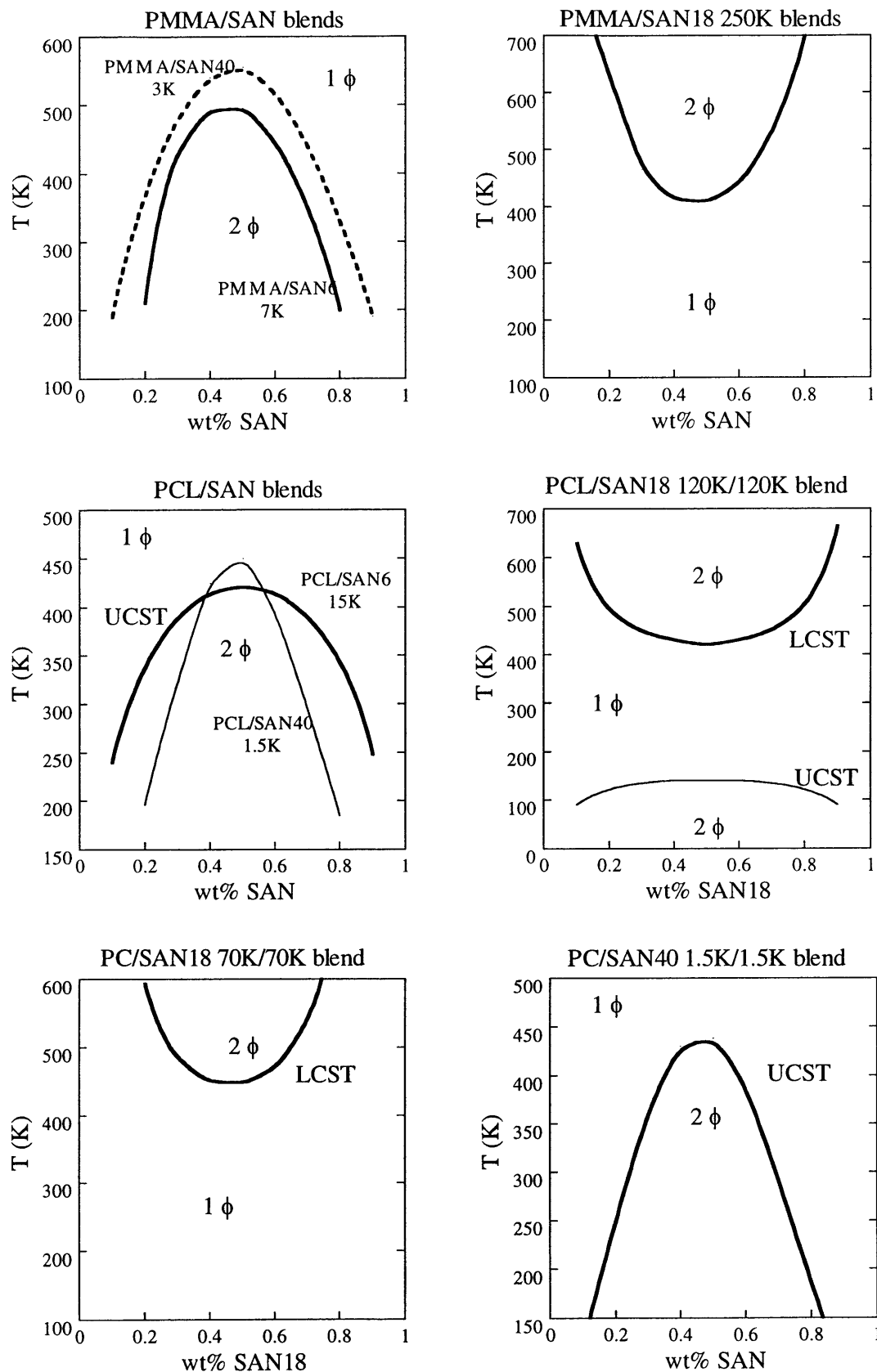
Figure VI.6: Predicted phase diagrams for PMMA/SAN, PCL/SAN and PC/SAN

Miscibility and the LCST are further predicted for intermediate molecular weight blends of PMMA and PC, in accord with the reported studies on this polymer pair[163-165], and also for blends of PMMA and PCL. For PMMA and PEO, on the other hand, moderate miscibility and UCST-type phase behavior are predicted for ~25K blends. This correlates well with the neutron scattering studies of Hopkinson and coworkers, who reported a decrease in scattering intensity and SANS-based χ with increasing temperature for PMMA/PEO blends, although a higher degree of thermodynamic compatibility is observed experimentally.[166] Earlier, Russell and coworkers also investigated this polymer pair with SANS, but reported a roughly constant χ across the whole T-range.[167] The predicted phase diagrams of these systems are shown in Figure VI.7.
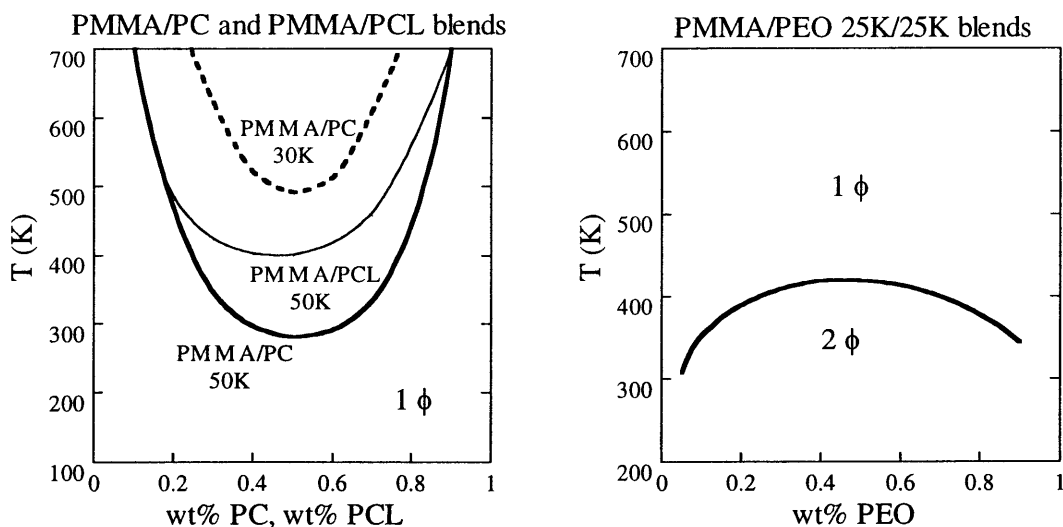
Figure VI.7: Predicted phase diagrams for PMMA/PC, PMMA/PCL and PMMA/PEO

In fact, the successful prediction of phase behavior for the more polar systems presented in this section using equation VI.23 in combination with the geometric rule of mixing for ε_{AB} indicates that strong specific interactions do not need to be invoked to

explain their miscibility. This is in contrast to PMMA/PVC and other methacrylate/PVC blends. Indeed, Berthelot's mixing rule predicts a large positive χ parameter and immiscibility for these blends, while their miscibility even for large molecular weights has been reported.[151] Similar predictions are further obtained for blends of PMMA and PVDF, two well-known compatible polymers.[94,95] Hence, out of the 25 systems considered in this Chapter, the latter two appear to be the only ones for which a simple geometric average for the cross-interaction energy ε_{AB} is unsatisfactory. These are precisely the systems identified as "strongly interacting" in Chapter IV, and for which a matching of the homopolymer solubility parameters and densities does not necessarily result in miscibility. While the inadequacy of a geometric average for ε_{AB} of these polymer pairs involving increasingly strong dipole/dipole interactions is obvious, their phase behavior should still be captured by equation VI.23, provided a more accurate estimate of χ was available.

VI.5. SUMMARY

In this Chapter, a phenomenological free energy expression was derived for compressible polymer mixtures. Its ability to predict phase behavior as a function of temperature was demonstrated for homopolymer blends of 23 polymer pairs. Phase diagrams were calculated for each of these systems, which correlate predictively with the reported phase behaviors. In computing these phase diagrams, the following assumptions were made:

1. χ was assumed to follow Berthelot's rule of mixture and the Hildebrand solubility parameter formalism.[40]

2. Pure component cohesive energy densities were obtained using group contributions according to van Krevelen.[42]

3. An average hard core segmental volume $v = \sqrt{v_A v_B}$ and equal coordination numbers z were assumed for the mixed state.

4. Hard core and reduced densities of the pure components were obtained by extrapolating experimental PVT data[83] to 0K at 0 pressure (hard core state) assuming constant thermal expansion coefficients α taken from the melt state.

Even though some of these assumptions are clearly restrictive, excellent qualitative agreement between the predicted and observed temperature-dependent phase diagrams was obtained, with no adjustable parameters. However, given the necessity of reliable PVT data of the pure components, phase diagrams were calculated only for systems for which these were available. Indeed, while Chapter IV and V made use of a combination of GC/LF EOS calculations[88] to estimate PVT behavior of various homopolymers, this formalism tends to strongly overestimate the temperature dependence of the density and, thereby, α. This, in turn, results in erroneous phase diagram predictions when used in the context of equation VI.23 since a small change in α strongly affects the location of the spinodal temperature, if not the type of phase behavior. Provided such data was available, we believe accurate phase diagrams could be predicted for numerous additional weakly interacting polymer pairs, including styrene/n-alkyl acrylates, as wells as PS/P(MMA-r-LMA), investigated in this thesis, and

countless other homopolymer/random copolymer systems. Although not attempted in this thesis, equation VI.21.b and 23 should also correctly predict phase diagrams for polymer solutions and, perhaps, small molecule systems. The success of equation VI.23 in combination with Berthelot's mixing rule in predicting phase diagrams for so many different polymer pairs and without requiring any experimental data on the mixture is a highly encouraging result, which contrasts with the compressible theories developed to date. Indeed, while some of these formalisms are clearly more rigorous than the phenomenological model proposed here, the price for this increased rigor is an apparent loss of predictive capability.

Towards the goal of quantitative phase diagram predictions, perhaps the most limiting assumption of the list above is that of constant thermal expansion coefficients. While, qualitatively, the predicted phase diagrams and trends in thermodynamic compatibility are excellent, the strong dependence of predicted spinodal temperatures on the values of α suggests that relaxing this assumption might yield better quantitative agreement with experimental spinodal curves. The impact of a constant α on the extrapolated values of the hard core parameters and resulting reduced densities further support these conclusions. A second potentially important source of deviations between predictions and experiments is the use of simple group contribution calculations for the evaluation of pure component cohesive energy densities. As explained in Chapter IV (section IV.1.1), the strong sensitivity of solubility parameter calculations on the particular formalism chosen complicate their use as a quantitative tool.

Nevertheless, the model presented in this Chapter provides a unique tool for phase diagram prediction that might be used for the design of new functional polymer blends

and block copolymers. Moreover, the phenomenological model based on equation VI.23 in combination with the assumptions listed above provides a simple explanation for the molecular origin of the LCST/LDOT in compatible polymer blends and block copolymers. Indeed, provided χ is small enough, which is achieved for polymer pairs with similar cohesive properties, phase separation upon heating arises naturally from a difference in free volume between the two components and its increase with increasing temperature due to a difference in thermal expansion coefficients. While this concept naturally emerged from most compressible theoretical treatments of polymer thermodynamics,[23,24,79,84-87,] starting with the work of McMaster in 1973[105], a simple mathematical expression of it in terms of the pure component properties only is given here for the first time.

Finally, while the model presented here in combination with Berthelot's mixing rule successfully predicts the phase behavior of all the weakly interacting systems considered, erroneous predictions are obtained for systems characterized by increasingly strong specific interactions. PMMA/PVC and PMMA/PVDF were given as two examples of such blends. It is expected that other systems involving even stronger interactions such as H-bonding and electrostatic interactions would also be poorly described. However, these failures point to the inadequacy of a geometric average for cross-interaction energies, rather than a failure of the free energy expression developed in this thesis, at capturing the thermodynamics of these systems

CHAPTER VII: CONCLUSIONS AND FUTURE WORK

PREAMBLE

Motivation for this thesis was drawn from one main premise, namely, that current applications of block copolymers are limited, in part because of a lack of control over their bulk thermodynamics and, more specifically, the appearance of order/disorder (solid-like/liquid-like) transitions. Indeed, from an application standpoint, the strong thermodynamic incompatibility typically found for block copolymers is highly advantageous, as it results in remarkably stable solid-like microphase separated morphologies that are of particular interest from an engineering standpoint. However, for melt-processing where flow is essential, the ability to access the segmentally mixed liquid state is clearly desirable. In an attempt to address this need, this thesis focused on, firstly, developing a better understanding of the molecular factors governing bulk thermodynamics in block copolymers and, secondly, developing simple predictive tools that could be used to molecularly design the behavior of new systems of commercial interest. The main conclusions drawn in this work and their impact from a materials science standpoint are summarized in this Chapter, along with some thoughts regarding future work.

VII.1. EXPERIMENTAL STUDIES

VII.1.1. Phase behavior of PS-*b*-P*n*AMA

Preliminary studies performed in collaboration with M. Pollard and T. P. Russell on PS-*b*-PBMA[82], a system previously found to display a LDOT[22,76], had revealed a unique pressure sensitivity of the ordering transition of this block copolymer. By applying 1kbar of hydrostatic pressure, its solid-like/liquid-like transition could be raised by 150°C, an unprecedented observation of pressure effects in block copolymers. Moreover, pressure forcing segmental mixing in this LDOT-type block copolymer implies "baroplasticity", a property that could be highly advantageous from a processing standpoint. Unfortunately, PS-*b*-PBMA, consisting of two high T_g blocks (T_g's above typical use temperatures), is not very attractive from a commercial standpoint, since its properties mimic those of glassy thermoplastics. However, the ability to design such "baroplastic" behavior into more relevant block copolymers, such as those consisting of a low T_g acrylate and a higher T_g second block, would be highly attractive.

To better understand the molecular origin of this strong pressure sensitivity, and perhaps identify new block copolymers with similar properties, the phase behavior of a family of diblock copolymers between styrene and a homologous series of *n*-alkyl methacrylates was investigated, both as a function of temperature and pressure. The results obtained on this family of materials, presented in Chapter III, revealed a strong dependence of the phase behavior of these block copolymers on the degree of branching of the methacrylate block. For very *short* ($n = 1$, MMA) and *long* ($n \geq 6$, HMA, OMA

and LMA) alkyl side chains, the classical UDOT-type phase behavior of block copolymers consisting of incompatible blocks is observed. For *intermediate side chain length* ($2 \leq n \leq 4$), however, the block copolymer is miscible at low temperatures and microphase separates upon heating through a LDOT. These results point to a strong influence of monomer structure on the block copolymer phase behavior. Indeed, given the chemistry involved in this family of materials, the presence of strong specific interactions between the non-polar styrene and the polar methacrylate segment cannot be deemed responsible for the compatibility observed for intermediate side chain lengths. At best, modest dipole/induced dipole interactions can occur between these two segments. Therefore, other effects, such as a fine balance between these weak interactions and favorable packing effects between the two monomers in the segmentally mixed state, must be invoked to explain the trend observed in these materials.

Interestingly, these effects manifest themselves quite dramatically in a systematic variation of the influence of hydrostatic pressure on the order/disorder transition of these materials. Indeed, for very short ($n=1$) and very long ($n=8$, 12) alkyl side chains, small pressure coefficients for the UDOT of the block copolymer are obtained, similar to those reported for other UDOT-type systems investigated in the literature. However, for alkyl side chain lengths ranging from $n=2$ to $n=6$, styrene/n-alkyl methacrylate block copolymers are characterized by unexpectedly large pressure coefficients, ranging in magnitude from 60 to $150°C/kbar$. These results, combined with those obtained as a function of temperature, point to a distinct linkage between packing and energetics which, for intermediate side chain lengths, is favorable to mixing at low temperatures and leads to the LDOT.

From an engineering standpoint, the large pressure coefficients of, not only the three LDOT-type systems (*n*=2, 3, 4), but also the UDOT-type PS-*b*-PHMA (*n*=6), are particularly interesting. Firstly, they demonstrate that UDOT-type block copolymers *can also* be characterized by strong pressure sensitivity. To our knowledge, it is the first time that pressure coefficients of this magnitude are reported for UDOT/UCST-type materials. Secondly, in all four of these systems, pressure can be used effectively to force segmental miscibility and, hence, liquid-like rheological properties. The ability to molecularly engineer such pressure- *and* temperature-tunable thermodynamic and rheological behavior into new systems was the subject of Chapters IV and V of this thesis.

VII.1.2 A predictive tool for the design of BCP phase behavior

VII.1.2.a GC/LF EOS calculations

In light of the systematic variation in phase behavior observed across the family of styrene/*n*-alkyl methacrylate BCP's, an attempt was made to identify pure component parameters that would correlate with these thermodynamic trends. To this end, simple group contribution (GC) calculations were used in combination with the Sanchez-Lacombe LF equation of state to calculate the solubility parameter (square root of the cohesive energy density) and mass density of the corresponding homopolymers of the various diblock copolymers investigated in Chapter III. These calculations showed that, not only the solubility parameter, but also the *density* of the alkyl methacrylate homopolymer, are closest to those of polystyrene for intermediate side chains, precisely

171

the systems exhibiting the highest degree of thermodynamic compatibility and pressure sensitivity. These calculations were further applied to a comprehensive list of well-known miscible polymer pairs, thereby distilling a new and very simple criterion for the design of thermodynamic compatibility in weakly interacting polymer blends: a match in mass density.

VII.1.2.b Molecular design of phase behavior in PS/PnAMA

The success of these simple calculations in capturing the general trends in phase behavior for the styrene/*n*-alkyl methacrylate family as well as many other polymer pairs inspired the following test of their predictive capabilities. A new styrene/methacrylate block copolymer that would exhibit the LDOT and the strong pressure effects that ensue was designed and synthesized, whereby the methacrylate block consisted of a random sequence of short and long alkyl side chain methacrylates both individually immiscible with polystyrene, and mutually immiscible, namely methyl (MMA, *n*=1) and lauryl methacrylate (LMA, *n*=12). The particular composition of the random methacrylate block, denoted P(MMA-*r*-LMA), was selected by matching its solubility parameter and density to those of polystyrene based on the GC/LF EOS calculations. The resulting block copolymer, denoted PS-*b*-P(MMA-*r*-LMA) and containing 53 wt% of MMA in the methacrylate block, was indeed found to exhibit LDOT behavior, with a dramatic pressure coefficient of 150°C/kbar! Moreover, the GC/LF EOS calculations applied to this family of materials showed that the miscibility window for PS-*b*-P(MMA-*r*-LMA) could be predicted quantitatively. Indeed, the calculations suggested that these

copolymers should be miscible for weight fractions of MMA in the methacrylate block ranging from 51 to 82 wt%. The results presented in Chapter IV showed that when the methacrylate content is decreased from 53 to 47 wt%, the phase behavior of the block copolymer changes from LDOT to UDOT, precisely following the trend in phase behavior observed for the homologous series of styrene/n-alkyl methacrylates. These results are central to this thesis since they demonstrate for the first time how the phase behavior of new block copolymers can be designed in a predictive manner via architectural modifications of the block segments. They further imply that the phase behavior of these weakly interacting block copolymers is sensitive to an average monomer structure, rather than the local details and chemical identity of the block segments, a highly attractive concept to polymer scientists and engineers.

VII.1.3 Styrene/acrylate "baroplastic" elastomers and adhesives

The simple semi-quantitative tool for the molecular design of miscibility into weakly interacting block copolymer melts identified in this thesis was further applied to the design of temperature and pressure-tunable block copolymers of commercial relevance, such as polystyrene-*block*-poly n-alkyl acrylates, denoted PS-*b*-PnAA. These materials are highly attractive candidate thermoplastic elastomers or adhesives which can now, for the first time, be prepared using new controlled/"living" free radical polymerization techniques such as atom transfer radical polymerization (ATRP). The ability to control the appearance of order/disorder (solid like/liquid-like) transitions by molecular design of these systems was demonstrated in Chapter V.

As expected based on the GC/LF EOS calculations applied to this new series of materials, a trend in phase behavior similar to that observed for PS-b-PnAMA was obtained. Hence, for short (n=1: PMA) and long side chains (n=6, 8, 12: PHA, POA and PLA), the acrylate block is incompatible with polystyrene and the copolymer exhibits the classical UDOT. In contrast, for n=4 (PBA), a phase diagram quite similar to that reported for PS-b-PBMA is observed, i.e., with both UDOT and LDOT-type phase behaviors. However, the temperature of the UDOT for equivalent molecular weights appears to be shifted to higher temperature for the styrene/acrylate system.

Accordingly, this material as well as several PS-b-P(MA-r-LA) block copolymers, molecularly designed in the same manner as the PS-b-P(MMA-r-LMA) system, are all characterized by large pressure coefficients, on the order of $100°C$/kbar, although the former only display UDOT-type phase behavior. These last experimental results amply demonstrate how new baroplastic elastomers can be designed to exhibit strong pressure sensitivity. Together with the results obtained for PS-b-PHMA ($dT_{UDOT}/dP = -60°C$/kbar) they further confirm that UDOT-type block copolymers can also be characterized by large pressure coefficients. From an applications standpoint, the results presented in Chapter V demonstrate how industrially amenable synthetic routes such as ATRP can be successfully combined with the molecular design tool identified in this thesis to impart pressure and temperature-tunable phase behavior into new acrylic block copolymers of commercial relevance. Given the fact that current polymer processing technologies often involve the application of pressure on the polymer melt, such behavior could have a direct economic impact. In the next section, this idea is explored and a new class of true baroplastic elastomers is proposed.

VII.1.4. "Baroplasticity" and a new class of green plastics

Based on these results, a new class of polymeric materials is proposed here, that could be processed *mainly* by the application of pressure, rather than temperature, thereby allowing them to be recycled multiply and with properties equivalent to the virgin material. Indeed, a large drawback of today's commercial plastics based on incompatible block copolymers such as PS-*b*-PI is their high viscosity in the melt due to the stability of the microphase separated state. Consequently, processing of these materials can only be achieved through the use of solvents, low molecular weight blocks, or very high temperatures so that a highly fluid state is achieved. While the first avenue is problematic from an environmental standpoint, the second results in materials with very poor mechanical properties due to the low entanglement density of these small polymer chains. High temperatures, on the other hand, inevitably lead to alterations of the chemical structure, resulting in a dramatically reduced performance. Therefore, taking advantage of the baroplastic behavior identified in this thesis would not only result in a dramatic lowering of the processing costs but also allow for multiple recycling by limiting the exposure of the material to high temperatures. Moreover, this could be achieved using classical processing techniques such as compression molding, etc., since these naturally involve the application of pressure on the polymer melt. Suggestions regarding the types of block copolymers that would be ideal for this purpose are outlined below.

Today's commercial elastomers based on block copolymers typically involve a very low-T_g material as the majority component and a high-T_g block such as PS or

PMMA as the second block. What appears unappreciated is that excellent mechanical properties can also be achieved by choosing a second block with a T_g closer to room temperature, yielding elastomers still suitable for many applications involving low temperatures only. A plethora of block copolymer compositions can be readily identified, in which one of the component blocks has a very low T_g and the second component has a T_g above the service temperature of the material, but below $100°C$. By further making a judicious choice of composition using the design criterion identified in this thesis to impart a strongly pressure sensitive UDOT, UDOT+LDOT or LDOT-type phase behavior, new materials with highly attractive rheological properties could be designed. Indeed, at room temperature, microphase separation would impart elastomeric properties to these copolymers. However, under the application of pressure at temperatures hardly exceeding the T_g of the hard block, these materials could be processed from the melt in the liquid, segmentally-mixed, state via compression molding, for example. Such a new elastomeric block copolymer based on PBMA and PBA was successfully synthesized using ATRP that displays excellent mechanical properties at room temperature. While a thorough investigation of its phase behavior was not carried out in this thesis and is suggested as future work, preliminary results indicate this material might be the first true baroplastic elastomer, since it was successfully compression molded at ~60°C under a pressure of 500 psi! It is hoped that such materials might partly address the current needs for recyclable plastics.

VII.2. THEORY

VII.2.1. A phenomenological compressible free energy expression

Besides their direct implication from an engineering standpoint, the systematic

trends in phase behavior with monomer structure and pure component properties revealed

in this thesis suggest that a simple free energy expression might be able to capture these

observations.

The simple design tool based on GC/LF EOS calculations identified and utilized

in this thesis successfully predicts whether or not miscibility will be encountered for a

given polymer pair. However, it does not allow one to predict the type of phase diagram

to be expected, namely LDOT/LCST versus UDOT/UCST, crucial information for the

design of new functional materials. In an attempt to address this last need, a

phenomenological free energy expression for compressible polymer mixtures was

derived in Chapter VI. Given the similarity in phase behavior for block copolymers and

the corresponding homopolymer blends, its extension to the former is straightforward and

was not discussed in this thesis. The ability of this model to qualitatively predict phase

diagrams for the homopolymer pairs investigated in this thesis and many others reported

in the literature was demonstrated.

This phenomenological free energy expression was derived in a similar fashion as

the well-known Flory-Huggins theory, assuming random mixing (mean-field

approximation). However, in deriving expressions for the changes in enthalpy and

entropy upon mixing, the free volume of the pure components and the mixture, defined as the difference between the total volume and the hard core (0K) volume, were accounted for. The final expression for the change in free energy per unit volume, obtained upon ignoring changes in volume on mixing and assuming an average hard core monomer volume $v=(v_A v_B)^{1/2}$ in the mixture, is given by equation VI.21.b, repeated here:

$$\Delta g_{mix} = RT\left[\frac{\phi_A \tilde{\rho}_A}{N_A v_A}\ln\varphi_A + \frac{\phi_B \tilde{\rho}_B}{N_B v_B}\ln\varphi_B\right] + \frac{\phi_A \phi_B \tilde{\rho}_A \tilde{\rho}_B}{v}(RT\chi^{FH}) + \phi_A \phi_B\left[(\tilde{\rho}_A - \tilde{\rho}_B)(\delta_A^{2} - \delta_B^{2})\right]$$

In predicting phase diagrams for various weakly interacting polymer pairs using this expression, Berthelot's mixing rule and the Hildebrand solubility parameter formalism were assumed for the evaluation of χ^{FH}:

$$\chi^{FH} = \frac{v(\delta_{A_o} - \delta_{B_o})^2}{RT}$$

Extrapolation of Tait-equation fits to experimental density data to zero K at P=0, assuming constant thermal expansion coefficients α (the melt state values), was used to extract hard core densities and segmental volumes. Finally, solubility parameters of the pure components were obtained using GC calculations according to Van Krevelen. In this fashion, qualitative phase diagrams could be successfully predicted for 23 polymer pairs and this without requiring any experimental data on the mixture.

Equation VI.21.b further provides a simple molecular explanation for the LDOT/LCST. Indeed, provided χ is small enough, which is achieved for weakly interacting polymer pairs with matching solubility parameters and densities, phase separation upon heating at an experimentally accessible temperature arises naturally from a difference in the thermal expansion coefficients of the two components. In contrast, when this difference is very small or when χ is large, UDOT/UCST-type phase behavior

is observed instead. This explanation suggests some simple molecular criteria for the design of phase behavior of new functional polymer blends and block copolymers. Hence, based on these considerations, the candidate baroplastic PBMA-*b*-PBA described above is expected to display UDOT- rather than LDOT-type phase behavior, in analogy to the PEMA/PEA system investigated in Chapter VI. However, such phase behavior arises mainly from free volume effects (third term of equation VI.21.b) rather than a large χ, suggesting that strong pressure effects might be expected for these UDOT-type block copolymers.

VII.2.2. Future work

VII.2.2.a. Pure component thermodynamic properties

As explained in the last section of Chapter VI, phase diagrams were predicted only for systems for which accurate pure component experimental PVT data was available. These data where then extrapolated to 0K (hard core state) assuming constant α's. However, an attractive alternative avenue to obtain the pure component thermodynamic parameters necessary for phase diagram predictions using equation VI.21.b might consist in molecular dynamics and energy minimization simulations. Indeed, Choi *et al.*[170] recently reported on the use of the commercial software Cerius in combination with the force field UNIVERSAL to simulate the density, cohesive energy density and hard core (0K) parameters of PS and PVME. These simulated densities and cohesive energy densities, obtained from hypothetical polymer chains of as little as 20

segments, were found to be in good agreement with experimentally determined values as well as those obtained from GC calculations. The advantage of such a procedure clearly relies in its predictive nature, thereby allowing one to estimate the thermodynamic properties of new polymers, including random copolymers of various compositions, instead of measuring them using a PVT apparatus. Moreover, this approach might also yield hard core state parameters with improved physical meaning in comparison with the extrapolated values used in this thesis. The potential use of these simulations in combination with the free energy model derived in this thesis might offer an attractive approach for the design of phase behavior into new systems.

Alternatively, a much simpler, although less accurate and powerful, approach to obtain the thermodynamic information necessary for phase diagram predictions using equation VI.21.b might be the built-in group contribution-like databases of commercial software packages such as Biosym. Indeed, certain modules of this software can be used to predict polymer densities as a function of temperature, solubility parameters, thermal expansion coefficients above and below the glass transition, etc.[171] While the values predicted in this fashion would clearly lack the accuracy of experimentally determined ones or those obtained from molecular dynamics simulation, these estimations might be attractive from an engineering standpoint, serving as rough guidelines for the choice of random copolymer compositions and chemistries for the design of new functional polymer blends and block copolymers.

The two approaches outlined here might be particularly useful in the area of biomaterials. Indeed, these materials mainly involve biodegradable polymers such as lactides or glycolides, for which PVT data are currently not available in the literature.

However, the ability to design tunable phase behaviors in these new materials has direct implications from an applications standpoint. This is not only for processing reasons, but also, and more importantly, because of the strong influence of blending or block copolymerization on the biodegradable properties and lifetimes of these polymers.[172,173]

VII.2.2.b. Beyond T-dependent polymer blend phase behavior

The success of equation VI.21.b (in combination with the assumptions listed above) at capturing the qualitative trends in phase behavior for several weakly interacting polymer pairs suggests that it might also be used to predict the phase behavior of polymer solutions, small molecule mixtures, and perhaps even inorganic alloys. Moreover, the compressible free energy expression derived here should also capture the effect of pressure on polymer blend and block copolymer phase behavior. Although this was attempted by the author, the inconclusive predictions were not incorporated in the document. Curiously, it was found that equation VI.21.b successfully predicts a large pressure coefficient of ~ 120°C/kbar for the LCST of PS/PBMA, which correlates extremely well with the observed pressure sensitivity of this polymer pair. However, when the same calculations are performed on blends of PS and PI, an equivalently large and negative pressure coefficient was predicted for the UCST of this system. This is clearly in contrast with the reported pressure dependence of PS/PI block copolymers, which display a decrease in thermodynamic compatibility with pressure of about 20°C/kbar. The origin of this discrepancy between experiments and predictions is unclear. However, it is important to note that the extrapolation procedure using constant

α's used in this thesis appears to systematically overestimate the free volume term (third term of equation VI.21.b) in comparison to the purely enthalpic χ-term. While the consequences of this error are minor for systems with matching cohesive properties, for which χ is small, they become serious for systems governed by unfavorable enthalpic interactions, such as PS/PI or PS/PB. Improved predictions, both as a function of temperature and pressure, might be obtained by taking into account the temperature dependence of α in extracting the hard core parameters.

APPENDIX

A.III. IRPA FITTING PARAMETERS

Table A.I: IRPA FITTING PARAMETERS FOR PS-B-PNAMA

Copolymer	T range (°C)	N	χ at 150°C	a_{MA} (Å)	Incoh. scatt. I_{inc} (cm^{-1})	Scaling factor
19K PS$_{d8}$-b-LMA	150-210	122	0.083	15 ± 1	-	0.1 ± 0.05
23K PS-b-OMA	120-200	175	0.056	12.3 ± 0.4	~ 0.35 ± 0.02	~ 0.02
28.6 K PS-b-HMA	150-215	221	0.044	10.8 ± 0.5	~ 0.065 ± 0.001	0.005 ± 0.0002
85K PS-b-PBMA	110-150	672	0.014	8.8 ± 0.4	-	12.5 ± 0.5
110K PS-b-PPMA	100-175	972	0.0008	8.6 ± 0.5	~ 0.068 ± 0.001	0.0015 ± 0.0002
70K PS-b-PEMA	120-185	643	0.0156	8.3 ± 0.5	~ 0.53 ± 0.03	0.0075 ± 0.0005

A.IV. GROUP CONTRIBUTION/EOS CALCULATIONS

A.IV.1. Solubility parameters

The solubility parameters of the homopolymers and random copolymers

considered in this thesis were obtained according to Van Krevelen, using the group

contributions listed in reference 42. The expression for δ used includes contributions

from dispersive forces (δ_d), dipole/dipole (δ_p) and hydrogen bonding (δ_H) interactions.

Equation A.IV.1 relates the total solubility parameter δ to these three contributions:

$$\delta = \sqrt{\delta_d{}^2 + \delta_p{}^2 + \delta_H{}^2}$$
(A.IV.1)

The three components of δ are given by:

$$\delta_d = \frac{\sum_i F_{d_i}}{V}$$
(A.IV.2.a)

$$\delta_p = \frac{\sqrt{\sum_i F_{p_i}^2}}{V}$$
(A.IV.2.b)
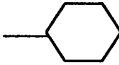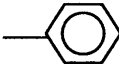
$$\delta_H = \sqrt{\frac{\sum_i E_{H_i}}{V}}$$
(A.IV.2.c)

where F_{di} is the contribution to dispersive forces, F_{pi} the contribution to polar

forces, and E_{Hi} the contribution to hydrogen bonding energy for chemical group i, and V

is the molar volume. In most cases, V was taken directly from Tables 4.5-4.7 of reference

42. For the polymers for which this values was not listed, V was calculated using the

group contributions listed in Table 4.9 of the reference. Table A.IV.1 gives the group

contributions F_{di}, F_{pi}, E_{Hi} for the chemical groups most commonly encountered in vinyl polymers, while Tables A.IV.3 through A.IV.5 give the molar volume V, calculated δ and EOS parameters (see below) for the homopolymers considered in this thesis.

TABLE A.IV.1: SOLUBILITY PARAMETER GROUP CONTRIBUTIONS FOR THE CHEMICAL GROUPS ENCOUNTERED IN VINYL MONOMERS.

Chemical group	F_{di} $(J^{1/2}cm^{3/2}/mol)$	F_{pi} $(J^{1/2}cm^{3/2}/mol)$	E_{Hi} (J/mol)
-CH$_3$	420	0	0
-CH$_2$-	270	0	0
-CH-	80	0	0
-C-	-70	0	0
=CH$_2$	400	0	0
=CH-	200	0	0
=C<	70	0	0
	1620	0	0
	1430	110	0
-Cl	450	550	400
-CN	430	1100	2500
-OH	210	500	20000
-O-	100	400	3000
-CO-	290	770	2000
-COOH	530	420	10000
-COO-	390	490	7000

A.IV.2. Specific volumes

Specific volumes were also estimated for each homopolymer using the recently

reported[88] combination of group contribution methods and lattice fluid (LF) equation of

state model, which was described in Chapter I, section I.3.2.a. The LF Sanchez-Lacombe

equation of state in the long chain limit:

$$\tilde{\rho}^2 + \tilde{P} + \tilde{T}[\ln(1 - \tilde{\rho}) + \tilde{\rho}] = 0 \qquad\qquad (A.IV.3)$$

was solved as a function of temperature for each homopolymer using equation of state

parameters P^*, T^* and ρ^* obtained from group contributions as follows:

$$
\begin{aligned}
P^* &= \sum P^*_i - P_o \\
T^* &= \sum T^*_i - T_o \\
\rho^* &= \sum \rho^*_i - \rho_o
\end{aligned}
\qquad\qquad (A.IV.4)
$$

where P_o, T_o and ρ_o are universal constants for all polymers (498.46 MPa, 666.95 K and

1.01947 g/cm^3 respectively) and P_i^*, T_i^* and ρ_i^* are the contributions to P^*, T^* and ρ^*

for chemical group i. These contributions are listed in reference 88 and those of interest

for the homopolymers studied in this thesis are given in Table A.IV.2.

The resulting equation of state parameters for each homopolymer are listed in

Table A.IV.3 through A.IV.5, along with the molar volume V and the solubility

parameter δ. Table A.IV.3 gives the values for polystyrene and the series of n-alkyl

methacrylates investigated in Chapters III and IV, Table A.IV.4 those for other systems

discussed but not investigated experimentally in this thesis, while Table A.IV.5 gives the

values for the series of n-alkyl acrylates discussed in Chapter V.

TABLE A.IV.2: GROUP CONTRIBUTIONS TO THE LF EOS PARAMETERS

Chemical Group	T_i^* (K)	P_i^* (MPA)	ρ_i^* (g/cm^3)
CH$_3$	-18.08	-105.41	-200.69
CH$_2$	-7.65	-29.67	-46.65
CH	70.40	-36.29	16.94
C	97.41	82.23	136.60
CH=CH	-129.64	-6.11	63.84
ACH	-114.89	-17.51	-18.53
ACCH	674.27	1.24	223.28
-COO-	-76.38	168.96	363.43
CH$_3$O	-72.69	-70.50	110.24
CH$_2$O	-8.14	7.89	182.84
CH$_2$Cl	-76.21	-2.06	257.75
CHCl	61.71	-46.78	491.19
CF$_2$	-24.47	-59.23	614.27
CHCN	193.71	76.22	257.19

Note that for the long alkyl side chain methacrylates and acrylates ($n \geq 6$), the EOS parameters as calculated from the GC listed in Table A.IV.2 yielded unrealistically low densities compared to those reported in the literature for some of these polymers.[83,129] In fact, it was found that treating these highly branched methacrylate repeat units as consisting of x units of MMA and (1-x) units of poly(ehtylene) (linear alkyl side chain), resulted in EOS parameters yielding more reasonable densities. For example, hexyl

methacrylate can be decomposed into one unit of MMA and 2.5 units of PE (5 CH_2),

yielding $x = 1/3.5$. Each EOS parameter is then calculated as a molar average of the

respective parameters of PMMA and PE, i.e:

$$X^*_{PHMA} = xX^*_{PMMA} + (1-x)X^*_{PE} \qquad \text{(A.IV.5)}$$

except for the hard core density, as explained in section A.IV.3 below.

The alternative EOS parameters obtained in this manner are listed in bold in Table

A.IV.3 and A.IV.5 while those obtained by simply summing the GC of the groups present

in the methacrylate repeat unit are in italic. The former were used in this thesis.

TABLE A.IV.3: EOS PARAMETERS AND δ FOR ALKYL METHACRYLATES

homopolymer	V_m (cm^3/mol)	δ ($J^{1/2}$/cm$^{3/2}$)	T* (K)	P* (MPa)	ρ* (g/cm^3)
PS	98	18.19	759	373	1.103
PMMA	86.5	19.65	644	500	1.272
PEMA	102.4	19.00	636	470	1.225
PPMA	118.7	18.75	628	440	1.171
PBMA	135	18.32	621	411	1.131
PHMA	169.1	17.89	*606*	*351*	*1.028*
			649	**449**	**1.02**
POMA	204.2	17.45	*591*	*292*	*0.945*
			649.5	**445**	**0.999**
PLMA	273.8	16.94	*560*	*173*	*0.760*
			650	**440**	**0.976**

TABLE A.IV.4: EOS PARAMETERS AND δ FOR MISCELLANEOUS POLYMERS

Homopolymer	V_m (cm³/mol)	δ ($J^{1/2}/cm^{3/2}$)	T^* (K)	P^* (MPa)	ρ^* (g/cm³)
PCHA	70.6	18.2	685	408	1.137
PCHMA	152.8	18.7	697[a]	426[a]	1.178[a]
PVME	59	18.5	657	353	1.1
PVEE	76	17.2	703	325	1.00
PIBVE	107.6	16.55	621	143	0.908
PPO	102	18.8	739	517	1.156
PE	32.8	16.5	652	430	0.930
PP	49.5	15.5	712	318	0.890
PIB	66.8	15.57	721	331	0.908
PB	60	15.7	522	424	0.990
			610[b]	456[b]	0.965[b]
PI	76	16.2	801	371	0.98
			621[c]	388[c]	0.96[c]
PC	254	19.47			
PCL	114	19.66			
PVC	45.1	21.73	721	413	1.464
PVF$_2$	-	-	635	401	1.587
PEO	38.9	21.3	651	468	1.156
PAN	48.1	28.94	853	536	1.230
PMAN	63.76	24.66	-	-	-
PMAnh	60.12	26.15	862	692	1.500

[a]: parameters from reference 83, not calculated with the GC.

[b]: parameters from reference 168 for 1,4 PB, compared to those calculated with the GC.

[c]: parameters from reference 168 for 1,4 PI, compared to those calculated with the GC

TABLE A.IV.5: EOS PARAMETERS AND δ FOR ALKYL ACRYLATES

homopolymer	V_m (cm^3/mol)	δ ($J^{1/2}$/cm$^{3/2}$)	T* (K)	P* (MPa)	ρ^* (g/cm^3)
PMA	70.6	20.43	635	487	1.252
PEA	89.4	19.56	628	457	1.206
PPA	103.37	19.00	619	423	1.160
PBA	119.74	18.60	612	398	1.112
PHA	152.48	18.09	597	339	1.019
			646	445	1.016
POA	185.22	17.77	582	279	0.933
			647	442	0.995
PLA	250.7	17.4	551	160	0.746
			649	438	0.973

A.IV.3. δ and v_{spec} for random copolymers

Solubility parameters and specific volumes where also calculated for the random copolymers considered in this thesis. For δ, essentially the same procedure as that described for homopolymers was followed. In each case, an equivalent copolymer repeat unit was defined, containing x mol % of monomer A and (1-x) of monomer B and equations A.IV.2 a-c for copolymers thus become:

$$\delta_d = \frac{x*(\sum_i F_{d_i}) + (1-x)*(\sum_j F_{d_j})}{x*V_A + (1-x)V_b} \qquad \text{(A.IV.5.a)}$$

$$\delta_p = \frac{\sqrt{x*(\sum_i F_{p_i}^2) + (1-x)*(\sum_j F_{p_j})}}{x*V_A + (1-x)*V_B} \qquad \text{(A.IV.5.b)}$$

$$\delta_H = \sqrt{\dfrac{x*(\sum_i E_{H_i})+(1-x)*(\sum_j E_{H_j})}{x*V_A+(1-x)*V_B}}$$ (A.IV.5.c)

where i and j are used as summation indexes for the chemical groups present in monomer A and B respectively.

Similar molar averages where employed to calculate P^* and T^*, namely:

$$P^* = xP_A^* + (1-x)P_B^*$$ (A.IV.6.a)

$$T^* = xT_A^* + (1-x)T_B^*$$ (A.IV.6.b)

However, for ρ^* which has units of g/cm^3 (close packed density), an average weighted by mass fraction rather than molar fraction was found to yield more realistic specific volumes, namely:

$$\rho^* = \dfrac{1}{\dfrac{m_A}{\rho_A^*}+\dfrac{m_B}{\rho_B^*}}$$ (A.IV.7)

instead of $\rho^* = x\rho_A^* + (1-x)\rho_B^*$.

Figure A.IV.1 shows the calculated specific volume of two styrene/acrylonitrile (SAN) copolymers containg 15 and 70 wt% AN respectively and for which data is available in the literature (see 83 and references therein). The calculated v_{spec} using a molar and a mass average for ρ^* are both shown. Clearly, the agreement between the experimental values and those calculated using a mass average is superior. Equations A.IV.6.a and b were thus used in combination with equation A.IV.7 to calculate specific volumes of the random copolymers invetigated in this thesis.
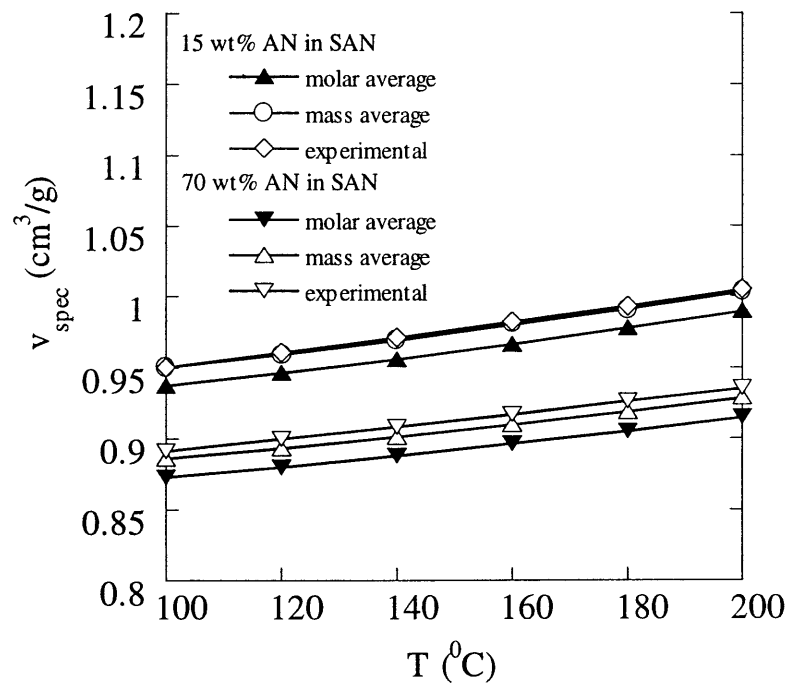
Figure A.IV.1: Calculated and measured v_{spec} as a function of temperature for two SAN random copolymers containing 15 and 70 wt% AN respectively.

A.VI. COMPRESSIBLE FREE ENERGY EXPRESSION

A.VI.1. Phenomenological van der Waals EOS and ΔS_{mix}

An expression for the change in configurational entropy upon mixing of a compressible mixture similar to that derived in section VI.1 can be obtained using a phenomenological van der Waals EOS:

$$\left(P + \frac{a}{V^2}\right)(V - b) = RT \tag{A.VI.1}$$

where a has units of (l^2atm/mol), i.e. (cm^3J/mol) and b has units of (l/mol) or (cm^3/mol).

In the vdw EOS formalism, the entropy S and internal energy E are given by:

$$E = -\frac{a}{V}$$
$$S = R\ln\left(\frac{V-b}{b}\right) \tag{A.VI.2}$$

Indeed, G, the Gibbs free energy, is $E + PV - TS$ and the EOS is obtained by minimizing G with respect to volume V ($\left.\frac{\partial G}{\partial V}\right|_{T,P} = 0$):

$$\frac{\partial G}{\partial V} = \frac{\partial}{\partial V}\left[-\frac{a}{V} + PV - RT\ln\left(\frac{V-b}{b}\right)\right] = \frac{a}{V^2} + P - RT\left(\frac{b}{V-b}\right)\frac{1}{b} = 0 \tag{A.VI.3}$$

or

$$(\frac{a}{V^2} + P)(V - b) = RT \tag{A.VI.4}$$

and equation A.IV.1 is recovered.

193

Applying this formalism to a compressible polymer mixture, and equating b to the hard core volume $V_{hc,i} = n_i N_i v_i$, the configurational entropy of the pure components is given by:

$$S^{pure} = S_A + S_B = R\left[n_A \ln\left(\frac{V_A - b_A}{b_A}\right) + n_B \ln\left(\frac{V_B - b_B}{b_B}\right) \right]$$

$$= \left[n_A \ln\left(\frac{V_A - n_A N_A v_A}{n_A N_A v_A}\right) + n_B \ln\left(\frac{V_B - n_B N_B v_B}{n_B N_B v_B}\right) \right]$$

(A.VI.5)

Likewise, the configurational entropy of the mixture in the vdw EOS formalism is given by:

$$S^{mixt} = S_A{}^{mixt} + S_B{}^{mixt} = R\left[n_A \ln\left(\frac{V - n_A N_A v_A - n_B N_B v_B}{n_A N_A v_A}\right) + n_B \ln\left(\frac{V - n_A N_A v_A - n_B N_B v_B}{n_B N_B v_B}\right) \right]$$

(A.VI.6)

while $\Delta S_{mix} = S^{pure} - S^{mixt}$ is given by:

$$\Delta S_{mix} / R = n_A \ln\left(\frac{V - n_A N_A v_A - n_B N_B v_B}{V_A - n_A N_A v_A}\right) + n_B \ln\left(\frac{V - n_A N_A v_A - n_B N_B v_B}{V_B - n_B N_B v_B}\right)$$

(A.VI.7)

or, making use of the definitions of reduced densities given by equations VI.5 and VI.6,

$$\Delta S_{mix} / R = n_A \ln\left(\frac{(1 - \tilde{\rho})V}{(1 - \tilde{\rho}_A)V_A}\right) + n_B \ln\left(\frac{(1 - \tilde{\rho})V}{(1 - \tilde{\rho}_B)V_B}\right)$$

(A.VI.8)

which is precisely equation A.VI.9.

A.VI.2. ΔE_{mix}: details of derivation of equation VI.21

The expression for the internal energy derived in Chapter VI (equation VI.18):

194

$$\Delta E_{mix} = n_A N_A f_B \left(RT\chi^{FH} \right) \tilde{\rho} + \frac{1}{2} \left[n_A N_A z \varepsilon_{AA} \left(\tilde{\rho} - \tilde{\rho}_A \right) + n_B N_B z \varepsilon_{BB} \left(\tilde{\rho} - \tilde{\rho}_B \right) \right] \qquad \text{(A.VI.9)}$$

can be further simplified and expressed in terms of the pure component properties as:

$$\Delta E_{mix} / V \approx \frac{n_A N_A f_B}{V} (kT\chi^{FH}) \tilde{\rho} + \frac{1}{2} \phi_A \phi_B \left[\left(\tilde{\rho}_A - \tilde{\rho}_B \right) \left(\delta_A^{\;2} - \delta_B^{\;2} \right) \right] \qquad \text{(A.VI.10)}$$

The derivations leading to the latter expression are given below.

The reduced density $\tilde{\rho}$ of the mixture is given by:

$$\tilde{\rho} = \frac{n_A N_A v_A + n_B N_B v_B}{V_A + V_B + \Delta V_{mix}} = \frac{n_A N_A v_A}{V_A} \frac{V_A}{V_A + V_B + \Delta V_{mix}} + \frac{n_B N_B v_B}{V_B} \frac{V_B}{V_A + V_B + \Delta V_{mix}}$$

$$\text{(A.VI.11)}$$

$$= \tilde{\rho}_A \left[\frac{V_A}{V_A + V_B + \Delta V_{mix}} \right] + \tilde{\rho}_B \left[\frac{V_B}{V_A + V_B + \Delta V_{mix}} \right]$$

However, given the magnitude of ΔV_{mix} ($\Delta V_{mix}/V \sim 10^{-4}$), the terms in brackets can

be approximated to first order (Taylor expansion around $\Delta V_{mix} = 0$) as:

$$\left[\frac{V_i}{V_A + V_B + \Delta V_{mix}} \right] \approx \phi_i \left[1 - \frac{\Delta V_{mix}}{V} \right] \qquad \text{(A.VI.12)}$$

as shown in Chapter VI, section VI.1.

Hence,

$$\tilde{\rho} \approx \left[1 - \frac{\Delta V_{mix}}{V} \right] \left(\phi_A \tilde{\rho}_A + \phi_B \tilde{\rho}_B \right) \qquad \text{(A.VI.13)}$$

where V is equal to $V_A + V_B$, and

$$\left(\tilde{\rho} - \tilde{\rho}_A \right) \approx (\phi_A - 1) \tilde{\rho}_A + \phi_B \tilde{\rho}_B - \left[\frac{\Delta V_{mix}}{V} \right] \left(\tilde{\rho}_A \phi_A + \tilde{\rho}_B \phi_B \right)$$

$$\text{(A.VI.14.a)}$$

$$= \phi_B \left(\tilde{\rho}_B - \tilde{\rho}_A \right) \left[1 - \frac{\Delta V_{mix}}{V} \right] - \left[\frac{\Delta V_{mix}}{V} \right] \tilde{\rho}_A$$

Likewise,

$$\left(\tilde{\rho}-\tilde{\rho}_B\right) \approx -\phi_A\left(\tilde{\rho}_B-\tilde{\rho}_A\right)\left[1-\frac{\Delta V_{mix}}{V}\right]-\left[\frac{\Delta V_{mix}}{V}\right]\tilde{\rho}_B \qquad (A.VI.14.b)$$

Inserting those expressions into the second term of the right hand side of equation A.VI.9

yields:

$$\frac{1}{2}\left[n_A N_A z\varepsilon_{AA}\left(\tilde{\rho}-\tilde{\rho}_A\right)+n_B N_B z\varepsilon_{BB}\left(\tilde{\rho}-\tilde{\rho}_B\right)\right]$$

$$\approx \frac{1}{2}\left(\tilde{\rho}_A-\tilde{\rho}_B\right)\left[1-\frac{\Delta V_{mix}}{V}\right]\left[\phi_A n_B N_B z\varepsilon_{BB}-\phi_B n_A N_A z\varepsilon_{AA}\right]+term2 \qquad (A.VI.15)$$

where *term2* is directly proportional to $\Delta V_{mix}/V$ and will be kept as *"term2"* for now.

However, since $\phi_i = \dfrac{n_i N_i v_i \Big/ \tilde{\rho}_i}{V}$, equation A.VI.15 reads:

$$\frac{1}{2}\left[n_A N_A z\varepsilon_{AA}\left(\tilde{\rho}-\tilde{\rho}_A\right)+n_B N_B z\varepsilon_{BB}\left(\tilde{\rho}-\tilde{\rho}_B\right)\right]-term2$$

$$\approx \frac{1}{2}\left(\tilde{\rho}_A-\tilde{\rho}_B\right)\left[1-\frac{\Delta V_{mix}}{V}\right]\frac{n_A N_A n_B N_B}{V}\left[\frac{v_A}{\tilde{\rho}_A}z\varepsilon_{BB}-\frac{v_B}{\tilde{\rho}_B}z\varepsilon_{AA}\right] \qquad (A.VI.16)$$

$$\approx \frac{1}{2}\left(\tilde{\rho}_A-\tilde{\rho}_B\right)\left[1-\frac{\Delta V_{mix}}{V}\right]\left(\frac{n_A N_A n_B N_B}{V}\right)\left(\frac{v_A v_B}{\tilde{\rho}_A\tilde{\rho}_B}\right)\left[\frac{\tilde{\rho}_B z\varepsilon_{BB}}{v_B}-\frac{\tilde{\rho}_A z\varepsilon_{AA}}{v_A}\right]$$

The final expression of equation A.IV.16 can now be expressed in terms of the pure

components solubility parameters. Indeed, as shown in Chapter IV (section IV.3.1,

equation IV.11)

$$\delta_i^2 = -\frac{1}{2}\frac{z\varepsilon_{ii}\rho_i}{M_{u_i}} \qquad (A.VI.17)$$

when ε_{ii} is defined as the negative nearest neighbor molar attractive interaction energy.

Since

196

$$\frac{\rho_i}{M_{u_i}} = \frac{\rho_i}{\rho_i^*} \frac{\rho_i^*}{M_{u_i}} = \tilde{\rho}_i \frac{1}{v_i},$$

(A.VI.18)

the expression for δ_i^2 reads:

$$\delta_i^2 = -\frac{1}{2}\frac{z\varepsilon_{ii}\tilde{\rho}_i}{v_i}$$

(A.VI.19)

which is exactly the argument inside the brackets in equation (A.VI.16) and thus,

$$\frac{1}{2}\left[n_A N_A z\varepsilon_{AA}\left(\tilde{\rho} - \tilde{\rho}_A\right) + n_B N_B z\varepsilon_{BB}\left(\tilde{\rho} - \tilde{\rho}_B\right)\right] - term2$$

$$\approx \left(\tilde{\rho}_A - \tilde{\rho}_B\right)\left[1 - \frac{\Delta V_{mix}}{V}\right]\left(\frac{n_A N_A n_B N_B}{V}\right)\left(\frac{v_A v_B}{\tilde{\rho}_A \tilde{\rho}_B}\right)\left[\delta_A^2 - \delta_B^2\right]$$

which, upon dividing by the total volume of the system, becomes:

$$\frac{1}{V}\left[\frac{1}{2}n_A N_A\left(\tilde{\rho} - \tilde{\rho}_A\right)z\varepsilon_{AA} + \frac{1}{2}n_B N_B\left(\tilde{\rho} - \tilde{\rho}_B\right)z\varepsilon_{BB}\right] \approx \left(\tilde{\rho}_A - \tilde{\rho}_B\right)\left[1 - \frac{\Delta V_{mix}}{V}\right]\phi_A\phi_B\left[\delta_A^2 - \delta_B^2\right] + term2/V$$

(A.VI.20)

In equation A.VI.20, *term2/V* is in turn given by:

$$-\frac{1}{2}\frac{1}{V}\frac{\Delta V_{mi}}{V}\left[n_A N_A\left(\tilde{\rho}_A\right)z\varepsilon_{AA} + n_B N_B\left(\tilde{\rho}_B\right)z\varepsilon_{BB}\right] = \frac{\Delta V_{mix}}{V}\left[\tilde{\rho}_A\phi_A\delta_A^2 + \tilde{\rho}_B\phi_B\delta_B^2\right]$$

(A.VI.21)

and its sign only depends on the **sign of** ΔV_{mix} since the term inside the brackets is always

positive. Thus, it tends to stabilize the mixture when $\Delta V_{mix} < 0$.

The total change in internal energy upon mixing thus reads:

$$\Delta E_{mix}/V \approx \frac{n_A N_A f_B}{V}\left(RT\chi^{FH}\right)\tilde{\rho} + \phi_A\phi_B\left[\left(\tilde{\rho}_A - \tilde{\rho}_B\right)\left(\delta_A^2 - \delta_B^2\right)\right] + \frac{\Delta V_{mix}}{V}\left[\tilde{\rho}_A\phi_A\delta_A^2 + \tilde{\rho}_B\phi_B\delta_B^2\right]$$

(A.VI.22)

In the final expression for ΔG_{mix} given in equation VI.21 of Chapter VI, the third

term has been omitted since it scales directly as $\Delta V_{mix}/V$ and $(1 - \Delta V_{mix}/V)$ has been further

197

approximated as 1. In this manner, phase diagrams could be predicted without requiring

any experimental data on the PVT properties of the mixture.

A.VI.3. Pure component properties for phase diagram predictions

Table A.VI.1 summarizes the values of the different pure component parameters

that were used in computing the phase diagrams presented in section VI.4. These

parameters are: the thermal expansion coefficient α_i (melt-state value), the extrapolated

(0K) hard core density ρ_i^*, the solubility parameter at 25°C obtained from GC, the hard

core cohesive energy density $\delta_{i_o}^2$, and the hard core segmental volume v_i. The repeat unit

molecular weight of each homopolymer is also given.

TABLE A.VI.1: PARAMETERS USED FOR PHASE DIAGRAM PREDICTIONS

homopolymer	ρ^* (g/cm^3)	α (10^{-4} K^{-1})	δ(298) (J$^{1/2}$/cm$^{3/2}$)	$\delta_{i_o}^2$ (J$^{1/2}$/cm$^{3/2}$)	M_u (g/mol)	v (cm^3/mol)
PS	1.24	5.13	18.19	385.54	104	83.96
PaMS	1.33	5.76	18.50	406.34	116	86.88
PMMA	1.42	5.48	19.65	454.62	100	70.42
PEMA	1.42	7.47	19.00	450.98	114	80.09
PBMA	1.32	7.38	18.30	417.27	142	107.46
POMA	1.15	5.8	17.45	361.95	198	171.67
PLMA	1.14	6.8	16.94	351.42	254	221.85
PCHMA	1.36	6.24	18.70	421.15	168	123.48
PVME	1.25	6.65	18.50	417.30	58	46.36
PEA	1.39	7.24	19.56	474.73	100	71.85
PB	1.06	5.67	16.20	310.84	54	50.98
PI	1.09	6.51	16.40	326.54	68	62.62
PIB	1.08	5.65	18.50[a]	405.02	56	51.59
P(E-r-B)66	1.14	7.1	18.71[a]	432.09	56	49.21
P(E-r-B)97	1.06	6.78	18.10[a]	400.96	56	52.82
PCL	1.32	6.39	19.66	467.62	114	86.64
PC	1.50	6.21	19.47	456.14	254	168.85
PEO	1.38	7.09	21.30	560.38	44	31.79
SAN6	1.28	5.92	18.6	412.71	98	76.65
SAN18	1.30	5.6	19.51	450.23	88.65	68.05
SAN40	1.31	5.16	21.57	542.60	75	57.40
PVC	1.79	7.40	21.73	588.69	63	35.09

a: solubility parameters determined from PVT data by Krishnamoorti et al.[58]

A.VI.4. Total change in entropy upon mixing $\Delta S_{mix,tot}$

The expression derived for the change in entropy upon mixing (equation VI.10) only includes a change in configurational entropy. However, the total entropy of mixing is readily obtained by taking the derivative of the total change in free energy with respect to temperature. Assuming constant α's and volume fractions, and using equation VI.21.b (repeated here):

$$\Delta g_{mix} = RT\left[\frac{\phi_A \tilde{\rho}_A}{N_A v_A}\ln\varphi_A + \frac{\phi_B \tilde{\rho}_B}{N_B v_B}\ln\varphi_B\right] + \phi_A \phi_B \tilde{\rho}_A \tilde{\rho}_B (\delta_{A_o} - \delta_{B_o})^2 + \phi_A \phi_B \left[(\tilde{\rho}_A - \tilde{\rho}_B)(\delta_A{}^2 - \delta_B{}^2)\right]$$

(VI.21.b)

the following expression for the entropy of mixing per unit volume is obtained:

$$\Delta s_{mix,tot} = -\left.\frac{\partial \Delta g_{mix}}{\partial T}\right|_{O,\phi_i}$$

$$= -R\left[\frac{(1-\alpha_A T)\phi_A \tilde{\rho}_A}{N_A v_A}\ln(\phi_A) + \frac{(1-\alpha_B T)\phi_{BA} \tilde{\rho}_{BA}}{N_B v_B}\ln(\phi_B)\right] + (\alpha_A + \alpha_B)\phi_A \phi_B \tilde{\rho}_A \tilde{\rho}_B (\delta_{A_o} - \delta_{B_o})^2$$

$$- \phi_A \phi_B \left[(\alpha_B \tilde{\rho}_B - \alpha_A \tilde{\rho}_A)(\delta_A{}^2 - \delta_B{}^2)\right] + \phi_A \phi_B \left[(\tilde{\rho}_A - \tilde{\rho}_B)(\alpha_A \delta_A{}^2 - \alpha_B \delta_B{}^2)\right]$$

(A.VI.23)

while the change in enthalpy upon mixing per unit volume is given by:

$$\Delta h_{mix} = \Delta g_{mix} + T\Delta s_{mix} = \Delta g_{mix} - T\left.\frac{\partial \Delta g_{mix}}{\partial T}\right|_{P,\phi_i}$$

(A.VI.24)

An expression entirely similar to equation A.VI.23 can also be obtained for the second derivative of the total change in entropy upon mixing with respect to composition, $s_{\phi\phi,tot}$.

BIBLIOGRAPHY

1. Hashimoto, T., Nagatoshi, K., Todo, A., Hasegawa, H. & Kawai, H. "Domain-Boundary Structure of Styrene-Isoprene Block Copolymer Films Cast from Toluene Solutions". *Macromolecules* **7**, 364 (1974).

2. Hashimoto, T., Shibayama, M., Fujimura, M. & Kawai, H. in *Block Copolymers-Science and Technology* (ed. Meier, D. J.) (MMI Press Symp. Series, Harwood, 1983).

3. Bates, F. S. & Fredrickson, G. H. "Block Copolymer Thermodynamics: Theory and Experiment". *Ann. Rev. Phys. Chem.* **41**, 525 (1990).

4. Hashimoto, T. "Order-Disorder Transition in Block Copolymers". in *Thermoplastic Elastomers* (eds. Holden, G., Legge, N. R., Quirk, R. & Shcroeder, H. E.) 429 (Hansen, Munich, Germany, 1996).

5. Hamley, I. *Block Copolymers* (Oxford U. P., Oxford, England, 1999).

6. Bates, F. S. & Fredrickson, G. H. "Block Copolymers-Designer Soft Materials". *Phys Today* **52**, 32 (1999).

7. Bates, F. S., Bair, H. E. & Hartney, M. "Block Copolymers near the Microphase Separation Transition. 1. Preparation and Physical Characterization of a Model System". *Macromolecules* **17**, 1987 (1984).

8. Quirk, R. P. & Morton, M. "Research on Anionic Triblock Copolymers". in *Thermoplastic Elastomers* (eds. Holden, G., Legge, N. R., Quirk, R. & Schroeder, H. E.) 71 (Hansen, Munich, Germany, 1996).

9. "Pressure Sensitive Adhesives and Products". in *Encyclopedia of Polymer Science and Engineering* 345-367 (John Wiley and Sons, NY, 1987).

10. Soo, P. P., Huang, B. Y., Jang, Y. I., Chiang, Y. M., Sadoway, D. R. & Mayes, A. M. "Rubbery block copolymer electrolytes for solid-state rechargeable lithium batteries". *J. Electrochem. Soc.* **146**, 32 (1999).

11. Mansky, P., Chaikin, P. M. & Thomas, E. L. "Monolayer Films of Diblock Copolymer Microdomains For Nanolithographic Applications". *J. Mat. Sci.* **30**, 1987 (1995).

12. Mansky, P., Harrison, C. K., Chaikin, P. M., Register, R. A. & Yao, N. "Nanolithographic templates from diblock copolymer thin films". *Appl. Phys. Lett.* **68**, 2586 (1996).

13. Park, M., Harrison, C., Chaikin, P. M., Register, R. A. & Adamson, D. H. "Block copolymer lithography: Periodic arrays of similar to 10(11) holes in 1 square centimeter". *Science* **276**, 1401 (1997).

14. Fasolka, M. J., Harris, D. J., Mayes, A. M., Yoon, M. & Mochrie, S. G. J. "Observed Substrate Topography-mediated Lateral Patterning of Diblock Copolymer Films". *Phys. Rev. Lett.* **79**, 3018 (1997).

15. Ciebien, J. F., Clay, R. T., Sohn, B. H. & Cohen, R. E. "Brief review of metal nanoclusters in block copolymer films". *New J. Chem.* **22**, 685 (1998).

16. Sohn, B. H., Cohen, R. E. & Papaefthymiou, G. C. "Magnetic properties of iron oxide nanoclusters within microdomains of block copolymers". *J. Magn. Magn. Mater.* **182**, 216 (1998).

17. Goldacker, T., Abetz, V., Stadler, R., Erukhimovich, I. & Leibler, L. "Non-centrosymmetric Superlattices in Block Copolymer Blends". *Nature* **398**, 137 (1999).

18. Fink, J., Urbas, A. M., Bawendi, M. G., Joannopoulos, J. D. & Thomas, E. L. "Block Copolymers as Photonic Bandgap Materials". *Journal of Lightwave Technology* **17**, 1963 (1999).

19. Urbas, A., Fink, Y. & Thomas, E. L. "One-dimensionally periodic dielectric reflectors from self- assembled block copolymer-homopolymer blends". *Macromolecules* **32**, 4748 (1999).

20. Discher, B. M., Won, Y. Y., Ege, D. S., Lee, J. C. M., Bates, F. S., Discher, D. E. & Hammer, D. A. "Polymersomes: Tough Vesicles Made From Diblock Copolymers". *Science* **284**, 1143 (1999).

21. Patten, T. E. & Matyjaszewski, K. "Atom Transfer Radical Polymerization and the Synthesis of Polymeric Materials". *Adv. Mater* **10**, 901 (1998).

22. Russell, T. P., Karis, T. E., Gallot, Y. & Mayes, A. M. "A Lower Critical Ordering Transition in a Diblock Copolymer Melt". *Nature* **368**, 729 (1994).

23. Yeung, C., Desai, R. C., Shi, A.-C. & Noolandi, J. "Lower Critical Ordering Temperature in Diblock Copolymer Melts". *Phys. Rev. Lett.* **72**, 1834 (1994).

24. Hino, T. & Prausnitz, J. M. "Lower and Upper Critical Ordering Temperatures in Compressible Diblock Copolymer Melts from a Perturbed Hard-Sphere-Chain Equation of State". *Macromolecules* **31**, 2636 (1998).

25. Utracki, L. A. *Polymer Alloys and Blends* (Hansen, Munich, Germany, 1990).

26. Winey, K. I., Gobran, D. A., Xu, Z., Fetters, L. J. & Thomas, E. L. "Compositional Dependence of the Order-Disorder Transition in Diblock Copolymers". *Macromolecules* **27**, 2392 (1994).

27. Han, C. D., Baek, D. M., Kim, J. K., Ogawa, T., Sakamoto, N. & Hashimoto, T. "Effect of Volume Fraction on the Order-Disorder Transition in Low-Molecular-Weight Polystyrene-block-Polyisoprene Copolymers .1. Order-Disorder Transition-Temperature Determined by Rheological Measurements". *Macromolecules* **28**, 5043 (1995).

28. LaMonte Adams, J., Graessley, W. & Register, R. "Rheology and the Miscrophase Separation Transition in Styrene-Isoprene Block Copolymers". *Macromolecules* **27**, 6026 (1994).

29. Bates, F. S., Rosedale, J. H. & Fredrickson, G. H. "Fluctuation Effects in a Symmetric Diblock Copolymer near the Order-Disorder Transition". *J. Chem. Phys* **92**, 6255 (1990).

30. Rosedale, J. H. & Bates, F. S. "Rheology of Ordered and Disordered Symmetric Poly(ethylenepropylene)-Poly(ethylethylene) Diblock Copolymers". *Macromolecules* **23**, 2329 (1990).

31. Rosedale, J. H., Bates, F. S., Almdal, K., Mortensen, K. & Wignall, G. D. "Order and Disorder in Symmetrical Diblock Copolymer Melts". *Macromolecules* **28**, 1429 (1995).

32. Russell, T. P., Hjelm, R. P. & Seeger, P. A. "Temperature Dependence of the Interaction Parameter of Polystyrene and Poly(methyl methacrylate)". *Macromolecules* **23**, 890 (1990).

33. Russell, T. P. "Changes in Polystyrene and Poly(methyl methacrylate) Interactions with Isotopic Substitution". *Macromolecules* **26**, 5819 (1993).

34. Menelle, A., Russell, T. P., Anastasiadis, S. H., Satija, S. K. & Majkrzak, C. F. "Ordering of Thin Diblock Copolymer Films". *Phys. Rev. Lett.* **68**, 67 (1992).

35. Anastasiadis, S. H., Russell, T. P., Satija, S. K. & Majkrzak, C. F. "Neutron Reflectivity Studies of the Surface-Induced Ordering of Diblock Copolymer Films". *Phys. Rev. Lett.* **62**, 1852 (1989).

36. Flory, P. J. "Thermodynamics of High Polymer Solutions". *J. Chem. Phys* **9**, 660 (1941).

37. Flory, P. J. *Principles of Polymer Chemistry* (Cornell University Press, Ithaca, New York, 1953).

38. Huggins, M. L. "Solutions of Long Chain Compounds". *J. Chem. Phys* **9**, 440 (1941).

39. Leibler, L. "Theory of Microphase Separation in Block Copolymers". *Macromolecules* **13**, 1602 (1980).

40. Hildebrand, J. H. & Scott, R. L. *The Solubility of Non-Electrolytes* (Van Nostrand-Reinhold, Princeton, NJ, 1950).

41. Grulke, E. A. in *Polymer Handbook* (eds. Bandrup, J. & Immergut, E. H.) VII-519 (John Wiley & Sons, NY, 1989).

42. van Krevelen, D. W. & Hoftyzer, P. J. *Properties of Polymers. Correlation with Chemical Structure* (Elsevier, New York, 1972).

43. Funk, E. W. & Prauznitz, J. M. "Thermodynamic Properties of Liquid Mixtures: Aromatic-Saturated Hydrocarbon Systems". *Ind. Eng. Chem.* **62**, 8 (1970).

44. Lacombe, R. H. & Sanchez, I. C. "Statistical Thermodynamics of Fluid Mixtures". *J. Phys. Chem.* **80**, 2568 (1976).

45. Coleman, M. M., Serman, C. J. & Bhagwagar, D. E. "A Practical Guide to Polymer Miscibility". *Polymer* **31**, 1187 (1989).

46. Krishnamoorti, R., Graessley, W. W., Balsara, N. P. & Lohse, D. J. "Structural Origin of Thermodynamic Interactions in Blends of Saturated Hydrocarbon Polymers". *Macromolecules* **27**, 3073 (1994).

47. Kumar, S. K. "Computer Simulations on the Free Energies and Phase Diagrams of Asymmetrically Interacting Blends". *Macromolecules* **30**, 5085 (1997).

48.   de Gennes, P. G. *Scaling Concepts in Polymer Physics* (Cornell University Press, Ithaca, New York, 1979).

49.   Bates, F. S. & Hartney, M. A. "Block Copolymers near the Microphase Separation Transition. 3. Small Angle Neutron Scattering Study of the Homogeneous Melt". *Macromolecules* **18**, 2478 (1985).

50.   Mori, K., Hasegawa, H. & Hashimoto, T. "Small-Angle X-Ray Scattering from Bulk Block Copolymers in Disordered State. Estimation of chi Values from Accidental Thermal Fluctuations". *Polym. J.* **17**, 799 (1985).

51.   Bates, F. S. "Measurement of the Correlation Hole in Homogeneous Block Copolymer Melt". *Macromolecules* **18**, 525 (1985).

52.   Dudowicz, J. & Freed, K. F. "Pressure Dependence of Polymer Fluids: Application of the Lattice Cluster Theory". *Macromolecules* **28**, 6625 (1995).

53.   Balsara, N. P., Fetters, L. J., Hadjichristidis, N., Lohse, D. J., Han, C. C., Graessley, W. W. & Krishnamoorti, R. "Thermodynamic Interactions in Model Polyolefin Blends Obtained by Small-Angle Neutron Scattering". *Macromolecules* **25**, 6137 (1992).

54.   Walsh, D. J., Graessley, W. W., Datta, S., Lohse, D. J. & Fetters, L. J. "Equation of State and Predictions of Miscibility for Hydrocarbon Polymers". *Macromolecules* **25**, 5236 (1992).

55.   Lohse, D. J., Fetters, L. J., Doyle, M. J., Wang, H. C. & Kow, C. "Miscibility in Blends of Model Polyolefins and Corresponding Diblock Copolymers - Thermal-Analysis Studies". *Macromolecules* **26**, 3444 (1993).

56.   Krishnamoorti, R., Graessley, W. W., Fetters, L. J., Garner, R. T. & Lohse, D. J. "Anomalous Mixing Behavior of Polyisobutylene with Other Polyolefins". *Macromolecules* **28**, 1252 (1995).

57.   Graessley, W. W., Krishnamoorti, R., Reichart, G., Balsara, N., Fetters, L. J. & Lohse, D. J. "Regular and Irregular Mixing in Blends of Saturated Hydrocarbon Polymers". *Macromolecules* **28**, 1260 (1995).

58.   Krishnamoorti, R., Graessley, W. W., Dee, G. T., Walsh, D. J., Fetters, L. J. & Lohse, J. "Pure Component Properties and Mixing Behavior in Polyolefin Blends". *Macromolecules* **29**, 367 (1996).

59. Reichart, G. C., Graessley, W. W., Register, R. A., Krishnamoorti, R. & Lohse, D. J. "Anomalous Attractive Interactions in Polypropylene Blends". *Macromolecules* **30**, 3036 (1997).

60. Alamo, R. G., Graessley, W. W., Krishnamoorti, R., Lohse, D. J., Londono, J. D., Mandelkren, L., Stehling, F. C. & Wignall, G. D. "Small Angle Neutron Scattering Investigations of Melt Miscibility and Phase Segregation in Blends of Linear and Branched Polyethylenes as a Function of Branch Content". *Macromolecules* **39**, 561 (1997).

61. Reichart, G. C., Graessley, W. W., Register, R. A., Krishnamoorti, R. & Lohse, D. J. "Measurement of Thermodynamic Interactions in Ternary Polymer Blends by Small-Angle Neutron Scattering". *Macromolecules* **30**, 3363 (1997).

62. Dudowicz, J. & Freed, K. F. "Effect of Monomer Structure and Compressibility on the Properties of Multicomponent Polymer Blends and Solutions .1. Lattice Cluster Theory of Compressible Systems". *Macromolecules* **24**, 5076 (1991).

63. Dudowicz, J., Freed, M. S. & Freed, K. S. "Effect of Monomer Structure and Compressibility on the Properties of Multicomponent Polymer Blends and Solutions .2. Application to Binary Blends". *Macromolecules* **24**, 5096 (1991).

64. Freed, K. F. & Dudowicz, J. "Influence of Short Chain Branching on the Miscibility of Binary Polymer Blends: Application to Polyolefin Mixtures". *Macromolecules* **29**, 625 (1996).

65. Foreman, K. W. & Freed, K. F. "Microscopic Parameters Influencing the Phase Separation in Compressible Blends of Linear Semiflexible Polymers". *J. Chem. Phys* **106**, 7422 (1997).

66. Sanchez, I. C. & Lacombe, R. H. "Statistical Thermodynamics of Polymer Solutions". *Macromolecules* **11**, 1145 (1978).

67. Fredrickson, G. H., Liu, A. & Bates, F. S. "Entropic Corrections to the Flory-Huggins Theory of Polymer Blends: Architectural and Conformational Effects". *Macromolecules* **27**, 2503 (1994).

68. Yethiraj, A., Curro, J. G. & Rajasekaran, J. J. "Thermodynamics and Local Structure in Vinyl Polymer Melts". *J. Chem. Phys* **103**, 2229 (1995).

69. Muller, M. "Effects of Structural Disparities in Polymer Blends: A Monte-Carlo Investigation". *Macromolecules* **28**, 6556 (1995).

70. Curro, J. G. "Intermolecular Structure and Thermodynamics of Vinyl Polymer Liquids: Freely-Jointed Chains". *Macromolecules* **27**, 4665 (1994).

71. Schweizer, K. S. "Analytical PRISM Theory of Structurally Asymmetric Polymer Blends and Copolymers". *Macromolecules* **26**, 6050 (1993).

72. Schweizer, K. S. & Singh, C. "Microscopic Solubility-Parameter Theory of Polymer Blends: General Predictions". *Macromolecules* **28**, 2063 (1995).

73. Singh, C. & Schweizer, K. S. "Coupled Enthalpic-Packing Effects on the Miscibility of Conformationally Asymmetric Polymer Blends". *Macromolecules* **30**, 1490 (1997).

74. Maranas, J. K., Mondello, M., Grest, G. S., Kumar, S. K., Debenedetti, P. G. & Graessley, W. W. "Liquid Structure, Thermodynamics, and Mixing Behavior of Saturated Hydrocarbon Polymers. 1. Cohesive Energy Density and Internal Pressure". *Macromolecules* **31**, 6991 (1998).

75. Maranas, J. K., Mondello, M., Grest, G. S., Kumar, S. K., Debenedetti, P. G. & Graessley, W. W. "Liquid Structure, Thermodynamics, and Mixing Behavior of Saturated Hydrocarbon Polymers. 2. Pair Distribution Functions and the Regularity of Mixing". *Macromolecules* **31**, 6998 (1998).

76. Karis, T. E., Russell, T. P., Gallot, Y. & Mayes, A. M. "Rheology of the Lower Critical Ordering Transition". *Macromolecules* **28**, 1129 (1995).

77. Bernstein, R. E., Cruz, C. A., Paul, D. R. & Barlow, J. W. "LCST Behavior in Polymer Blends". *Macromolecules* **10**, 681 (1977).

78. Freeman, P. I. & Rowlinson, J. S. "Lower Critical Points in Polymer Solutions". *Polymer* **1**, 20 (1960).

79. Sanchez, I. C. & Panayiotou, C. G. "Equation of State Thermodynamics of Polymer and Related Solutions". in *Models for Thermodynamic and Phase Equilibria Calculations* 187 (Marcel Dekker, Inc., New York, 1994).

80. Janssen, S., Schawhn, D., Mortensen, K. & Springer, T. "Pressure Dependence of the Flory-Huggins Interaction Parameter in Polymer Blends: A SANS Study and a

Comparison to the Flory-Orwoll-Vrij Equation of State". *Macromolecules* **26**, 5587 (1993).

81. Hammouda, B. & Bauer, B. J. "Compressibility of Two Polymer Blend Mixtures". *Macromolecules* **28**, 4505 (1995).

82. Pollard, M., Russell, T. P., Ruzette, A. V., Mayes, A. M. & Gallot, Y. "The Effect of Hydrostatic Pressure on the Lower Critical Ordering Transition in Diblock Copolymers". *Macromolecules* **31**, 6493 (1998).

83. Rodgers, P. A. "Pressure-Volume-Temperature Relationships for Polymeric Liquids: A Review of Equations of State and Their Characteristic Parameters for 56 Polymers". *J. Appl. Polym. Sci.* **48**, 1061 (1993).

84. Prigogine, I. *The Molecular Theory of Solutions* (North-Holland Publishing Co., Amsterdam, 1959).

85. Flory, P. J., Orwoll, R. A. & Vrij, A. "Statistical Thermodynamics of Chain Molecules I. An Equation of State for Normal Paraffin Hydrocarbons". *J. Am. Chem. Soc.* **86**, 3515 (1964).

86. Flory, P. J., Orwoll, R. A. & Vrij, A. "Statistical Thermodynamics of Chain Molecules II. Liquid Mixtures of Normal Paraffin Hydrocarbons". *J. Am. Chem. Soc.* **86**, 3515 (1964).

87. Patterson, D. *J. Polym. Sci., Part C* **16**, 3379 (1968).

88. Boudouris, D., Constantinou, L. & Panayatou, C. "A Group Contribution Estimation of the Thermodynamic Properties of Polymers". *Ind. Eng. Chem.* **36**, 3968 (1997).

89. Tang, H. & Freed, K. F. "Static Structure Factor of Compressible Polymer Blends and Diblock Copolymer Melts. 2. Constraints on Density Fluctuations". *Macromolecules* **24**, 958 (1991).

90. Dudowicz, J. & Freed, K. F. "Influence of Compressibility and Monomer Structure on Small Angle Neutron Scattering from Binary Blends.". *J. Chem. Phys* **96**, 9147 (1992).

91. Bidkar, U. R. & Sanchez, I. C. "Neutron Scattering From Compressible Polymer Blends: A Framework for Experimental Analysis and Interpretation of Interaction Parameters". *Macromolecules* **28**, 3963 (1995).

92. Dudowicz, J. & Freed, K. F. "Relation of Effective Interaction Parameters for Binary Blends and Diblock Copolymers: Lattice Cluster Theory Predictions and Comparison with Experiments". *Macromolecules* **26**, 213 (1993).

93. Hammouda, B., Bauer, B. J. & Russell, T. P. "Small-Angle Neutron Scattering from Deuterated Polystyrene/Poly(butyl methacrylate) Homopolymer Blend Mixtures". *Macromolecules* **27**, 2357 (1994).

94. Hadziioannou, G. & Stein, R. S. "Neutron Scattering Studies of Dimensions and of Interactions between Components in Polystyrene/Poly(vinyl methyl ether) and Poly(vinylidene fluoride)/Poly(methyl methacrylate) Amorphous Blends". *Macromolecules* **17**, 567 (1984).

95. Benedetti, E., Catanorchi, S., D'Alessio, A., Vergamini, P., Ciardelli, F. & Pracella, M. "FTIR Microscopic and DSC Analysis of Blends of Poly(vinylidene fluoride) with Isotactic and Syndiotactic Poly(methyl methacrylate)". *Polym. Int.* **45**, 373 (1998).

96. Nishi, T. & Kwei, T. K. "Cloud Point Curves for Poly(vinyl methyl ether) and Monodisperse Polystyrene Mixtures". *Polymer* **16**, 285 (1975).

97. Lu, F. J., Benedetti, E. & Hsu, S. L. "Spectroscopic Study of Polystyrene and Poly(vinyl methyl ether) Blends". *Macromolecules* **16**, 1525 (1983).

98. Garcia, D. "Fourrier-Transform Infrared Study of Polystyrene/Poly(vinyl methyl ether) Blends". *J. Polym. Sci., Polym. Phys. Ed.* **22**, 107 (1984).

99. Shibayama, M., Yang, H., Stein, R. & Han, C. "Study of Miscibility and Critical Phenomena of Deuterated Polystyrene and Hydrogenated Poly(vinyl methyl ether) by Small Angle Neutron Scattering". *Macromolecules* **18**, 2179 (1985).

100. Amelino, L., Martuscelli, E., Sellitti, C. & Silvestre, C. "Isotactic Polystyrene/Poly(vinyl methyl ether) Blends: Miscibility, Crystallization and Phase Structure". *Polymer* **31**, 1051 (1990).

101. Beaucage, G., Stein, R. S., Hashimoto, T. & Hasegawa, H. "Tacticity Effects on Polymer Blend Miscibility". *Macromolecules* **24**, 3443 (1991).

102. Hashimoto, T., Hasegawa, H., Hashimoto, T., Katayama, H., Kamigaito, M. & Sawamoto, M. "Synthesis and SANS Characterization of Poly(vinyl methyl ether)-block-Polystyrene". *Macromolecules* **30**, 6819 (1997).

103. Weeks, N. E., Karasz, F. E. & MacKnight, W. J. "Enthalpy of Mixing of Poly(2,6-dimethyl phenylene oxide) and Polystyrene". *J. Appl. Phys.* **48**, 4068 (1977).

104. Feng, H., Feng, Z., Ruan, H. & Shen, L. "A High-Resolution Solid-State NMR Study of the Miscibility, Morphology, and Toughening Mechanism of Polystyrene with Poly(2,6-dimethyl-1,4-phenylene oxide) Blends". *Macromolecules* **25**, 5981 (1992).

105. McMaster, L. P. "Aspects of Polymer-Polymer Thermodynamics". *Macromolecules* **6**, 760 (1973).

106. Hajduk, D. A., Urayama, P., Gruner, S. M. & Erramilli, S. "High-Pressure Effects on the Disordered Phase of Block Copolymer Melts". *Macromolecules* **28**, 7148 (1995).

107. Hajduk, D. A., Gruner, S. M., Erramilli, S., Register, R. A. & Fetters, L. J. "High-Pressure Effects on the Order/Disorder Transition in Block Copolymer Melts". *Macromolecules* **29**, 1473 (1996).

108. Steinhoff, B., Rüllmann, M., Wenzel, M., Junker, M., Alig, I., Oser, R., Stühn, B., Meier, G., Diat, O., Bösecke, P. & Stanley, H. B. "Pressure Dependence of the Order-to-Disorder Transition in Polystyrene/Polyisoprene and Polystyrene/Poly(methylphenylsiloxane) Diblock Copolymers". *Macromolecules* **31**, 36 (1998).

109. Schwahn, D., Frielinghaus, H., Mortensen, K. & Almdal, K. "Temperature and Pressure Dependence of the Order Parameter Fluctuations, Conformational Compressibility, and the Phase Diagram of the PEP-PDMS Diblock Copolymer". *Phys. Rev. Lett.* **77**, 3153 (1996).

110. Frielinghaus, H., Schwahn, D., Mortensen, K., Almdal, K. & Springer, T. "Composition Fluctuations and Coil Conformations in a Poly(ethylene-propylene)-Poly(ehtylethylene) Diblock Copolymer as a Function of Temperature and Pressure". *Macromolecules* **29**, 3263 (1996).

111. Prausnitz, J. M., Lichtenthaler, R. N. & de Azevedo, E. G. *Molecular Thermodynamics and Fluid Phase Equilibria* (Prentice-Hall, Englewood Cliffs, NJ, 1986).

112. Kasten, H. & Stühn, B. "Density Discontinuity at the Microphase Separation Transition of a Symmetric Diblock Copolymer". *Macromolecules* **28**, 4777 (1995).

113. Stühn, B. "The Relation between the Microphase Separation Transition and the Glass-Transition in Diblock Copolymers". *J. Polym. Sci., Polym. Phys. Ed.* **30**, 113 (1992).

114. Allen, R. D., Long, T. E. & McGrath, J. E. "Preparation of High-Purity, Anionic-Polymerization Grade Alkyl Methacrylate Monomer". *Polym. Bul.* **15**, 127 (1986).

115. Almdal, K., Roseldale, J. H. & Bates, F. S. "Order-Disorder Transition in Binary Mixtures of Nearly Symmetric Diblock Copolymers". *Macromolecules* **23**, 4336 (1990).

116. Hashimoto, T., Yamasaki, K., Koizumi, S. & Hasegawa, H. "Ordered Structure in Blends of Block Copolymers .1. Miscibility Criterion for Lamellar Block Copolymers". *Macromolecules* **26**, 2895 (1993).

117. Ihara, E., Morimoto, M. & Yasuda, H. "Living Polymerizations and Copolymerizations of Alkyl Acrylates by the Unique Catalysis of Rare Earth Metal Complexes". *Macromolecules* **28**, 7886 (1995).

118. Wang, J. S. & Matyjaszewski, K. "Controlled/"Living" Radical Polymerization. Atom Transfer Radical Polymerization in the Presence of Transition-Metal Complexes". *J. Am. Chem. Soc.* **117**, 5614 (1995).

119. Kano, M., Kamigaito, M., Sawamoto, M. & Higashimura, T. *Macromolecules* **26**, 1721 (1996).

120. Cassebras, M., Pascual, S., Polton, A., Tardi, M. & Vairon, J. P. "Synthesis of Di- and Triblock Copolymers of Styrene and Butyl Acrylate by Controlled Atom Transfer Radical Polymerization". *Macromol. Rapid Commun.* **20**, 261 (1999).

121. Shipp, D. A., Wang, J.-L. & Matyjaszewski, K. "Synthesis of Acrylate and Methacrylate Block Copolymers Using Atom Transfer Radical Polymerization". *Macromolecules* **31**, 8005 (1998).

122. Bates, F. S. "Block Copolymers near the Microphase Separation Transition. 2. Linear Dynamic Mechanical Properties". *Macromolecules* **17**, 2607 (1984).

123. Rosedale, J. H. & Bates, F. S. "Rheology of Ordered and Disordered Symmetric Poly(ethylenepropylene)-Poly(ethylethylene) Diblock Copolymers". *Macromolecules* **23**, 2329 (1990).

124. *Encyclopedia of Polymer Science and Engineering* (John Wiley & Sons, NY, 1987).

125. Fetters, L. J., Lohse, D. J., Witten, T. A. & Zirkel, A. "Connections between Polymer Molecular Weight, Density, Chain Dimensions, and Melt Viscoelastic Properties". *Macromolecules* **27**, 4639 (1994).

126. Freed, K. F. & Dudowicz, J. "On the Large Entropic Contribution the the Effective Interaction Parameter of Polystyrene-Poly(methyl methacrylate) Diblock Copolymer Systems". *J. Chem. Phys* **97**, 2105 (1992).

127. Harris, D. G. "Synthesis and Characterization of Poly(styrene-*b*-*n*-butyl methacrylate)". S. B. Thesis, Materials Science and Engineering, Massachusetts Institute of Technology, Cambridge (1998).

128. Brannock, G. R., Barlow, J. W. & Paul, D. R. "Blends of Styrene/Maleic Anhydride Copolymers with Polymethacrylates". *J. Polym. Sci. Polym. Phys.* **29**, 413 (1991).

129. Rogers, S. S. & Mandelkern, L. "Glass Formation in Polymers. I. The Glass Transitions of the Poly-(n-alkyl methacrylates)". *Journal of Physical Chemistry* **61**, 985 (1957).

130. Han, C. C., Bauer, J. B., Clark, J. C., Muroga, Y., Matsushita, Y., Okada, M., Tran-cong, Q., Chang, T. & Sanchez, I. C. "Temperature, Composition and Molecular Weight Dependence of the Binary Interaction Parameter of Polystyrene/Poly(vinyl methyl ether) Blends". *Polymer* **29**, 2001 (1988).

131. Nishimoto, M., Takami, T. A., Tohara, A. & Kasahara, H. "Miscibility of Blends of Poly(styrene-co-methacrylonitrile) and Methyl Methacrylate Based Copolymers". *Polymer* **36**, 1441 (1994).

132. Friedrich, C., Schwarzwälder, C. & Riemann, R.-E. "Rheological and Thermodynamic Study of the Miscible Blend Polystyrene/Poly(cyclohexyl methacrylate)". *Polymer* **37**, 2499 (1995).

212

133. Jang, F. H. & Woo, E. M. "Composition Dependence of Phase Stability and Cloud Point in Solution-Blended Mixtures of Polystyrene with Poly(cyclohexyl methacrylate)". *Polymer* **40**, 2231 (1999).

134. Siol, W. "Polymer Compatibility - A Consequence of Repulsive Groups within the Monomer Units". *Makromol. Chem., Macromol. Symp.* **44**, 47 (1991).

135. Hseih, D. T., Peiffer, D. G., Rabeony, M., Siakali-Kioulafa, E. & Hadjichristidis, N. "Miscible Polymer Mixture Driven by Segmental Microconformation". *Macromolecules* **26**, 4978 (1993).

136. Jabbari, E. & Peppas, N. A. "Comparison of Interdiffusion at the Polystyrene-Poly(vinyl methyl ether) and Polystyrene-Poly(isobutyl vinyl ether) Interfaces". *Polym. Int.* **38**, 65 (1995).

137. Fowler, M. E., Barlow, J. W. & Paul, D. R. "Effect of Copolymer Composition on the Miscibility of Blends of Styrene-Acrylonitrile Copolymers with Poly(methyl methacrylate)". *Polymer* **28**, 1177 (1987).

138. Nishimoto, M., Keskkula, H. & Paul, D. R. "Miscibility of Blends of Polymers Based on Styrene, Acrylonitrile and Methyl Methacrylate". *Polymer* **30**, 1279 (1989).

139. Nishimoto, M., Keskkula, H. & Paul, D. R. "Blends of Poly(styrene-*co*-acrylonitrile) and Methyl Methacrylate Based Copolymers". *Macromolecules* **23**, 3633 (1990).

140. Hahn, K., Schmitt, B. J., Kirschey, M., Kirste, R. G., Salie, H. & Schimtt-Strecker, S. "Structure and Thermodynamics in Polymer Blends. Neutron Scattering Measurements on Blends of Poly(methyl methacrylate) and Poly(styrene-co-acrylonitrile)". *Polymer* **33**, 5150 (1992).

141. Cowie, J. M. G., Watson, L. M. & MccEwen, I. J. "The Effect of Replacing the α-Hydrogen with a Methyl Group on the Miscibility in Systems Containing Styrene, Methacrylonitrile and Methyl Methacrylate". *Polym. Bul.* **31**, 729 (1993).

142. Nishimoto, M., Takami, Y., Tohara, A. & Kasahara, H. "Miscibility of Blends of Poly(styrene-*co*-methacrylonitrile) and Methyl Methacrylate Based Copolymers". *Polymer* **36**, 1441 (1995).

143. Rosedale, J. H., Bates, F. S., Almdal, K., Mortensen, K. & Wignall, G. D. "Order and Disorder in Symmetrical Diblock Copolymer Melts". *Macromolecules* **28**, 1429 (1995).

144. Yamaguchi, D., Bodycomb, J., Koizumi, S. & Hashimoto, T. "Ordered Structure in Blends of Block Copolymers. 4. Location of the Short Diblock". *Macromolecules* **32**, 5884 (1999).

145. Yamaguchi, M. & Miyata, H. "Influence of Stereoregularity of Polypropylene on Miscibility with Ethylene-1-Hexene Copolymer". *Macromolecules* **32**, 5911 (1999).

146. Lohse, D., Fetters, L. J. & Richter, Internal Report D. 30 (Exxon Research and Engineering Co., Annadale, NJ, 1999).

147. Witten, T. A., Milner, S. T. & Wang, Z.-G. in *Multiphase Macromolecular Systems* (ed. Culberton, B. M.) (Plenum, NY, 1989).

148. Fetters, L. J., Lohse, D. J. & Graessley, W. W. "Chain Dimensions and Entanglement Spacings in Dense Macromolecular Systems". *J. Polym. Sci. Polym. Phys. Ed.* **37**, 1023 (1998).

149. Fetters, L. J., Lohse, D. J., Milner, S.T. & Graessley, W. W. "Packing Length Influence in the Linear Polymer Melts on the Entanglement, Critical, and Reptation Molecular Weights". *Macromolecules* **32**, 6847 (1999).

150. Hasegawa, H., Sakamoto, N., Takeno, H., Jinnai, H., Hashimoto, T., Schwahn, D., Frielinghaus, H., Janssen, S., Imai, M. & Mortensen, K. "Small-angle Neutron Scattering Studies on Phase Behavior of Block Copolymers". *J. Phys. Chem. Sol.* **60**, 1307 (1999).

151. Walsh, D. J. & McKeown, G. J. "Compatibility of Polyacrylates and Polymethacrylates with Poly(vinyl chloride): 1. Compatibility and Temperature Variation". *Polymer* **21**, 1331 (1980).

152. Walsh, D. J. & Cheng, G. L. "The Miscibility of Polyacrylates with PVC: *In Situ* Polymerization and the Miscibility of Poly(methyl acrylate) and poly(ethyl acrylate)". *Polymer* **25**, 495 (1984).

153. Tremblay, C. & Prud'Homme, R. E. "Miscible Blends of Amorphous Polymers". *J. Polym. Sci., Polym. Phys. Ed.* **22**, 1857 (1984).

154. Temin, S. C. "Adhesive Compositions". in *Encyclopedia of Polymer Science and Engineering* 547-577 (John Wiley and Sons, NY, 1987).

155. Hagman, J. F. & Crary, J. W. "Acrylic Elastomers". in *Encyclopedia of Polymer Science and Engineering* 307-334 (John Wiley and Sons, NY, 1987).

156. Zoller, P. & Hoehn, H. "Pressure-Volume-Temperature Properties of Blends of Poly(2,6-dimethyl-1,4-phenylene ether) with Polystyrene". *J. Polym. Sci., Polym. Phys. Ed.* **20**, 1385 (1982).

157. Callaghan, T. A. & Paul, D. R. "Interaction Energies for Blends of Poly(methyl methacrylate), Polystyrene, and Poly(*alpha*-methylstyrene) by the Critical Molecular-Weight Method". *Macromolecules* **26**, 2439 (1993).

158. Cowie, J. M. G., Ferguson, R., Fernandez, M. D., McEwen, I. J. "Miscibility of Some Methacrylate and Acrylate Homopolymer Blends". *Macromolecules.* **25**, 3170 (1992).

159. Chiu, S.-C., Smith, T. G. "Compatibility of Poly(ε-caprolactone) (PCL) and Poly(styrene-*co*-acrylonitrile) (SAN) Blends. II. The Influence of the AN Content in SAN Copolymer upon Blend Compatibility". *J. Appl, Polym. Sci.* **29**, 1797 (1984).

160. Svoboda, P., Kressler, J., Ougizawa, T., Inoue, T. "FTIR and Calorimetric Analyses of the Specific Interactions in Poly(ε-caprolactone)/Poly(styrene-*co*-acrylonitrile) Blends Using Low Molecular Weight Analogues". *Macromolecules* **30**, 1973 (1997).

161. Callaghan, T. A., Takakuwa, K., Paul, D. R. "Polycarbonate-SAN Copolymer Interaction". *Polymer* **34**, 3797 (1993).

162. Li, H., Yang, Y., Fujitsuka, R., Ougizawa, T., Inoue, T. "Studies on Miscibility in Polycarbonate/Poly(styrene-*co*-acrylonitrile) Blends by Ellipsometry". *Polymer* **40**, 927 (1999).

163. Kim, W. N., Burns, C. "Blends of Polycarbonate and Poly(methyl methacrylate) and the Determination of the Polymer-Polymer Interaction Parameter of the Two Polymers". *Macromolecules* **20**, 1876 (1987).

164. Nishimoto, M., Paul, D. R. "Miscibility of Polycarbonate with Methyl Methacrylate-based Copolymers". *Polymer* **32**, 1274 (1991).

165.   Callaghan, T. A., Paul, D. R. "Estimation of the Interaction Energies by the Critical Molecular Weight Method: 1. Blends with Polycarbonates". *J. Polym. Sci.: Part B: Polym. Phys.* **32**, 1813 (1994).

166.   Hopkinson, I., Kiff, F. T., Richards, R. W., King, S. M., Farren, T. "Isotopic Labeling and Composition Dependence of Interaction Parameters in Polyethylene Oxide/Polymethyl Methacrylate Blends". *Polym.* **36**, 3523 (1995).

167.   Ito, H., Russell, T. P., Wignall, G. D. "Interactions in Mixtures of Poly(ethylene oxide) and Poly(methyl methacrylate)". *Macromolecules* **20**, 2213 (1987).

168.   Yi, Y. X. & Zoller, P. "An Experimental and Theoretical Study of the PVT Equation of State of Butadiene and Isoprene Elastomers to 200°C and 200 MPa". *J. Polym. Sci.: Part B: Polym. Phys.* **31**, 779 (1993).

169.   Milner, S. T., Witten, T. A. & Cates, M. E. "Theory of the Grafted Polymer Brush". *Macromolecules* **21**, 2610 (1988).

170.   Choi, K., Jo W. H. & Hsu S. L. "Determination of Equation-of-State Parameters by Molecular Simulations and Calculation of the Spinodal Curve for Polystyrene/Poly(vinyl methyl ether) Blends". *Macromolecules* **31**, 1366 (1998).

171.   Fasolka, M. J. *Private communication.*

172.   Domb, A. J. "Degradable Polymer Blends: I. Screening of Miscible Polymers". *J. Polym. Sci.: Part A: Polym. Chem.* **31**, 1973 (1993).

173.   Eguiburu, J. L., Fernandez-Berridi, M. J. & San Roman, J. "Blends of Amorphous and Crystalline Polylactides with Poly(methyl methacrylate) and Poly(methyl acrylate): a Miscibility Study" *Polym.* **39**, 6891 (1998).

BIOGRAPHICAL NOTE

Anne-Valérie Ruzette was born on February 25, 1973 to Marie-Rose and Alexis Ruzette, in Namur, Belgium, where she grew up. She was married to Cyrille Foillard on January 9, 1999.

Education
Institut Sainte Marie, Namur, Belgium (Sept. 1984-June 1990)

Catholic University of Louvain-la-Neuve, Belgium (Sept. 1990-June 1995)
  Engineering degree in Materials Science and Engineering

Massachusetts Institute of Technology (Sept. 1995-present)
Doctoral Program, Department of Materials Science and Engineering
  PhD: Materials Science and Engineering
  Advisor: Anne M. Mayes

Awards and Honors
1. Chateaubriand Postdoctoral Fellowship (CNRS, UMR 167, France) (2000-2001)
2. IBM Graduate Student Fellowship (1999-2000)
3. Materials Research Society Graduate Student Award (Silver Medal) (Fall Meeting 1999)
4. Belgian and American Educational Foundation Fellowship (1997-1998)
5. Fulbright Fellowship (1995-1996)

Research Experience
Massachusetts Institute of Technology
Research Assistant: with Professor Anne M. Mayes, Dept. of Materials Science and Engineering. (Jan. 1996-present).

  Studies include:
  1. Molecular Design of Ordering Transition in Block Copolymers
  2. Salt-Induced Microphase Separation in Block Copolymer Electrolytes

Catholic University of Louvain-la-Neuve, Belgium
Undergradute research in Metal Matrix Composites under Professor F. Delannay, Dept. of Materials Science and Engineering. (1994-1995)

Massachusetts Institute of Technology
Summer internship. Research in Intermetallic Compounds under Professor Andreas Mortensen, Dept. of Materials Science and Engineering. (summer 1994)

Teaching Experience
Massachusetts Institute of Technology
Teaching Assistant. Introduction to Solid State Chemistry (3.091) - Fall Term 1999, under Prof. D. R. Sadoway.

Catholic University of Louvain-la-Neuve, Belgium
Teaching Assistant. Thermodynamics and Physical Chemistry- Fall Term 1995, under Prof. J.-M. Streydio.

Selected Publications
1. *"A Simple Free Energy Model for Weakly Interacting Polymer Blends and Solutions"*, A.-V. G. Ruzette and A. M. Mayes, *In Preparation*
2. *"A Simple Model for Baroplastic Behavior in Block Copolymer Melts"*, A.-V. G. Ruzette, P. Banerjee, A. M. Mayes and T. P. Russell, *In Preparation*
3. *"Salt-Induced Microphase Separation in Block Copolymer Electrolytes"*, A.-V. G. Ruzette, P. Soo, A. M. Mayes and D. R. Sadoway, *In Preparation*
4. *"Pressure-Dependence of Phase Behavior in Styrene/n-Alkyl Methacrylate and Styrene/n-Alkyl Acrylate Block Copolymers"*, A.-V. G. Ruzette, P. Banerjee, A. M. Mayes, T. P. Russell, S. Kline, *In Preparation*
5. *"Phase Behavior of Diblock Copolymers of Styrene and n-Alkyl Methacrylates"*, A.-V. G. Ruzette, P. Banerjee, A. M. Mayes, M. Pollard, T. P. Russell, T. Slawecki, R. Hjelm, P. Thiyagarajan and R. Jerome, *Macromolecules* **1998**, *31*, 8509-8516.
6. *"The Effect of Hydrostatic Pressure on the Lower Critical Ordering Transition in Diblock Copolymers"*, M. Pollard, T. P. Russell, A.-V. G. Ruzette, A. M. Mayes, Y. Gallot, *Macromolecules* **1998**, *31*, 6493-6498.
7. *"On the Control of Interfacial Reaction in Squeeze Cast Aluminum Matrix Composites"*, A.-V. G. Ruzette, F. Boland, C. Colin, J.-M. Gilot and F. Delannay, Key Engineering Materials, Vols. 116-117, pp 229-240, Trans Tech Publications, Switzerland (**1995**).

Selected Presentations
1. *"Molecular Design of Ordering Transitions in Block Copolymers"*, MIT Program in Polymer Science and Technology, Fall 1999 seminar series, Cambridge, MA. (invited talk)
2. *"Molecular Design of Miscibility into Block Copolymers"*, Materials Research Society, Fall 1999 Meeting, Boston, MA. (contributed talk)
3. *"Controlling Bulk Thermodynamics of Block Copolymers"*, CNRS/Elf-Atochem, Paris, France. (invited talk)
4. *"Salt Induced Microphase Separation: Design of New Block Copolymer Electrolytes for Rechargeable Lithium Batteries"*, American Physical Society, March 1999 meeting, Atlanta, GA. (contributed talk)
5. *"Phase behavior of Diblock Copolymers of Styrene and n-Alkyl Methacrylates"*, American Physical Society, March 1998 meeting, Los Angeles, Ca. (contributed talk)
6. *"Lower Critical Ordering Transition in Diblock Copolymers of Styrene and n-Alkyl Methacrylates"*, American Physical Society, March 1997 meeting, Kansas City, MO. (contributed talk)